NASA/CR—2005–214006

The *M*-Integral for Computing Stress Intensity Factors in Generally Anisotropic Materials

P.A. Wawrzynek and B.J. Carter
Fracture Analysis Consultants, Inc., Ithaca, New York

L. Banks-Sills, Consultant
Tel Aviv University, Tel Aviv, Israel

Prepared for Marshall Space Flight Center
under Contract NAS8–36801
and sponsored by the
Space Shuttle Main Engine Program
managed at the Marshall Space Flight Center

July 2005

The NASA STI Program Office…in Profile

Since its founding, NASA has been dedicated to the advancement of aeronautics and space science. The NASA Scientific and Technical Information (STI) Program Office plays a key part in helping NASA maintain this important role.

The NASA STI Program Office is operated by Langley Research Center, the lead center for NASA's scientific and technical information. The NASA STI Program Office provides access to the NASA STI Database, the largest collection of aeronautical and space science STI in the world. The Program Office is also NASA's institutional mechanism for disseminating the results of its research and development activities. These results are published by NASA in the NASA STI Report Series, which includes the following report types:

- TECHNICAL PUBLICATION. Reports of completed research or a major significant phase of research that present the results of NASA programs and include extensive data or theoretical analysis. Includes compilations of significant scientific and technical data and information deemed to be of continuing reference value. NASA's counterpart of peer-reviewed formal professional papers but has less stringent limitations on manuscript length and extent of graphic presentations.

- TECHNICAL MEMORANDUM. Scientific and technical findings that are preliminary or of specialized interest, e.g., quick release reports, working papers, and bibliographies that contain minimal annotation. Does not contain extensive analysis.

- CONTRACTOR REPORT. Scientific and technical findings by NASA-sponsored contractors and grantees.

- CONFERENCE PUBLICATION. Collected papers from scientific and technical conferences, symposia, seminars, or other meetings sponsored or cosponsored by NASA.

- SPECIAL PUBLICATION. Scientific, technical, or historical information from NASA programs, projects, and mission, often concerned with subjects having substantial public interest.

- TECHNICAL TRANSLATION. English-language translations of foreign scientific and technical material pertinent to NASA's mission.

Specialized services that complement the STI Program Office's diverse offerings include creating custom thesauri, building customized databases, organizing and publishing research results…even providing videos.

For more information about the NASA STI Program Office, see the following:

- Access the NASA STI Program Home Page at ***http://www.sti.nasa.gov***

- E-mail your question via the Internet to help@sti.nasa.gov

- Fax your question to the NASA Access Help Desk at 301–621–0134

- Telephone the NASA Access Help Desk at 301–621–0390

- Write to:
  NASA Access Help Desk
  NASA Center for AeroSpace Information
  7121 Standard Drive
  Hanover, MD 21076–1320
  301–621–0390

NASA/CR—2005–214006

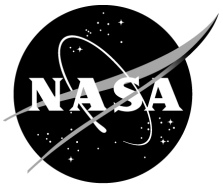

The *M*-Integral for Computing Stress Intensity Factors in Generally Anisotropic Materials

P.A. Wawrzynek and B.J. Carter
Fracture Analysis Consultants, Inc., Ithaca, New York

L. Banks-Sills, Consultant
Tel Aviv University, Tel Aviv, Israel

Prepared for Marshall Space Flight Center
under Contract NAS8–36801
and sponsored by the
Space Shuttle Main Engine Program
managed at the Marshall Space Flight Center

National Aeronautics and
Space Administration

Marshall Space Flight Center • MSFC, Alabama 35812

July 2005

Available from:

NASA Center for AeroSpace Information
7121 Standard Drive
Hanover, MD 21076–1320
301–621–0390

National Technical Information Service
5285 Port Royal Road
Springfield, VA 22161
703–487–4650

TABLE OF CONTENTS

LIST OF FIGURES

LIST OF FIGURES (Continued)

CONTRACTOR REPORT

THE *M*-INTEGRAL FOR COMPUTING STRESS INTENSITY FACTORS IN GENERALLY ANISOTROPIC MATERIALS

1. INTRODUCTION

The objective of this project is to develop and demonstrate a capability for computing stress intensity factors in generally anisotropic materials. These objectives have been met.

The primary deliverable of this project is this report and the information it contains. In addition, we have delivered the source code for a subroutine that will compute stress intensity factors for anisotropic materials encoded in both the C and Python programming languages and made available a version of the FRANC3D program that incorporates this subroutine.

Single crystal super alloys are commonly used for components in the hot sections of contemporary jet and rocket engines. Because these components have a uniform atomic lattice orientation throughout, they exhibit anisotropic material behavior. This means that stress intensity solutions developed for isotropic materials are not appropriate for the analysis of crack growth in these materials. Until now, a general numerical technique did not exist for computing stress intensity factors of cracks in anisotropic materials and cubic materials in particular. Such a capability was developed during the project and is described and demonstrated herein.

1.1 Background

Expressions for the stress and displacement fields near the tip of a crack in an anisotropic material were first published by Sih, Paris, and Irwin [1965]. Their results were used by a number of authors to create numerical techniques for computing stress intensity factors in such materials (e.g., Atluri *et al.* [1975], Boone *et al.* [1987], and Tohgo *et al.* [1993]). However, a restriction not strongly emphasized in the original or any of the subsequent papers is that these results are only valid for the case where the plane of analysis (typically a plane perpendicular to the crack front) is a plane of material symmetry.

The expressions for the stress and displacement field near a crack front in a generally anisotropic material were first published by Hoenig [1982]. These results do not appear to be widely referenced in the literature and it does not appear that a numerical technique for computing stress intensity factors based on these results has been developed previously. The Hoenig paper contains a significant number of typographical errors. We believe that these have all been identified and corrected in the work reported herein.

1.2 Anisotropic Material Properties

The primary materials of concern for the present study are single-crystal alloys. These materials exhibit cubic behavior, which means that they can be characterized by three properties (usually E, G, and v) and their orientation is given by three angles. The current implementation supports the more general case of arbitrarily oriented orthotropic materials, which are characterized by nine properties (E_1, E_2, E_3, G_{12}, G_{23}, G_{13}, ν_{12}, ν_{23}, and ν_{13}) and three angles. The fully general case of a material with 21 independent material properties could be accommodated easily in the current software, but as it is rare to assume such general behavior in engineering practice, this is not currently supported in order to simplify the interface.

As mentioned, three angles are required to specify the orientation of the material axes relative to the Cartesian axes. There are a number of conventions for this. Here we adopted the use of Euler angles, which are commonly used in many finite element applications. Our convention conforms to that used by the ANSYS software, where the first rotation, θ_z, is about the original z-axis. The second rotation, θ_x, is about the rotated x-axis, and the third rotation, θ_y, is about the rotated y-axis. In all cases, a "right-handed" rule is used to determine the sign of the rotation.

The remainder of this report is divided into seven sections. In the following section, the expressions for the stress and displacement fields near crack fronts in anisotropic materials are developed. In Section 3, the M-integral is formulated for anisotropic materials. In Section 4, the details of the present implementation of the M-integral are described. In Section 5, the results of verification studies with prescribed nodal displacements are presented. In Section 6, the results of verification studies of cracks in thick center-crack plates are presented. In Section 7, the results of a large number of analyses of cracks in single-crystal Brazilian disk specimens are summarized. Finally, Section 8 summarizes the report.

2. CRACK-FRONT STRESS AND DISPLACEMENT FIELDS

2.1 General Anisotropy

The stress and displacement fields in the vicinity of a crack-front in a general anisotropic material were presented by Hoenig [1982] based on the Lekhnitskii [1963] formalism. These are given by

$$\begin{Bmatrix} \sigma_{xx} \\ \sigma_{yy} \\ \sigma_{xy} \\ \sigma_{zx} \\ \sigma_{yz} \end{Bmatrix} = \frac{1}{\sqrt{2\pi r}} \begin{Bmatrix} \mathrm{Re}\left(\sum_{i=1}^{3} \frac{\mu_i^2 N_{ij}^{-1} K_j}{Q_i} \right) \\ \mathrm{Re}\left(\sum_{i=1}^{3} \frac{N_{ij}^{-1} K_j}{Q_i} \right) \\ -\mathrm{Re}\left(\sum_{i=1}^{3} \frac{\mu_i N_{ij}^{-1} K_j}{Q_i} \right) \\ \mathrm{Re}\left(\sum_{i=1}^{3} \frac{\mu_i \lambda_i N_{ij}^{-1} K_j}{Q_i} \right) \\ -\mathrm{Re}\left(\sum_{i=1}^{3} \frac{\lambda_i N_{ij}^{-1} K_j}{Q_i} \right) \end{Bmatrix} \tag{1}$$

and

$$u_i = \sqrt{\frac{2r}{\pi}}\, \mathrm{Re}\left(\sum_{j=1}^{3} m_{ij} N_{jl}^{-1} K_l Q_j \right), \tag{2}$$

where Re represents the real part of the quantity in parenthesis, two repeated indices obey the summation convention from 1 to 3, the coordinates x, y, z, r, and θ refer to the crack coordinates illustrated in Figure 1, and K_j are the stress intensity factors K_I, K_{II}, and K_{III}. It is assumed that the stresses and displacements are functions only of the in-plane coordinates, r and θ.

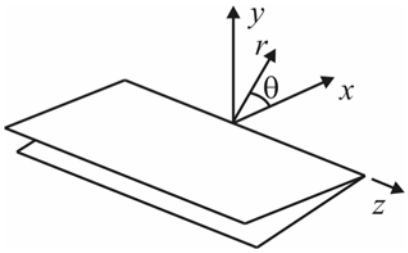

Figure 1. Local crack front coordinate system used throughout this report.

The quantities p_i, λ_i, m_{ij}, N_{ij}, and Q_i, are derived from the material compliance tensor, $\overline{S}_{ijkl}$ (where $\overline{\varepsilon}_{ij} = \overline{S}_{ijkl}\overline{\sigma}_{kl}$). The overbar indicates quantities specified in the Cartesian coordinate system. Before extracting the quantities, it is necessary to rotate the tensor to the crack-front coordinate system, S_{ijkl}, and contract it to a 6x6 matrix, S_{ij}, where i = 1..6. It is common in many branches of solid mechanics to work with the contracted form of the constitutive matrix. However, there are two different conventions for the ordering of the elements in the matrix. Both are used in this work. In the theoretical Sections (2 and 3), indices of the contracted matrix are taken in the order $\{x, y, z, yz, xz, xy\}$. This is consistent with the Hoenig and Sih papers and much of the literature for orthotropic materials (principally composites). However, in the actual code and those portions of the report concerning the implementation, the contracted matrix indices are taken in the order $\{x, y, z, xy, yz, zx\}$. This is consistent with most finite element software and much of the finite element literature.

For plane stress conditions, the full compliance matrix is employed. For generalized plane strain conditions (which are assumed in the implementation and throughout this report), a reduced compliance matrix is obtained from

$$S'_{ij} = S_{ij} - \frac{S_{i3}S_{3j}}{S_{33}} \tag{3}$$

where i,j = 1..6, S'_{ij} is symmetric, and $S'_{i3} = S'_{3i} = 0$.

The parameters μ_i, i = 1..3, are the eigenvalues of the compatibility equations with positive imaginary parts. These are found from the characteristic sixth order polynomial equation

$$l_4(\mu)l_2(\mu) - l_3^2(\mu) = 0 \tag{4}$$

where

$$\begin{aligned} l_2(\mu) &= S'_{55}\mu^2 - 2S'_{45}\mu + S'_{44} \\ l_3(\mu) &= S'_{15}\mu^3 - (S'_{14} + S'_{56})\mu^2 + (S'_{25} + S'_{46})\mu - S'_{24} \\ l_4(\mu) &= S'_{11}\mu^4 - 2S'_{16}\mu^3 + (2S'_{12} + S'_{66})\mu^2 - 2S'_{26}\mu + S'_{22} \end{aligned} \tag{5}$$

Solution of eqn. 4 leads to three pairs of complex conjugate roots. The three with positive imaginary parts are chosen. The parameters λ_i are given by

$$\lambda_i = -\frac{l_3(\mu_i)}{l_2(\mu_i)}, \quad i = 1..3. \tag{6}$$

The parameters m_{ij} are given by

$$
\begin{aligned}
m_{1i} &= S'_{11}\mu_i^2 - S'_{16}\mu_i + S'_{12} + \lambda_i\left(S'_{15}\mu_i - S'_{14}\right) \\
m_{2i} &= S'_{21}\mu_i - S'_{26} + S'_{22}/\mu_i + \lambda_i\left(S'_{25} - S'_{24}/\mu_i\right). \\
m_{3i} &= S'_{41}\mu_i - S'_{46} + S'_{42}/\mu_i + \lambda_i\left(S'_{45} - S'_{44}/\mu_i\right)
\end{aligned} \tag{7}
$$

The matrix N_{ij} is defined as

$$
N_{ij} = \begin{bmatrix} 1 & 1 & 1 \\ -\mu_1 & -\mu_2 & -\mu_3 \\ -\lambda_1 & -\lambda_2 & -\lambda_3 \end{bmatrix}, \tag{8}
$$

which has an inverse

$$
N_{ij}^{-1} = \frac{1}{|N|}\begin{bmatrix} \mu_2\lambda_3 - \mu_3\lambda_2 & \lambda_3 - \lambda_2 & \mu_2 - \mu_3 \\ \mu_3\lambda_1 - \mu_1\lambda_3 & \lambda_1 - \lambda_3 & \mu_3 - \mu_1 \\ \mu_1\lambda_2 - \mu_2\lambda_1 & \lambda_2 - \lambda_1 & \mu_1 - \mu_2 \end{bmatrix} \tag{9}
$$

and $|N|$ is the determinate of N_{ij}. Finally,

$$
Q_i = \sqrt{\cos\theta + \mu_i \sin\theta} \tag{10}
$$

2.2 Special Anisotropies

There are special anisotropies for which the above development is mathematically degenerate. These include monoclinic and cubic materials oriented such that $z = 0$ is a plane of material symmetry. Hoenig [1982] gives expressions for the stresses and displacements for the degenerate cases. However, the implementation follows the more widely referenced expressions given earlier by Sih *et. al.* [1965]. These stress and displacement expressions are

$$
\begin{Bmatrix} \sigma_{xx} \\ \sigma_{yy} \\ \sigma_{xy} \\ \sigma_{zx} \\ \sigma_{yz} \end{Bmatrix} = \frac{1}{\sqrt{2\pi r}} \begin{Bmatrix} K_I \,\mathrm{Re}\left[\left(\frac{\mu_1\mu_2}{\mu_1-\mu_2}\right)\left(\frac{\mu_2}{Q_2} - \frac{\mu_1}{Q_1}\right)\right] + K_{II}\,\mathrm{Re}\left[\left(\frac{1}{\mu_1-\mu_2}\right)\left(\frac{\mu_2^2}{Q_2} - \frac{\mu_1^2}{Q_1}\right)\right] \\ K_I \,\mathrm{Re}\left[\left(\frac{1}{\mu_1-\mu_2}\right)\left(\frac{\mu_1}{Q_2} - \frac{\mu_2}{Q_1}\right)\right] + K_{II}\,\mathrm{Re}\left[\left(\frac{1}{\mu_1-\mu_2}\right)\left(\frac{1}{Q_2} - \frac{1}{Q_1}\right)\right] \\ K_I \,\mathrm{Re}\left[\left(\frac{\mu_1\mu_2}{\mu_1-\mu_2}\right)\left(\frac{1}{Q_1} - \frac{1}{Q_2}\right)\right] + K_{II}\,\mathrm{Re}\left[\left(\frac{1}{\mu_1-\mu_2}\right)\left(\frac{\mu_1}{Q_1} - \frac{\mu_2}{Q_2}\right)\right] \\ -K_{III}\,\mathrm{Re}\left[\frac{\mu_3}{Q_3}\right] \\ K_{III}\,\mathrm{Re}\left[\frac{1}{Q_3}\right] \end{Bmatrix} \tag{11}
$$

and

$$\begin{Bmatrix} u_1 \\ u_2 \\ u_3 \end{Bmatrix} = \sqrt{\frac{2r}{\pi}} \begin{Bmatrix} K_I \,\mathrm{Re}\left[\left(\frac{1}{\mu_1-\mu_2}\right)\left(\mu_1 p_2 Q_2 - \mu_2 p_1 Q_1\right)\right] + K_{II}\,\mathrm{Re}\left[\left(\frac{1}{\mu_1-\mu_2}\right)\left(p_2 Q_2 - p_1 Q_1\right)\right] \\ K_I \,\mathrm{Re}\left[\left(\frac{1}{\mu_1-\mu_2}\right)\left(\mu_1 q_2 Q_2 - \mu_2 q_1 Q_1\right)\right] + K_{II}\,\mathrm{Re}\left[\left(\frac{1}{\mu_1-\mu_2}\right)\left(q_2 Q_2 - q_1 Q_1\right)\right] \\ K_{III}\,\mathrm{Re}\left[\frac{Q_3}{S'_{45}+\mu_3 S'_{44}}\right] \end{Bmatrix} \quad (12)$$

In these expressions, μ_1 and μ_2 are the roots of the equation

$$S'_{11}\mu^4 - 2S'_{16}\mu^3 + \left(2S'_{12} + S'_{66}\right)\mu^2 - 2S'_{26}\mu + S'_{22} = 0 \quad (13)$$

with positive imaginary parts.

μ_3 is the root of the equation

$$S'_{44}\mu^2 + 2S'_{45}\mu + S'_{55} = 0. \quad (14)$$

with a positive imaginary part.

The parameters p_j and q_j are defined as

$$\begin{aligned} p_j &= S'_{11}\mu_j^2 - S'_{16}\mu_j + S'_{12} \\ q_j &= S'_{12}\mu - S'_{26} + S'_{22}/\mu_j \end{aligned} \quad i = 1,2 \quad (15)$$

Finally,

$$Q_i = \sqrt{\cos\theta + \mu_i \sin\theta}\,. \quad (16)$$

3. *M*-INTEGRAL FORMULATION

3.1 The Relationship Between *J* and *K*

As a first step in formulating an *M*-integral for anisotropic materials, the relationship between the *J*-integral and the stress intensity factors must be established.

The J-integral developed by Rice [1968] is given by

$$J = \int_{\Gamma} \left(W n_x - T_i \frac{\partial u_i}{\partial x} \right) ds \tag{17}$$

where, for 2-D, the integration path Γ is illustrated in Figure 2, W is the strain energy density

$$W = \tfrac{1}{2} \sigma_{ij} \varepsilon_{ij} \tag{18}$$

n_i is the outer normal to Γ, $T_i = \sigma_{ij} n_j$, u_i is the displacement vector, and ds is the differential arc length along Γ.

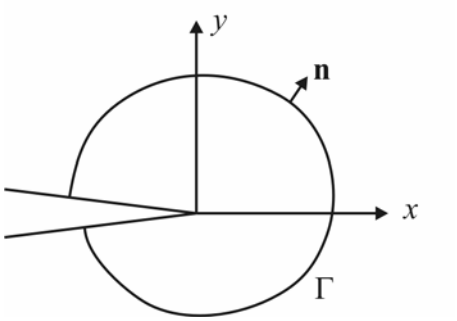

Figure 2. The integration contour for the 2-D *J*-integral.

By means of the crack closure integral, Hoenig [1982] developed the relationship between the *J*-integral and the stress intensity factors as

$$J = -\tfrac{1}{2} \left(K_I \, \mathrm{Im}\left[m_{2i} N_{ij}^{-1} K_j \right] + K_{II} \, \mathrm{Im}\left[m_{1i} N_{ij}^{-1} K_j \right] + K_{III} \, \mathrm{Im}\left[m_{3i} N_{ij}^{-1} K_j \right] \right) \tag{19}$$

where Im is the imaginary part of the bracketed quantities and summation is applied to repeated indices.

For monoclinic or cubic materials oriented such that $z = 0$ is a symmetry plane, the relationship between *J* and *K* is

$$J = \tfrac{1}{2}\,\mathrm{Im}\left[\left(S'_{26} - \left(\frac{\mu_1+\mu_2}{\mu_1\mu_2}\right)S'_{22}\right)K_I^2 + \left(\left[\mu_1+\mu_2\right]S'_{11} - S'_{16}\right)K_{II}^2 + \left(\mu_1\mu_2 S'_{11} - \frac{1}{\mu_1\mu_2}S'_{22}\right)K_I K_{II}\right] + \tfrac{1}{2}\sqrt{S'_{44}S'_{55} - S'^2_{45}}\,K_{III}^2 \tag{20}$$

3.2 The *M*-Integral Expressions

Yau *et. al.* [1980] developed the *M*-integral from the *J*-integral as a way to extract the stress intensity factors for the three fracture modes from the global energy release rate. To obtain the *M*-integral from eqn. 19, two solutions are assumed and superposed. This is possible if the material is assumed to be linear elastic. Define

$$\begin{aligned} \sigma_{ij} &= \sigma_{ij}^{(1)} + \sigma_{ij}^{(2)} \\ \varepsilon_{ij} &= \varepsilon_{ij}^{(1)} + \varepsilon_{ij}^{(2)} \\ u_i &= u_i^{(1)} + u_i^{(2)} \\ K_i &= K_i^{(1)} + K_i^{(2)} \end{aligned} \quad . \tag{21}$$

Substitution of the stress, strain, and displacement fields into the J-integral expression (eqn. 17) leads to

$$J = J^{(1)} + J^{(2)} + M^{(1,2)} \tag{22}$$

where

$$\begin{aligned} J^{(1)} &= \int_\Gamma \left(W^{(1)} n_1 - T_i^{(1)} \frac{\partial u_i^{(1)}}{\partial x_1}\right) ds \\ J^{(2)} &= \int_\Gamma \left(W^{(2)} n_1 - T_i^{(2)} \frac{\partial u_i^{(2)}}{\partial x_1}\right) ds \\ M^{(1,2)} &= \int_\Gamma \left(W^{(1,2)} n_1 - T_i^{(1)} \frac{\partial u_i^{(2)}}{\partial x_1} - T_i^{(2)} \frac{\partial u_i^{(1)}}{\partial x_1}\right) ds \end{aligned} \tag{23}$$

The interaction strain energy density is given by

$$W^{(1,2)} = \sigma_{ij}^{(1)} \varepsilon_{ij}^{(2)} = \sigma_{ij}^{(2)} \varepsilon_{ij}^{(1)} \tag{24}$$

and $M^{(1,2)}$ is the *M*-integral.

The superposed stress intensity factors in eqn. 21 can be substituted into eqn. 19 to yield

$$
\begin{aligned}
J = J^{(1)} + J^{(2)} - \tfrac{1}{2}\Big[& K_I^{(1)} \operatorname{Im}\left(m_{2i} N_{ij}^{-1} K_j^{(2)}\right) + K_I^{(2)} \operatorname{Im}\left(m_{2i} N_{ij}^{-1} K_j^{(1)}\right) \\
& + K_{II}^{(1)} \operatorname{Im}\left(m_{1i} N_{ij}^{-1} K_j^{(2)}\right) + K_{II}^{(2)} \operatorname{Im}\left(m_{1i} N_{ij}^{-1} K_j^{(1)}\right) \\
& + K_{III}^{(1)} \operatorname{Im}\left(m_{3i} N_{ij}^{-1} K_j^{(2)}\right) + K_{III}^{(2)} \operatorname{Im}\left(m_{3i} N_{ij}^{-1} K_j^{(2)}\right)\Big]
\end{aligned} \tag{25}
$$

where

$$
\begin{aligned}
J^{(1)} &= -\tfrac{1}{2}\Big[K_I^{(1)} \operatorname{Im}\left(m_{2i} N_{ij}^{-1} K_j^{(1)}\right) + K_{II}^{(1)} \operatorname{Im}\left(m_{1i} N_{ij}^{-1} K_j^{(1)}\right) + K_{III}^{(1)} \operatorname{Im}\left(m_{3i} N_{ij}^{-1} K_j^{(1)}\right)\Big] \\
J^{(2)} &= -\tfrac{1}{2}\Big[K_I^{(2)} \operatorname{Im}\left(m_{2i} N_{ij}^{-1} K_j^{(2)}\right) + K_{II}^{(2)} \operatorname{Im}\left(m_{1i} N_{ij}^{-1} K_j^{(2)}\right) + K_{III}^{(2)} \operatorname{Im}\left(m_{3i} N_{ij}^{-1} K_j^{(2)}\right)\Big].
\end{aligned} \tag{26}
$$

Equating eqn. 22 and eqn. 25, and noting eqn. 23, leads to the definition of the *M*-integral as

$$
\begin{aligned}
M = -\tfrac{1}{2}\Big[& K_I^{(1)} \operatorname{Im}\left(m_{2i} N_{ij}^{-1} K_j^{(2)}\right) + K_I^{(2)} \operatorname{Im}\left(m_{2i} N_{ij}^{-1} K_j^{(1)}\right) \\
& + K_{II}^{(1)} \operatorname{Im}\left(m_{1i} N_{ij}^{-1} K_j^{(2)}\right) + K_{II}^{(2)} \operatorname{Im}\left(m_{1i} N_{ij}^{-1} K_j^{(1)}\right) . \\
& + K_{III}^{(1)} \operatorname{Im}\left(m_{3i} N_{ij}^{-1} K_j^{(2)}\right) + K_{III}^{(2)} \operatorname{Im}\left(m_{3i} N_{ij}^{-1} K_j^{(2)}\right)\Big]
\end{aligned} \tag{27}
$$

To this point, the *J*- and *M*-integrals have been presented as contour integrals. It is well known that in the context of finite elements the evaluation of area and volume integrals lead to more accurate and stable results than direct integration along a contour. Li *et. al.* (1985) introduced the 2-D equivalent domain integral (EDI) form of the *J*-integral that transforms eqn. 17 to an area integral. An analogous technique can be used to formulate a 3-D equivalent domain version of the *M*-Integral where the integration takes place over a volume. The resulting expressions are

$$
\begin{aligned}
J^{(k)} &= \int_V \left(\sigma_{ij}^{(k)} \frac{\partial u_i^{(k)}}{\partial x_1} - W^{(k)} \delta_{1j} \right) \frac{\partial q}{\partial x_j} dV \qquad i = 1,2,3 \quad k, j = 1,2 \\
M^{(1,2)} &= \int_V \left(\sigma_{ij}^{(1)} \frac{\partial u_i^{(2)}}{\partial x_1} + \sigma_{ij}^{(2)} \frac{\partial u_i^{(1)}}{\partial x_1} - W^{(1,2)} \delta_{1j} \right) \frac{\partial q}{\partial x_j} dV \quad i = 1,2,3 \quad j = 1,2 \\
A_q &= \int_L q_t \, ds \, .
\end{aligned} \tag{28}
$$

where δ_{ij} is the Kronecker delta and q is a function that is 1 at the stress intensity evaluation point and zero on the outer boundary of the domain of integration; q_t is the value of the q function along the crack front. The domain of integration is a cylinder that encloses a portion of the crack front. This is illustrated in Figure 3. The q function can be thought of as a virtual crack extension. This is illustrated in Figure 4.

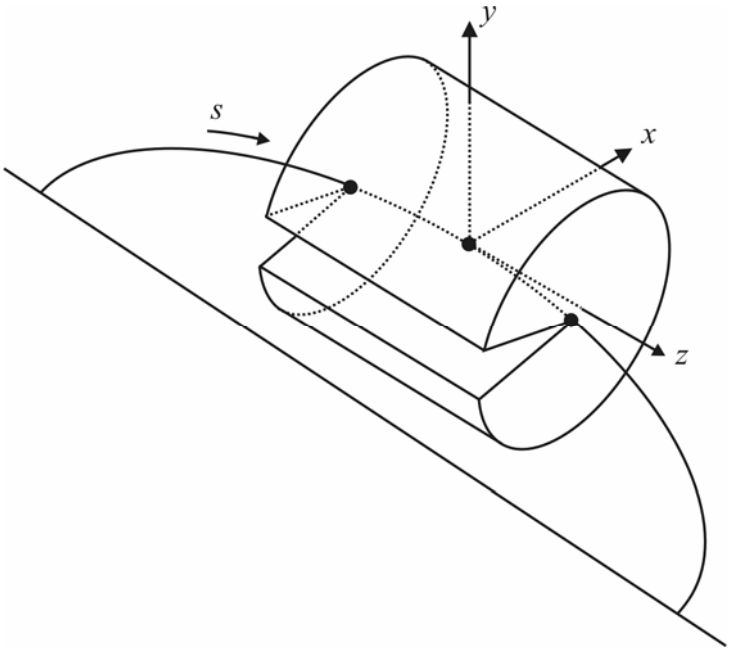

Figure 3. Domain of integration for computing the 3-D *M*-integral.

In order to evaluation the M-integral numerically, two solutions are chosen. Solution (1) is the finite element solution for the problem of interest. Solution (2) is an auxiliary solution; three solutions are chosen in order to obtain $K_I^{(1)}$, $K_{II}^{(1)}$, and $K_{III}^{(1)}$. These are denoted (2a), (2b), and (2c) and are chosen as follows

Solution	K_I	K_{II}	K_{III}
(2a)	1.0	0.0	0.0
(2b)	0.0	1.0	0.0
(2c)	0.0	0.0	1.0

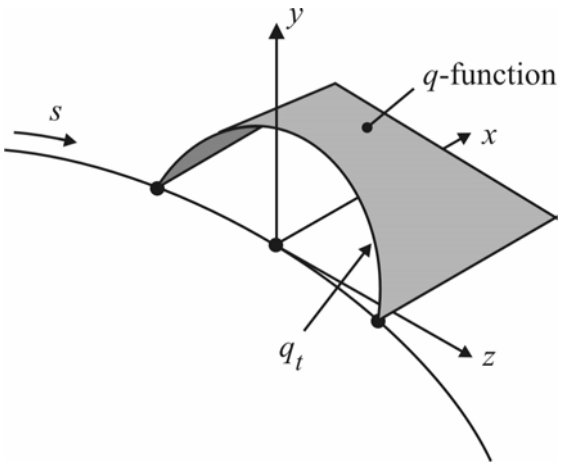

Figure 4. The *q* function used in evaluating the 3-D *M*-integral.

Substituting these into eqn. 27 yields the following expressions for *M*

$$
\begin{aligned}
M^{(1,2a)} &= -\tfrac{1}{2}\left[2K_I^{(1)}\,\mathrm{Im}\left(m_{2i}N_{i1}^{-1}\right) + K_{II}^{(1)}\,\mathrm{Im}\left(m_{1i}N_{i1}^{-1}+m_{2i}N_{i2}^{-1}\right)+ K_{III}^{(1)}\,\mathrm{Im}\left(m_{3i}N_{i1}^{-1}+m_{2i}N_{i3}^{-1}\right)\right]\\
M^{(1,2b)} &= -\tfrac{1}{2}\left[K_I^{(1)}\,\mathrm{Im}\left(m_{2i}N_{i2}^{-1}+m_{1i}N_{i1}^{-1}\right) + 2K_{II}^{(1)}\,\mathrm{Im}\left(m_{1i}N_{i2}^{-1}\right)+ K_{III}^{(1)}\,\mathrm{Im}\left(m_{3i}N_{i2}^{-1}+m_{1i}N_{i3}^{-1}\right)\right] \qquad (29)\\
M^{(1,2c)} &= -\tfrac{1}{2}\left[K_I^{(1)}\,\mathrm{Im}\left(m_{2i}N_{i3}^{-1}+m_{3i}N_{i1}^{-1}\right) + K_{II}^{(1)}\,\mathrm{Im}\left(m_{1i}N_{i3}^{-1}+m_{3i}N_{i2}^{-1}\right)+ 2K_{III}^{(1)}\,\mathrm{Im}\left(m_{3i}N_{i3}^{-1}\right)\right]
\end{aligned}
$$

and

$$
\begin{aligned}
M^{(1,2a)} &= \int_A\left(\sigma_{ij}^{(1)}\frac{\partial u_i^{(2a)}}{\partial x_1}+\sigma_{ij}^{(2a)}\frac{\partial u_i^{(1)}}{\partial x_1}-W^{(1,2a)}\delta_{1j}\right)\frac{\partial q}{\partial x_j}\,dA\\
M^{(1,2b)} &= \int_A\left(\sigma_{ij}^{(1)}\frac{\partial u_i^{(2b)}}{\partial x_1}+\sigma_{ij}^{(2b)}\frac{\partial u_i^{(1)}}{\partial x_1}-W^{(1,2b)}\delta_{1j}\right)\frac{\partial q}{\partial x_j}\,dA \qquad (30)\\
M^{(1,2c)} &= \int_A\left(\sigma_{ij}^{(1)}\frac{\partial u_i^{(2c)}}{\partial x_1}+\sigma_{ij}^{(2c)}\frac{\partial u_i^{(1)}}{\partial x_1}-W^{(1,2c)}\delta_{1j}\right)\frac{\partial q}{\partial x_j}\,dA
\end{aligned}
$$

These can be combined into one system of equations,

$$
\begin{bmatrix}
2\,\mathrm{Im}\left(m_{2i}N_{i1}^{-1}\right) & \mathrm{Im}\left(m_{1i}N_{i1}^{-1}+m_{2i}N_{i2}^{-1}\right) & \mathrm{Im}\left(m_{3i}N_{i1}^{-1}+m_{2i}N_{i3}^{-1}\right)\\
\mathrm{Im}\left(m_{2i}N_{i2}^{-1}+m_{1i}N_{i1}^{-1}\right) & 2\,\mathrm{Im}\left(m_{1i}N_{i2}^{-1}\right) & \mathrm{Im}\left(m_{3i}N_{i2}^{-1}+m_{1i}N_{i3}^{-1}\right)\\
\mathrm{Im}\left(m_{2i}N_{i3}^{-1}+m_{3i}N_{i1}^{-1}\right) & \mathrm{Im}\left(m_{1i}N_{i3}^{-1}+m_{3i}N_{i2}^{-1}\right) & 2\,\mathrm{Im}\left(m_{3i}N_{i3}^{-1}\right)
\end{bmatrix}
\begin{Bmatrix} K_I^{(1)}\\ K_{II}^{(1)}\\ K_{III}^{(1)}\end{Bmatrix}
=\begin{Bmatrix} M^{(1,2a)}/A_q\\ M^{(1,2b)}/A_q\\ M^{(1,2c)}/A_q\end{Bmatrix} \qquad (31)
$$

that can be solved for the stress intensity factors. The terms in the coefficient matrix are obtained from eqs. 7 and 9 and depend on the material properties and orientation.

Terms in the right-hand-side vector (eqn. 30) are obtained from the finite element results and eqs. 1 and 2.

For the special case where $z = 0$ is a plane of material symmetry, the corresponding expressions for the M-integral are

$$
\begin{aligned}
M^{(1,2a)} &= \mathrm{Im}\left[\left(S'_{26}-\left(\frac{\mu_1+\mu_2}{\mu_1\mu_2}\right)S'_{22}\right)K_I^{(1)}+\frac{1}{2}\left(\mu_1\mu_2 S'_{11}-\frac{1}{\mu_1\mu_2}S'_{22}\right)K_{II}^{(1)}\right]\\
M^{(1,2b)} &= \mathrm{Im}\left[\frac{1}{2}\left(\mu_1\mu_2 S'_{11}-\frac{1}{\mu_1\mu_2}S'_{22}\right)K_I^{(1)}+\left((\mu_1+\mu_2)S'_{11}-S'_{16}\right)K_{II}^{(1)}\right] \qquad (32)\\
M^{(1,2c)} &= \sqrt{S'_{44}S'_{55}-S'^{\,2}_{45}}\,K_{III}^{(1)}\,.
\end{aligned}
$$

These can be arranged into the system of equations

$$\begin{bmatrix} \mathrm{Im}\left(S'_{26} - \left(\frac{\mu_1 + \mu_2}{\mu_1 \mu_2} \right) S'_{22} \right) & \frac{1}{2}\mathrm{Im}\left(\mu_1 \mu_2 S'_{11} - \frac{1}{\mu_1 \mu_2} S'_{22} \right) & 0 \\ \frac{1}{2}\mathrm{Im}\left(\mu_1 \mu_2 S'_{11} - \frac{1}{\mu_1 \mu_2} S'_{22} \right) & \mathrm{Im}\left((\mu_1 + \mu_2) S'_{11} - S'_{16} \right) & 0 \\ 0 & 0 & \sqrt{S'_{44} S'_{55} - S'^2_{45}} \end{bmatrix} \begin{Bmatrix} K_I^{(1)} \\ K_{II}^{(1)} \\ K_{III}^{(1)} \end{Bmatrix} = \begin{Bmatrix} \dfrac{M^{(1,2a)}}{A_q} \\ \dfrac{M^{(1,2b)}}{A_q} \\ \dfrac{M^{(1,2c)}}{A_q} \end{Bmatrix}. \tag{33}$$

where the terms in the right-hand-side vector are determined from eqn. 30 using eqs. 11 and 12 to determine the stresses and displacements.

4. *M*-INTEGRAL IMPLEMENTATION

4.1 Integration Domains and *q*-Functions

There are two important aspects of the implementation of the 3-D *M*-integral that do not follow directly from the formulation. These are the selection of the elements that will participate in the integration domain, and the related issue of selecting the virtual crack extension, the *q*-function.

Our experience with 2-D implementations of the *J*-integral indicates that accurate stress intensity factors can be computed using eight triangular quarter-point elements around the crack tip. We obtain accurate results integrating only in these crack-tip elements. Other authors, however, report more accurate results when the integration is performed in "rings" of elements that are remote from, but completely encircle the crack tip (e.g., Banks-Sills and Sherman [1992]). In 3-D, unlike in 2-D, the domain of integration cannot be remote from the crack-front. That is, the crack-front elements must be included in the integration domain, if not, it cannot be demonstrated that the *J*-integral (or *M*-integral) is path independent.

Considering this experience and constraints, we have implemented the two options of evaluating the *M*-integral: either in the crack-front elements only (Fig. 5-8), or in the crack-front elements plus the first ring of elements surrounding the crack-front elements (Fig 9-12). The crack-front elements are assumed to be 15-noded wedge elements with the appropriate side nodes moved to the quarter-points. The elements in the next ring out from the crack front are assumed to be 20-noded brick elements.

Related to the selection of elements in the integration domain is the selection of an appropriate virtual crack extension or *q*-function. Banks-Sills and Sherman studied this issue in some detail [1988]. They determined that the most accurate results are obtained if the integral is evaluated at the corner node of an element with a linear variation of the *q*-function along the crack front in both sets of elements adjacent to the evaluation point. This *q*-variation is illustrated in the right of Figures 5 and 9. For the purposes of this report, this is denoted as $q^{(1)}$. This type of *q*-function has the attractive feature that it can be used for nodes where the crack-front meets a free surface, as shown in Figures 6, 7, 10, and 11, which are denoted as $q^{(2)}$ and $q^{(3)}$.

An alternative *q*-function that extends only the mid-side node is shown in Figures 8 and 12 (denoted $q^{(4)}$). Banks-Sills and Sherman found that this extension was less accurate than the corner node extensions. However, this extension does overcome complications that arise for curved crack fronts.

Curved crack fronts are usually approximated by piecewise linear segments. For anisotropic materials, one must consider the orientation of the material coordinate system relative to the crack front coordinate system. For cases $q^{(2)}$, $q^{(3)}$, and $q^{(4)}$ the relative orientation of the material coordinate system can be determined from the tangent of the participating crack front segment and the local normal to the crack plane. For case $q^{(1)}$, two crack front segments participate in the

integration domain, and, in general, their tangents will not be equal. This means that the local material coordinate system orientation is ambiguous. How this ambiguity is resolved in the current implementation is presented in Section 4.2.2. However, the accuracy of this resolution has not been assessed.

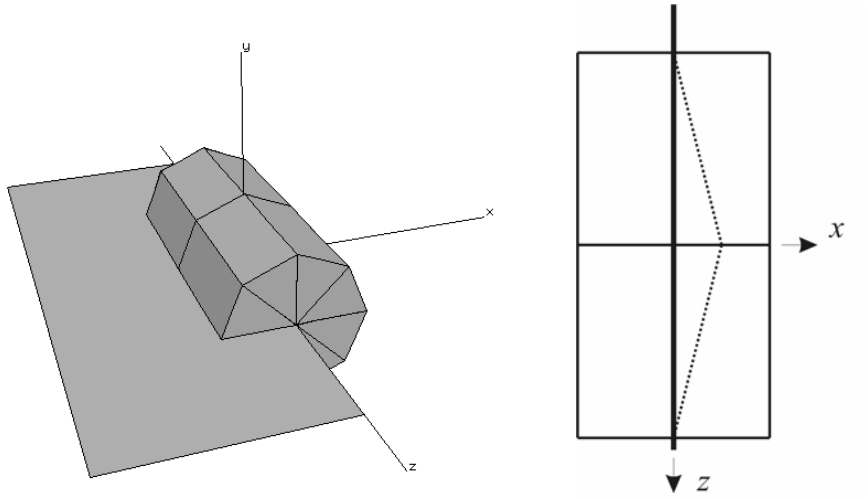

Figure 5. The domain of integration and the virtual crack extension for $q^{(1)}$ using one ring of elements.

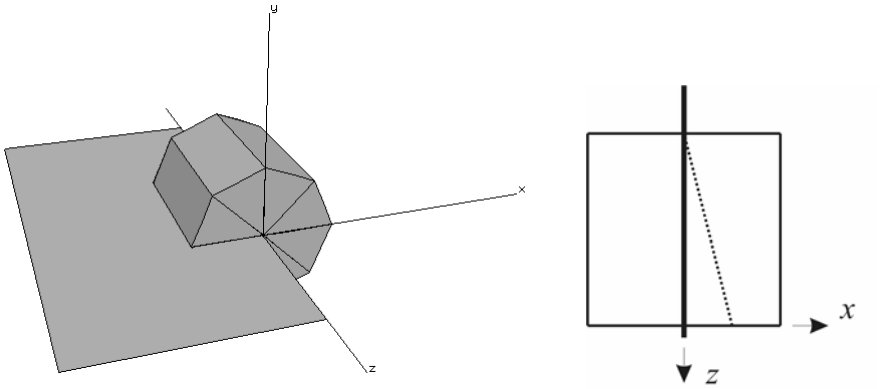

Figure 6. The domain of integration and the virtual crack extension for $q^{(2)}$ using one ring of elements.

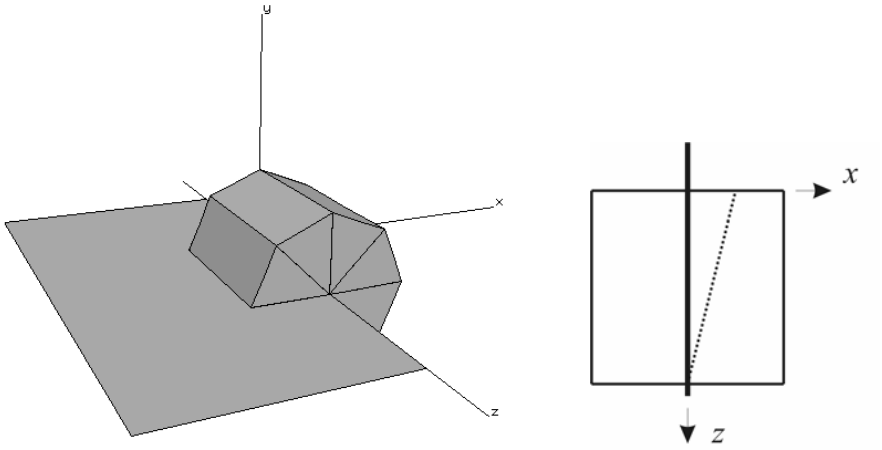

Figure 7. The domain of integration and the virtual crack extension for $q^{(3)}$ using one ring of elements.

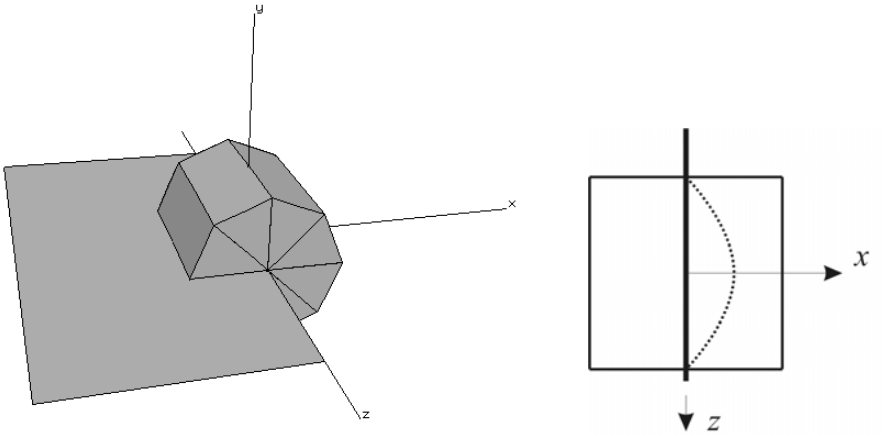

Figure 8. The domain of integration and the virtual crack extension for $q^{(4)}$ using one ring of elements.

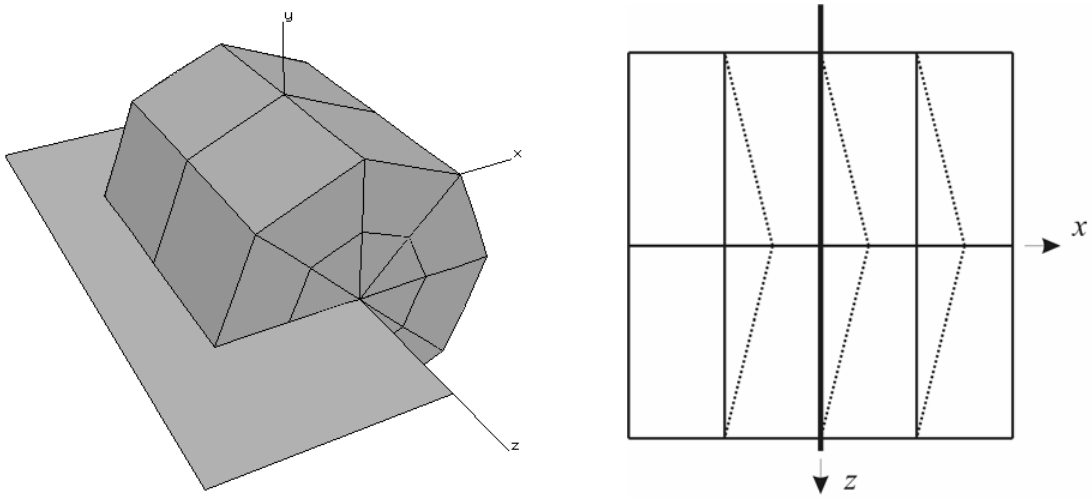

Figure 9. The domain of integration and the virtual crack extension for $q^{(1)}$ using two rings of elements.

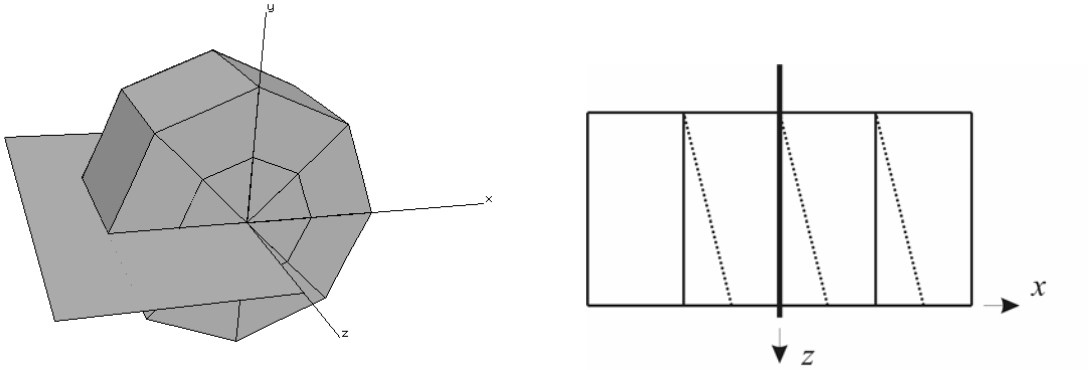

Figure 10. The domain of integration and the virtual crack extension for $q^{(2)}$ using two rings of elements.

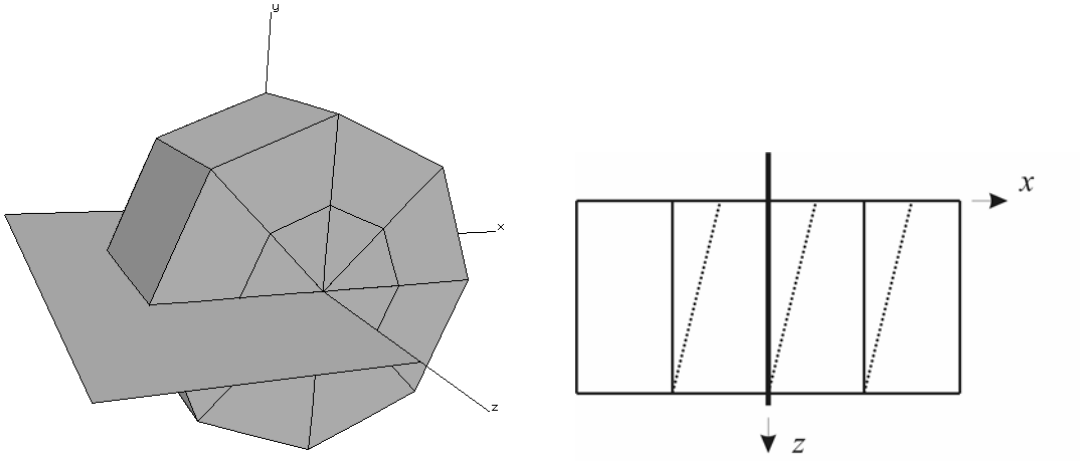

Figure 11. The domain of integration and the virtual crack extension for $q^{(3)}$ using two rings of elements.

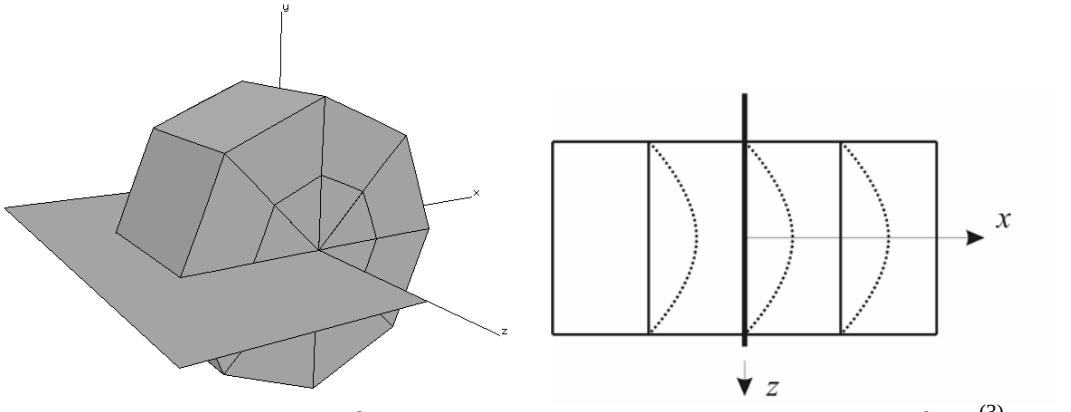

Figure 12. The domain of integration and the virtual crack extension for $q^{(3)}$ using two rings of elements.

A study of the relative accuracy of the combinations of element domains and *q*-functions has been performed. The results are reported in Section 5.

4.2 Detailed Implementation Steps

The following sub-sections detail the steps in the current implementation of the *M*-integral for anisotropic materials.

4.2.1 Compute material constitutive matrices

Material properties are specified by nine material properties: E_1, E_2, E_3, ν_{12}, ν_{23}, ν_{13}, G_{12}, G_{23}, and G_{31}. The orientation of the material coordinate system relative to the Cartesian coordinate system of the model is specified by three Euler angles, θ_z, θ_x, and θ_y.

The material compliance matrix for an orthotropic material in the local material coordinate system is

$$\left[\hat{S}\right] = \begin{bmatrix} 1/E_1 & -\nu_{12}/E_2 & -\nu_{13}/E_3 & 0 & 0 & 0 \\ & 1/E_2 & -\nu_{23}/E_3 & 0 & 0 & 0 \\ & & 1/E_3 & 0 & 0 & 0 \\ & & & 1/G_{12} & 0 & 0 \\ & & & & 1/G_{23} & 0 \\ sym & & & & & 1/G_{23} \end{bmatrix}. \qquad (34)$$

This is inverted to obtain the local material stiffness matrix

$$\hat{C} = \hat{S}^{-1}. \qquad (35)$$

A 3x3 transformation matrix that will rotate the local material coordinate axis to the material coordinate axes in the Cartesian space is determined from the Euler angles as

$$[t] = \begin{bmatrix} \cos(\theta_z)\cos(\theta_y) - \sin(\theta_z)\sin(\theta_x)\sin(\theta_y) & -\sin(\theta_z)\cos(\theta_x) & \cos(\theta_z)\sin(\theta_y) + \sin(\theta_z)\sin(\theta_x)\cos(\theta_y) \\ \sin(\theta_z)\cos(\theta_y) + \cos(\theta_z)\sin(\theta_x)\sin(\theta_y) & \cos(\theta_z)\cos(\theta_y) & \sin(\theta_z)\cos(\theta_y) - \cos(\theta_z)\sin(\theta_x)\cos(\theta_y) \\ -\cos(\theta_x)\sin(\theta_y) & \sin(\theta_x) & \cos(\theta_x)\sin(\theta_y) \end{bmatrix}. \qquad (36)$$

Components of the 3x3 rotation matrices are used to formulate 6x6 matrices that rotate the material stiffness and compliance matrices. These two matrices are different, and are given by

$$[R_s]=\begin{bmatrix} t_{11}^2 & t_{12}^2 & t_{13}^2 & t_{11}t_{12} & t_{12}t_{13} & t_{13}t_{11} \\ t_{21}^2 & t_{22}^2 & t_{23}^2 & t_{21}t_{22} & t_{22}t_{23} & t_{23}t_{21} \\ t_{31}^2 & t_{32}^2 & t_{33}^2 & t_{31}t_{32} & t_{32}t_{33} & t_{33}t_{31} \\ 2t_{11}t_{21} & 2t_{12}t_{22} & 2t_{13}t_{23} & t_{11}t_{22}+t_{12}t_{21} & t_{12}t_{23}+t_{13}t_{22} & t_{13}t_{21}+t_{11}t_{23} \\ 2t_{21}t_{31} & 2t_{22}t_{32} & 2t_{23}t_{33} & t_{21}t_{32}+t_{22}t_{31} & t_{22}t_{33}+t_{23}t_{32} & t_{23}t_{31}+t_{21}t_{33} \\ 2t_{31}t_{11} & 2t_{32}t_{12} & 2t_{33}t_{13} & t_{31}t_{12}+t_{32}t_{11} & t_{32}t_{13}+t_{33}t_{12} & t_{33}t_{11}+t_{31}t_{13} \end{bmatrix} \tag{37}$$

and

$$[R_c]=\begin{bmatrix} t_{11}^2 & t_{12}^2 & t_{13}^2 & 2t_{11}t_{12} & 2t_{12}t_{13} & 2t_{13}t_{11} \\ t_{21}^2 & t_{22}^2 & t_{23}^2 & 2t_{21}t_{22} & 2t_{22}t_{23} & 2t_{23}t_{21} \\ t_{31}^2 & t_{32}^2 & t_{33}^2 & 2t_{31}t_{32} & 2t_{32}t_{33} & 2t_{33}t_{31} \\ t_{11}t_{21} & t_{12}t_{22} & t_{13}t_{23} & t_{11}t_{22}+t_{12}t_{21} & t_{12}t_{23}+t_{13}t_{22} & t_{13}t_{21}+t_{11}t_{23} \\ t_{21}t_{31} & t_{22}t_{32} & t_{23}t_{33} & t_{21}t_{32}+t_{22}t_{31} & t_{22}t_{33}+t_{23}t_{32} & t_{23}t_{31}+t_{21}t_{33} \\ t_{31}t_{11} & t_{32}t_{12} & t_{33}t_{13} & t_{31}t_{12}+t_{32}t_{11} & t_{32}t_{13}+t_{33}t_{12} & t_{33}t_{11}+t_{31}t_{13} \end{bmatrix}. \tag{38}$$

The material matrices are then rotated into the Cartesian system by

$$[\overline{C}]=[R_c][\hat{C}][R_c]^T \quad \text{and} \quad [\overline{S}]=[R_s][\hat{S}][R_s]^T. \tag{39}$$

4.2.2 Compute the crack-front coordinate system

For cases $q^{(2)}$, $q^{(3)}$, and $q^{(4)}$, the local *z*-axis is equal to the tangent to the crack-front segment that is participating in the integration. The local *y*-axis is parallel to the local normal to the crack surface. The local *x*-axis is perpendicular to the local *y*- and *z*-axes.

As mentioned above, the local crack front coordinate system for $q^{(1)}$ is ambiguous. In the current implementation, the local crack front axes are determined from the coordinates of the nodes that are shared by the crack-front elements on either side of the evaluation location. This is illustrated in Figure 13.

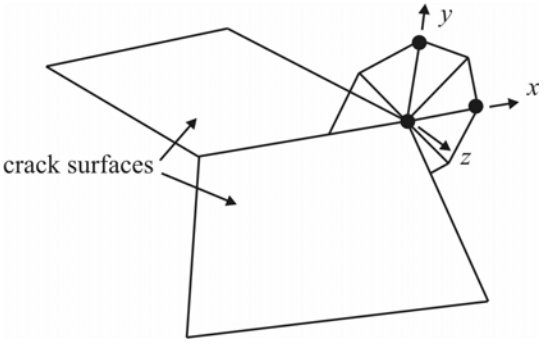

Figure 13. The definition of the local crack-front coordinates for case $q^{(1)}$, based on specified nodal coordinates

4.2.3 Transform nodal coordinates, displacements, and material matrices

The *M*-integral implementation requires that all input nodal coordinates, finite element displacements, and the material stiffness and compliance matrices be rotated to the local crack-front coordinate system. Furthermore, it requires that the nodal coordinates be translated so that the *M*-evaluation point is at the local coordinate origin.

If the components of the normalized crack-front axes specified in the model Cartesian coordinate system are given by *x*', *y*', and *z*', then the 3x3 matrix that will transform nodal coordinates and displacements in the Cartesian system into the crack-front system is given by

$$[t'] = \begin{bmatrix} x'_x & y'_x & z'_x \\ x'_y & y'_y & z'_y \\ x'_z & y'_y & z'_z \end{bmatrix}. \tag{40}$$

The corresponding transformations are

$$\{x^*\} = [t']\{x - x_{origin}\} \quad \text{and} \quad \{u^*\} = [t']\{u\}. \tag{41}$$

The material rotation matrices are similar to those given in eqs. 37 and 38, but use components of the t' matrix. The corresponding transformations are

$$[C] = [R'_c][\overline{C}][R'_c]^T \quad \text{and} \quad [S] = [R'_s][\overline{S}][R'_s]^T. \tag{42}$$

4.2.4 Determine the nature of the isotropy/anisotropy

Components of the compliance matrix are examined to determine if the material is 1) isotropic, 2) the local *z* = 0 plane is a plane of material symmetry, or 3) the material is generally anisotropic.

For the isotropic and *z* = 0 symmetry cases, the compliance matrix will have distinct patterns of zero and non-zero entries. *z* = 0 symmetry will have the pattern

$$[S] = \begin{bmatrix} * & * & * & * & 0 & 0 \\ * & * & * & * & 0 & 0 \\ * & * & * & * & 0 & 0 \\ * & * & * & * & 0 & 0 \\ 0 & 0 & 0 & 0 & * & * \\ 0 & 0 & 0 & 0 & * & * \end{bmatrix}. \tag{43}$$

The first check is to see if any of the upper right 6 entries of the compliance matrix are non-zero. If so, the material is assumed to be generally anisotropic.

An isotropic material has the pattern

$$[S]=\begin{bmatrix} * & * & * & 0 & 0 & 0 \\ * & * & * & 0 & 0 & 0 \\ * & * & * & 0 & 0 & 0 \\ 0 & 0 & 0 & * & 0 & 0 \\ 0 & 0 & 0 & 0 & * & 0 \\ 0 & 0 & 0 & 0 & 0 & * \end{bmatrix}. \qquad (44)$$

The second check is to see if the 14, 24, 34, or 56 elements are zero. If so, and the following conditions hold

$$S_{11} = S_{22} = S_{33}, \quad S_{12} = S_{13} = S_{23}, \quad S_{44} = S_{55} = S_{66}, \quad \text{and} \quad S_{44} = S_{11}/2(1-S_{12}/S_{11}) \qquad (45)$$

the material is assumed to be isotropic. Otherwise, $z = 0$ symmetry is assumed.

4.2.5 Compute anisotropic parameters

If the material has been determined to be $z = 0$ symmetric, then the μ's are determined by finding the roots to eqs. 13 and 14.

If the material has been determined to be generally anisotropic, then the μ's, λ's, m's, and N^{-1} are determined from eqs. 4 through 9.

4.2.6 Compute the auxiliary nodal displacements

For all elements in the domain of integration, we determine the nodal displacements associated with the three auxiliary solutions, $u^{(2a)}$, $u^{(2b)}$, $u^{(2c)}$. The generalized plane strain expressions for these values are given by eqs. 2 and 12 for the general anisotropy case and the $z = 0$ symmetry case, respectively. For isotropic materials in plane strain, the expression is

$$\begin{Bmatrix} u_x \\ u_y \\ u_z \end{Bmatrix} = \frac{1}{G}\sqrt{\frac{r}{2\pi}} \begin{bmatrix} \cos\frac{\theta}{2}\left(1-2\nu+\sin^2\frac{\theta}{2}\right) & \sin\frac{\theta}{2}\left(2-2\nu+\cos^2\frac{\theta}{2}\right) & 0 \\ \sin\frac{\theta}{2}\left(2-2\nu-\cos^2\frac{\theta}{2}\right) & \cos\frac{\theta}{2}\left(-1+2\nu+\sin^2\frac{\theta}{2}\right) & 0 \\ 0 & 0 & 2\sin\frac{\theta}{2} \end{bmatrix} \begin{Bmatrix} K_I \\ K_{II} \\ K_{III} \end{Bmatrix}. \qquad (46)$$

These expressions give the displacements as a function of the in-plane coordinates r and θ. A general approach for determining these must account for curved crack fronts where the "ends" of the element may not be perpendicular to the crack front. The technique for doing this in the

current implementation is illustrated in Figure 14. The evaluation point x has element parametric coordinates ξ, η, and ζ. The associated point on the crack plane, x', is determined from the parametric coordinates ξ and η in the quadrilateral region that is the intersection of the evaluation ring with the crack plane. The associated point on the crack front, x'', is determined from the parametric coordinate ξ and the associated crack-front segment. r is the magnitude of the vector from x'' to x, and θ is the angle between this vector and the vector from x'' to x'.

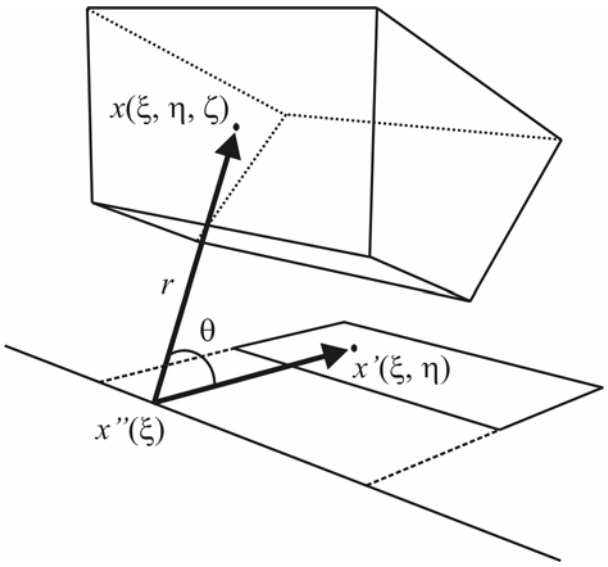

Figure 14. A schematic of how the coordinates r and θ are determined.

4.2.7 Compute displacement derivatives

For each integration point within an element, we compute $\frac{\partial u^{(1)}}{\partial x}$, $\frac{\partial u^{(2a)}}{\partial x}$, $\frac{\partial u^{(2b)}}{\partial x}$, and $\frac{\partial u^{(2c)}}{\partial x}$. This is done using standard finite element interpolation. The expression for the displacement derivatives is

$$\left[\partial u/\partial x\right] = \left[J\right]^{-1}\left[\partial N/\partial \xi\right]\{u\} \tag{47}$$

where J is the Jacobian matrix and N represents the element shape functions. The Jacobian is computed from the product of the shape function derivatives with respect to the parametric coordinates and the element's nodal coordinates:

$$\left[J\right] = \left[\partial N/\partial \xi\right]\{x\}. \tag{48}$$

4.2.8 Compute local stresses

For each integration point, we compute the local element stresses. For the finite element stresses, $\sigma^{(1)}$, the expression is

$$\begin{Bmatrix} \sigma_x \\ \sigma_y \\ \sigma_z \\ \sigma_{xy} \\ \sigma_{yz} \\ \sigma_{zx} \end{Bmatrix} = [C] \begin{Bmatrix} \partial u_x/\partial x \\ \partial u_y/\partial y \\ \partial u_z/\partial z \\ \partial u_x/\partial y + \partial u_y/\partial x \\ \partial u_y/\partial z + \partial u_z/\partial y \\ \partial u_z/\partial x + \partial u_x/\partial z \end{Bmatrix}. \tag{49}$$

For the auxiliary solutions ($\sigma^{(2a)}$, $\sigma^{(2b)}$, and $\sigma^{(2c)}$), stresses are given by eqn. 1 for the general anisotropy case, eqn. 11 for $z = 0$ symmetry, and for the case of isotropy by

$$\begin{Bmatrix} \sigma_x \\ \sigma_y \\ \sigma_{xy} \\ \sigma_{yz} \\ \sigma_{zx} \end{Bmatrix} = \frac{1}{\sqrt{2\pi r}} \begin{bmatrix} \cos\frac{\theta}{2}\left(1-\sin\frac{\theta}{2}\sin\frac{3\theta}{2}\right) & -\sin\frac{\theta}{2}\left(2+\cos\frac{\theta}{2}\cos\frac{3\theta}{2}\right) & 0 \\ \cos\frac{\theta}{2}\left(1+\sin\frac{\theta}{2}\sin\frac{3\theta}{3}\right) & \sin\frac{\theta}{2}\cos\frac{\theta}{2}\cos\frac{3\theta}{2} & 0 \\ \sin\frac{\theta}{2}\cos\frac{\theta}{2}\cos\frac{3\theta}{2} & \cos\frac{\theta}{2}\left(1-\sin\frac{\theta}{2}\sin\frac{3\theta}{2}\right) & 0 \\ 0 & 0 & \cos\frac{\theta}{2} \\ 0 & 0 & -\sin\frac{\theta}{2} \end{bmatrix} \begin{Bmatrix} K_I \\ K_{II} \\ K_{III} \end{Bmatrix}. \tag{50}$$

For all cases, σ_z comes from the plane strain condition

$$\sigma_z = \left(S_{31}\sigma_x + S_{32}\sigma_y + S_{34}\sigma_{xy} + S_{35}\sigma_{yz} + S_{36}\sigma_{zx}\right)/S_{33}\,. \tag{51}$$

4.2.9 Compute the contribution to the M-integral

The *M*-integral is evaluated numerically using Gauss integration. It has contributions from all Gauss points for all elements in the integration domain. The expressions for the numerical integration is

$$\begin{aligned} M^{(1,2a)} &= \sum_{elem=1}^{\#elem}\sum_{gp=1}^{\#gp} w_{gp}\left|J_{gp}\right|\left(\sigma_{ij}^{(1)}\frac{\partial u_i^{(2a)}}{\partial x_1} + \sigma_{ij}^{(2a)}\frac{\partial u_i^{(1)}}{\partial x_1} - W^{(1,2a)}\delta_{1j}\right)\frac{\partial q}{\partial x_j} \\ M^{(1,2b)} &= \sum_{elem=1}^{\#elem}\sum_{gp=1}^{\#gp} w_{gp}\left|J_{gp}\right|\left(\sigma_{ij}^{(1)}\frac{\partial u_i^{(2b)}}{\partial x_1} + \sigma_{ij}^{(2b)}\frac{\partial u_i^{(1)}}{\partial x_1} - W^{(1,2b)}\delta_{1j}\right)\frac{\partial q}{\partial x_j} \\ M^{(1,2c)} &= \sum_{elem=1}^{\#elem}\sum_{gp=1}^{\#gp} w_{gp}\left|J_{gp}\right|\left(\sigma_{ij}^{(1)}\frac{\partial u_i^{(2c)}}{\partial x_1} + \sigma_{ij}^{(2c)}\frac{\partial u_i^{(1)}}{\partial x_1} - W^{(1,2c)}\delta_{1j}\right)\frac{\partial q}{\partial x_j} \end{aligned} \tag{52}$$

where w_{gp} is the Gauss integration weight and $|J_{gp}|$ is the determinate of the Jacobian matrix evaluated at the integration point. Summation convention is assumed with $i = 1, 2, 3$ and $j = 1, 2, 3$.

The current implementation uses 27 integration points for brick elements and 28 integration points for wedge (crack-front) elements.

4.2.10 Compute the area of the virtual extension

A_q is the area of the virtual extension along the crack front. For cases $q^{(2)}$, $q^{(3)}$, and $q^{(4)}$ only one crack-front segment participates in the integration. If this is denoted l, and, noting that the virtual extension at the evaluation point is 1,

$$A_q^{(2)} = A_q^{(3)} = \tfrac{1}{2} l \quad \text{and} \quad A_q^{(4)} = \tfrac{2}{3} l \tag{53}$$

For case $q^{(1)}$, two crack-front segments participate in the integration. If these are denoted l_1 and l_2, then

$$A_q^{(1)} = \tfrac{1}{2}\left(l_1 + l_2\right). \tag{54}$$

4.2.11 Compute the stress intensity factors

Finally, the stress intensity factors are computed. Eqn. 31 is used for general anisotropy, eqn 33 for $z = 0$ symmetry, and for isotropy, the expression is

$$\begin{bmatrix} \dfrac{2\left(1-\nu^2\right)}{E} & 0 & 0 \\ 0 & \dfrac{2\left(1-\nu^2\right)}{E} & 0 \\ 0 & 0 & \dfrac{2\left(1+\nu\right)}{E} \end{bmatrix} \begin{Bmatrix} K_I \\ K_{II} \\ K_{III} \end{Bmatrix} = \begin{Bmatrix} M^{(1,2a)} / A_q \\ M^{(1,2b)} / A_q \\ M^{(1,2c)} / A_q \end{Bmatrix}. \tag{55}$$

5. PRESCRIBED DISPLACEMENT TESTS

An initial series of tests were performed to verify the implementation. In these tests, no finite element analysis was performed. Rather, nodal displacements for all elements participating in the *M*-integral evaluation were determined from eqs. 2, 12, and 46, assuming unit stress intensity values. The *M*-integral is evaluated, and the computed stress intensity values are compared to the prescribed values.

The purpose of these tests is two-fold. First, as verification; if the *M*-integral evaluation is encoded correctly, then the computed stress intensity factor should be close to the prescribed value. Second, the absolute difference between the prescribed and computed values give a quantitative assessment of the "intrinsic" error in the computations and an indication of the relative performance of differing q functions and numbers of element rings. By intrinsic error, we mean those errors that arise due to the approximate numerical techniques used to evaluate the integrals.

Table 1 shows the computed stress intensity factors for isotropy, $z = 0$ symmetry, and general anisotropy. For each, all three fracture modes are examined for both 1 and 2 element rings around the crack front for four different q functions.

Of all the tests, the largest error was 4.7%. This was for general anisotropy, mode I, one ring of elements, and $q^{(4)}$. In general, all the $q^{(4)}$ tests with one ring of elements performed poorly. If these are discounted, then the largest error for the one-ring tests was 0.89%. Among the two-ring tests the largest error was 0.46%.

Based on these tests, the following conclusions are drawn:

1. All combinations of element rings and q functions produce accurate results with the exception of $q^{(4)}$ with one ring of elements. This configuration should be avoided.

2. In general the two-ring configurations are slightly more accurate than the one-ring configurations, but the difference is not significant.

6. THICK PLATE ANALYSES

A series of finite element analyses were performed to verify the performance of the *M*-integral calculations. The models were essentially very thick center-cracked plates. The objective was to make the plates thick enough that plane-strain conditions would be approximated near the center of the plate.

The geometry of the model is shown in Figure 15. The plate is simply supported as shown in Figure 16a. Two load cases, mode I (Figure 16b) and mode II (Figure 16c) were analyzed. All length and force units are normalized with respect to those used for the material properties.

Table 1. Computed stress intensity factors for prescribed nodal displacements.

		prescribed K_I			prescribed K_{II}			prescribed K_{III}		
rings	$q^{(n)}$	K_I	K_{II}	K_{III}	K_I	K_{II}	K_{III}	K_I	K_{II}	K_{III}
Isotropic										
1	1	1.0089	0.0	0.0	0.0	1.0062	0.0	0.0	0.0	1.0070
	2	1.0089	0.0	0.0	0.0	1.0062	0.0	0.0	0.0	1.0070
	3	1.0089	0.0	0.0	0.0	1.0062	0.0	0.0	0.0	1.0070
	4	0.9591	0.0	0.0	0.0	0.9647	0.0	0.0	0.0	0.9562
2	1	0.9984	0.0	0.0	0.0	0.9987	0.0	0.0	0.0	0.9992
	2	0.9984	0.0	0.0	0.0	0.9987	0.0	0.0	0.0	0.9992
	3	0.9984	0.0	0.0	0.0	0.9987	0.0	0.0	0.0	0.9992
	4	0.9984	0.0	0.0	0.0	0.9987	0.0	0.0	0.0	0.9992
Z symmetry										
1	1	1.0080	0.0	0.0	0.0	1.0065	0.0	0.0	0.0	1.0069
	2	1.0080	0.0	0.0	0.0	1.0065	0.0	0.0	0.0	1.0069
	3	1.0080	0.0	0.0	0.0	1.0065	0.0	0.0	0.0	1.0069
	4	0.9534	0.0	0.0	0.0	0.9624	0.0	0.0	0.0	0.9543
2	1	1.0034	0.0	0.0	0.0	1.0009	0.0	0.0	0.0	1.0001
	2	1.0034	0.0	0.0	0.0	1.0009	0.0	0.0	0.0	1.0001
	3	1.0034	0.0	0.0	0.0	1.0009	0.0	0.0	0.0	1.0001
	4	1.0034	0.0	0.0	0.0	1.0009	0.0	0.0	0.0	1.0001
general anisotropy										
1	1	1.0078	0.0	-0.0007	0.0	1.0064	0.0	-0.0013	0.0	1.0073
	2	1.0078	0.0	-0.0007	0.0	1.0064	0.0	-0.0013	0.0	1.0073
	3	1.0078	0.0	-0.0007	0.0	1.0064	0.0	-0.0013	0.0	1.0073
	4	0.9529	0.0	-0.0024	0.0	0.9702	0.0	-0.0062	0.0	0.9591
2	1	1.0046	0.0	0.0018	0.0	0.9968	0.0	0.0045	0.0	0.9980
	2	1.0046	0.0	0.0018	0.0	0.9968	0.0	0.0045	0.0	0.9980
	3	1.0046	0.0	0.0018	0.0	0.9968	0.0	0.0045	0.0	0.9980
	4	1.0046	0.0	0.0018	0.0	0.9968	0.0	0.0045	0.0	0.9980

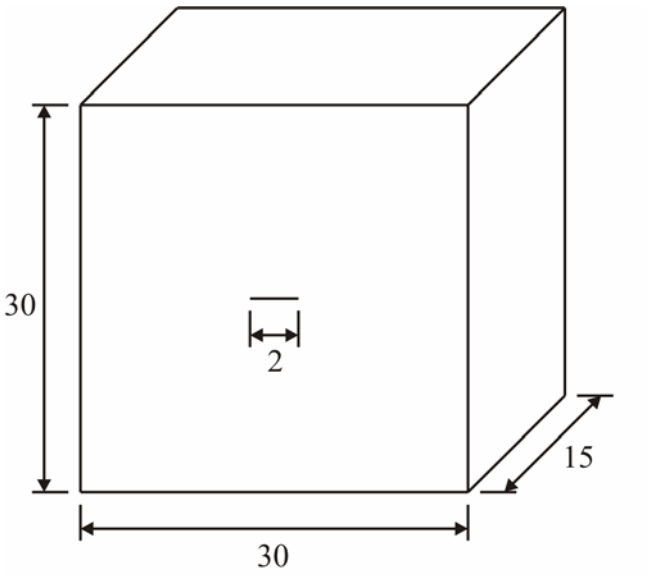

Figure 15. The geometry used for the thick plate analysis.

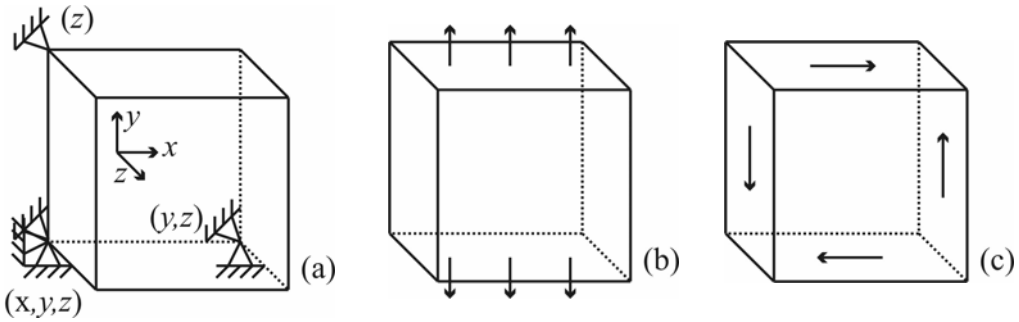

Figure 16. The simply supported boundary conditions (a), and the mode I (b) and II (c) load cases used in the analyses.

Three sets of material properties were investigated

Isotropic:

$E = 1000.0, \quad \nu = 0.25$

Cubic material oriented with z = 0 symmetry:

$E_1 = E_2 = E_3 = G_{12} = G_{23} = G_{13} = 1000.0$

$\nu_{12} = \nu_{23} = \nu_{13} = 0.25$

$\theta_z = 45.0°, \quad \theta_x = \theta_y = 0.0°$

Cubic material oriented with a general orientation:

$E_1 = E_2 = E_3 = G_{12} = G_{23} = G_{13} = 1000.0$

$\nu_{12} = \nu_{23} = \nu_{13} = 0.25$

$\theta_z = \theta_x = \theta_y = 45.0°$

The model and meshes were generated with FRANC3D. The finite element analysis was performed with ANSYS. The resulting nodal displacements were read back into FRANC3D where the *M*-integrals were evaluated to determine the stress intensity factors.

The same mesh was used for all analyses; it is shown in Figure 17, with a detail of the crack region shown in Figure 18. The mesh is predominantly 10-noded tetrahedral elements. 15-noded quarter point wedge elements are used around the crack front. One ring of 20-noded brick elements is used around the crack-front elements. 13-noded pyramid elements are used to transition from the brick elements to the tetrahedral elements in the bulk of the mesh.

Because of the simple loading and the simple supports, the well-known *K* solution for a center-cracked plate is valid for all three material behaviors. The relative errors between the theoretical solution and the numerical solutions are shown graphically in Figure 19. It is expected that there will be a relatively large error near the surfaces of the plate where plane strain conditions are not satisfied. It can be seen that near the center of the plate the M-integral solutions are very accurate.

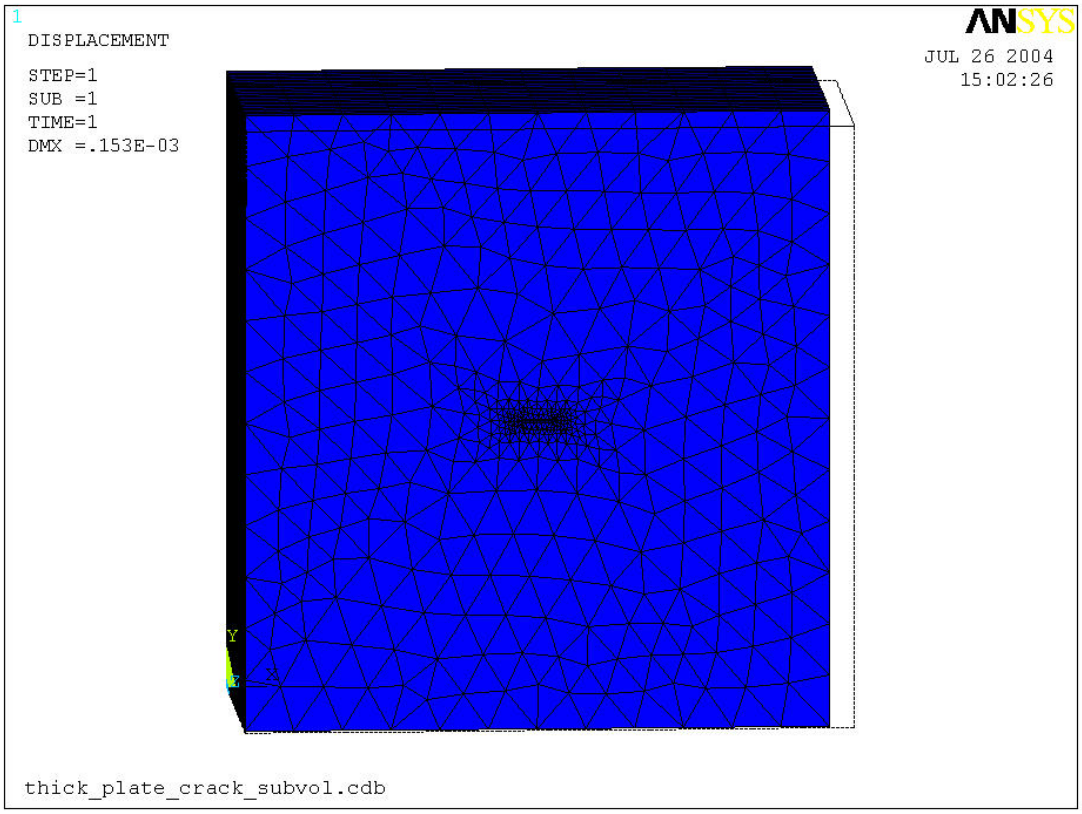

Figure 17. The mesh used for the thick plate verification analyses.

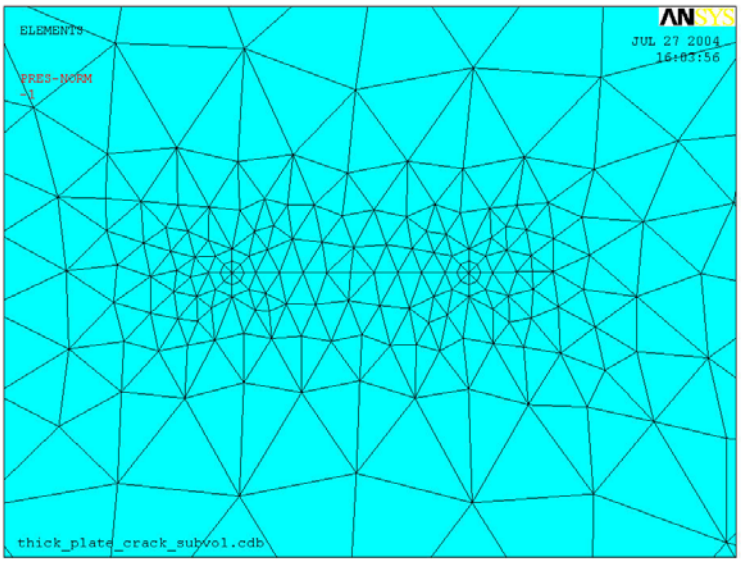

Figure 18. A detail of the thick plate mesh showing the crack region.

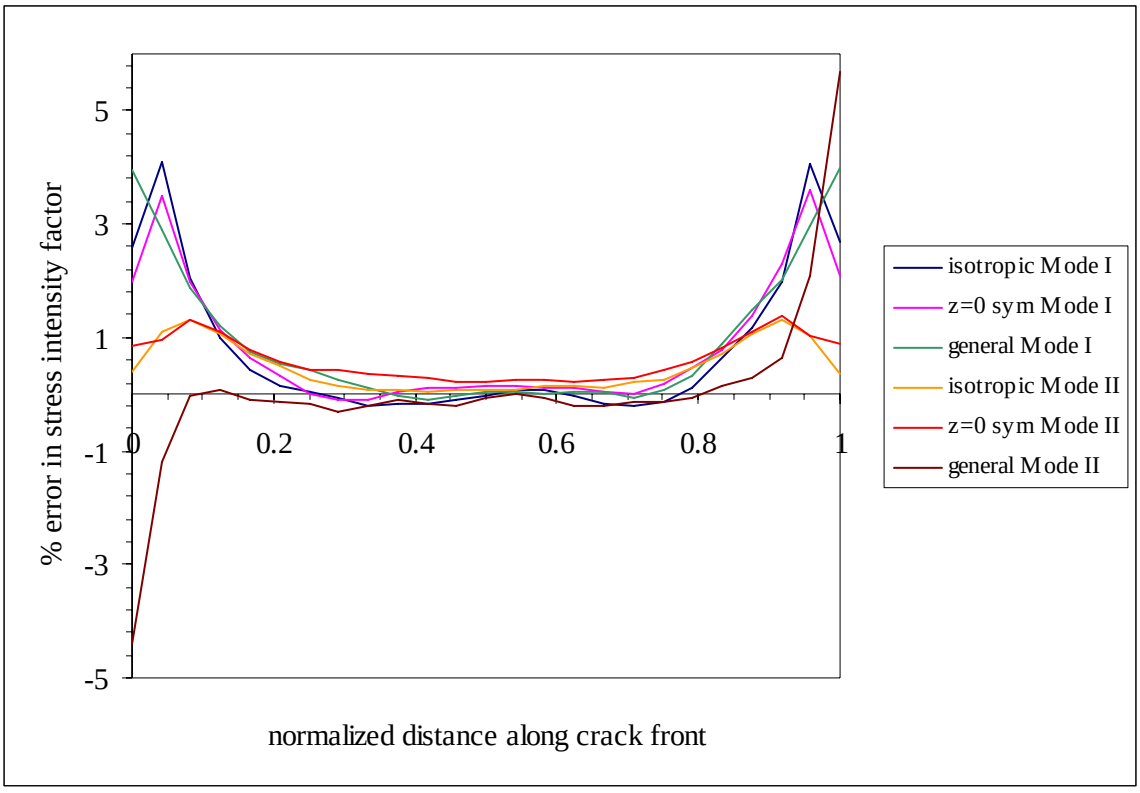

Figure 19. The relative errors between the theoretical and numerical solutions for the stress intensity factors for a thick center-cracked plate.

7. BRAZILIAN DISK ANALYSIS

A large number of analyses were performed to determine a stress intensity solution for a Brazilian disk test specimen. The specimen geometry is shown in Figure 20. The material properties considered are those for a typical single crystal nickel alloy used in an engine hot section. An isotropic material was considered as well. In testing, it is observed that the two ends of the crack do not usually grow at the same rate, therefore, a range of a_1 and a_2 lengths are considered.

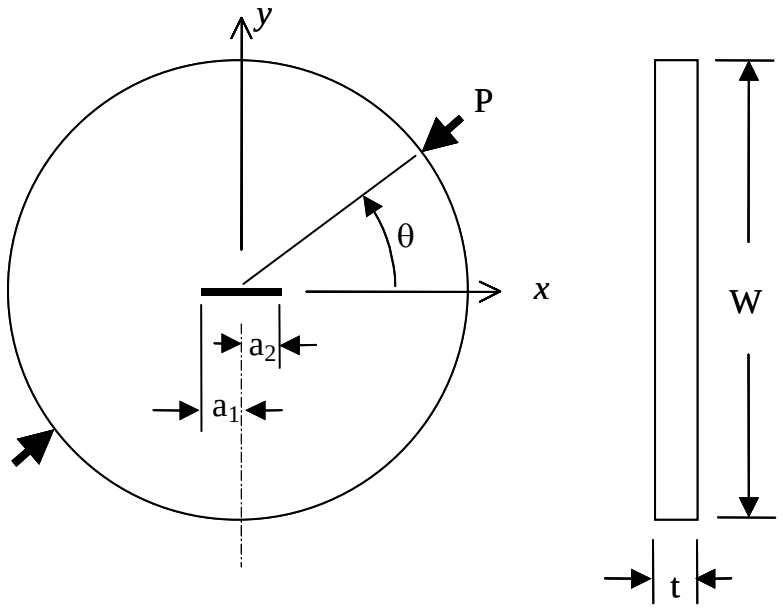

Figure 20. The geometry of the Brazilian disk test specimen.

The single crystal material has cubic symmetry. This means that $E = E_{001} = E_{010} = E_{100}$, $\nu = \nu_{001/010} = \nu_{001/100} = \nu_{010/100}$, and $G = G_{001/010} = G_{001/100} = G_{010/100}$. The properties used here are $E/G = 0.952$ and $\nu = 0.4$. The properties used for the isotropic material are $E/G = 2.8$ and $\nu = 0.4$.

Two different material orientations were considered for the anisotropic material, <111/1$\underline{1}$0> and <111/11$\underline{2}$> where <*y/x*> defines the orientation of the local crack front axes relative to the material axes. These orientations are shown graphically in Figure 21, where the red axes indicate the local crack front-axes. The corresponding Euler angles are $\theta_z = 50.7685$, $\theta_x = -24.0948$, and $\theta_y = 26.5650$, for the <111/1$\underline{1}$0> case, and $\theta_z = -35.2644$, $\theta_x = -45.0$, and $\theta_y = -90.0$, for the <111/11$\underline{2}$> case.

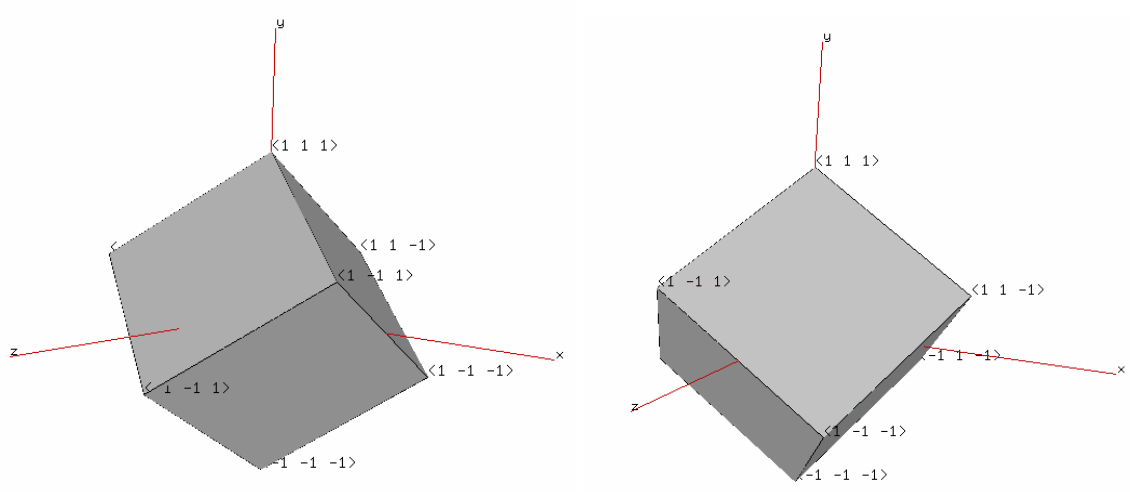

Figure 21. A graphical illustration of the cubic material orientation relative to the local crack-front axes.

Twenty-eight crack configurations were considered. These are shown in Table 2. Eleven load orientations, θs, were considered. The isotropic and <111/11$\underline{2}$> material configurations give symmetric results for negative and positive θ angles. For these cases, 0°, 4°, 8°, 12°, 16° and 20° were analyzed. For the <111/11$\underline{2}$> material orientation, –4°, –8°, –12°, –16°, and –20° were analyzed in addition to the positive angles.

Table 2. Analyzed crack configuration.

$2a_1/W$	$2a_2/W$
0.2	0.2, 0.3, 0.4, 0.5, 0.6, 0.7, 0.8
0.3	0.3, 0.4, 0.5, 0.6, 0.7, 0.8
0.4	0.4, 0.5, 0.6, 0.7, 0.8
0.5	0.5, 0.6, 0.7, 0.8
0.6	0.6, 0.7, 0.8
0.7	0.7, 0.8
0.8	0.8

A typical mesh used in these analyses is shown in Figure 22 (with greatly magnified displacements). The meshes were two elements thick and periodic boundary conditions were applied to the front and back surfaces to enforce plane strain behavior. The meshes were predominantly 15-noded wedge elements, with quarter-point wedge elements used at the crack fronts and 20-noded brick elements used in the first ring of elements surrounding the crack-front elements. The M-integral was evaluated using $q^{(1)}$.

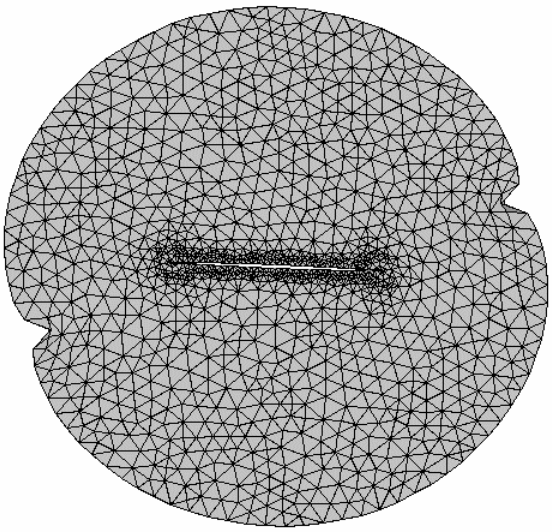

Figure 22. A typical mesh used in the disk analyses (with greatly magnified displacements).

Typical analysis results for are shown graphically in Figure 23. Complete analysis results are given in graphical and tabular form in the appendices.

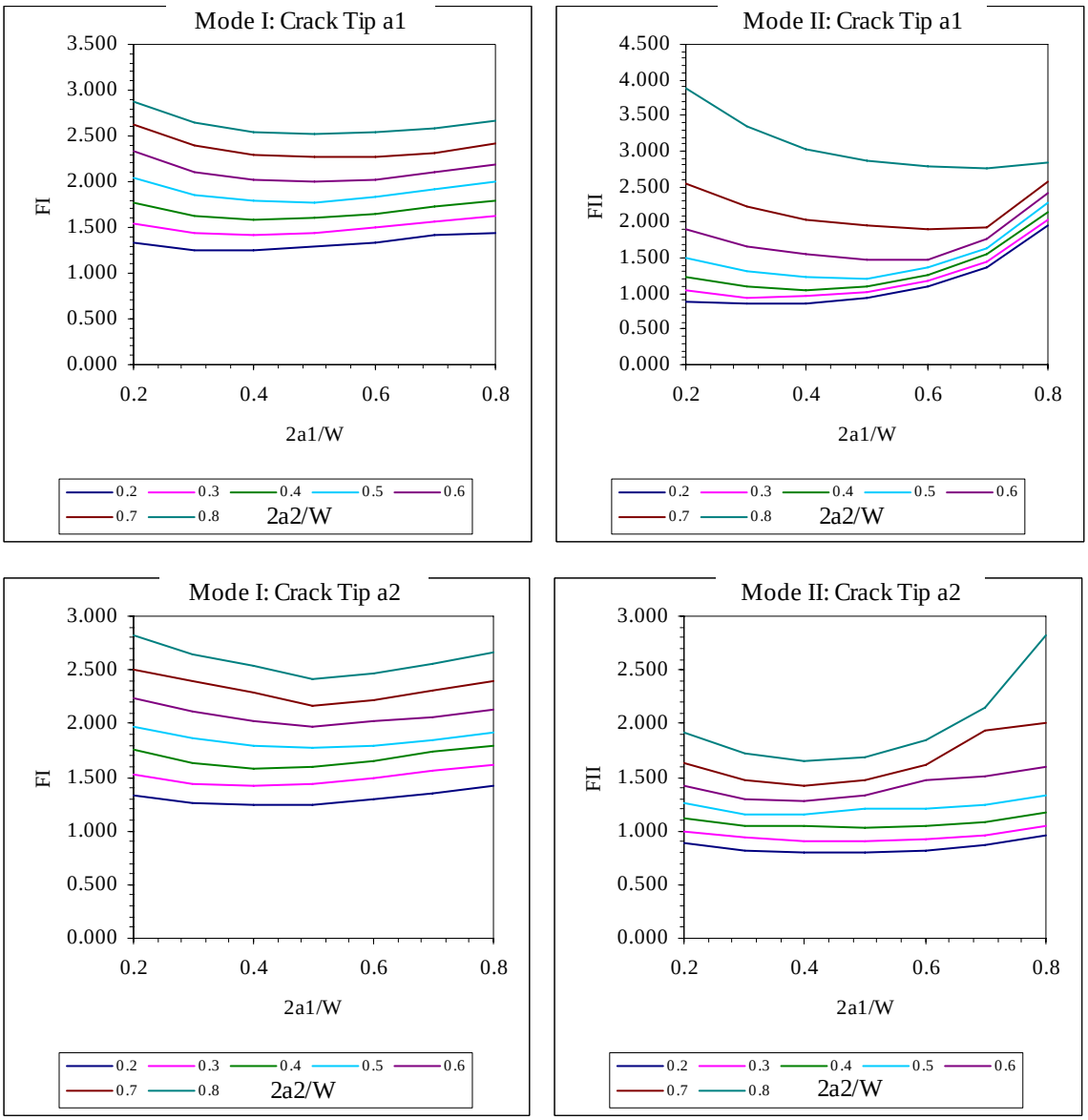

Figure 23. Typical Brazilian disk analysis results, where

$$F_n = \frac{K_n \pi W t}{P\sqrt{2\pi(a_1 + a_2)}}, \text{ with } n = \text{I, II.}$$

8. SUMMARY

This report describes the successful effort to develop and verify a numerical technique for extracting stress intensity factors from finite element results for anisotropic materials. The report can be summarized as follows:

- Expressions for the stress and displacement fields near a crack front in anisotropic material are presented.

- The expressions for the *M*-integral that can be used to determine the mode-wise stress intensity factors in such materials are developed.

- The details of an implementation of the anisotropic *M*-integral are presented.

- The M-integral is shown to give consistent and accurate results for test cases where nodal displacements are prescribed to be the theoretical near crack-front values.

- The M-integral is shown to give accurate results for a simple model with a known stress intensity factor solution.

- The new capability is used to develop the *K*-solution for crack growth in an anisotropic Brazilian disk specimen.

REFERENCES

Atluri S.N., Kobayashi A.S., Nakagaki M., "A finite-element program for fracture mechanics analysis of composite material." In: Sendeckyj G.P., editor. *Fracture Mechanics of Composites, ASTM-STP 593*. American Society for Testing and Materials, 1975. p.~86-98.

Banks-Sill, L. and Sherman, D., "On quarter-point three-dimensional finite elements in linear elastic fracture mechanics," *Int J Fracture* 1989; 41:177-196.

Banks-Sill, L. and Sherman, D., "On the computation of stress intensity factors for three-dimensional geometries by means of the stiffness derivative and J-integral methods," *Int J Fracture* 1992; 53:1-20.

Boone T.J., Wawrzynek P.A., and Ingraffea A.R., "Finite element modeling of fracture propagation in orthotropic materials," *Engng Fract Mech.* 1987; 26:185-201.

Hoenig A., "Near-tip behavior of a crack in a plane anisotropic elastic body," *Engng Fract Mech*. 1982; 16(3):393-403.

Lekhnitskii S.G., *Theory of Elasticity of an Anisotropic Body*. San Francisco: Holden-Day, 1950, in Russian, 1963, in English, translated by Fern P.

Rice J.R., "A path independent integral and the approximate analysis of strain concentration by notches and cracks," *J Appl Mech.* 1968; 35:379-386.

Sih G.C. Paris P.C. Irwin G.R., "On cracks in rectilinearly anisotropic bodies," *Int J Fract Mech.* 1965; 1:189--302.

Tohgo K., Wang A.S.D., and Chou T., "A criterion for splitting crack initiation in unidirectional fiber-reinforced composites," *J Compos Ma*. 1993; 27:1054-1076.

Yau J.F., Wang S.S., Corten H.T., "A mixed-mode crack analysis of isotropic solids using conservation laws of elasticity," *J Appl Mech.* 1980; 47:335-341.

APPENDIX A: BRAZILIAN DISK ANALYSIS RESULTS

This appendix contains stress intensity factor results for the Brazilian disk specimens.

Analyses were performed for a cubic material with properties E/G = 0.952 and ν = 0.4 and for an isotropic material with properties E/G = 2.8 and ν = 0.4. Two material orientations relative to the crack-font were considered for the cubic material, <111/1$\underline{1}$0> and <111/11$\underline{2}$> where <*y/x*> defines the orientation of the local crack front axes relative to the material axes.

For the isotropic material and the cubic material in the <111/1$\underline{1}$0> orientation, θ angles of 0°, 4°, 8°, 12°, 16° and 20° were analyzed. Due to material symmetries, these results are symmetric about θ = 0°. The cubic material in the <111/11$\underline{2}$> orientation is not symmetric about θ = 0°. For that case, –4°, –8°, –12°, –16°, and –20° were analyzed in addition to the positive angles.

A total of 644 analyses were performed.

The first part of this appendix contains the stress intensity factor values in tabular form. Each page contains the data for one load orientation for one material type/orientation.

The second part of this appendix contains plots of normalized stress intensity factors for Modes I and II. The normalized stress intensity factors are defined as

$$F_n = \frac{K_n \pi W t}{P\sqrt{2\pi(a_1 + a_2)}} \quad \text{where } n = \text{I, II.}$$

<111/11$\underline{2}$0>, $\theta = 20°$

Mode I:

2a1/W		2a2/W 0.2	0.3	0.4	0.5	0.6	0.7	0.8
0.2	tip 1	0.128	0.127	0.107	0.058	-0.035	-0.200	-0.495
	tip 2	0.128	0.147	0.163	0.174	0.175	0.163	0.124
0.3	tip 1		0.147	0.127	0.078	-0.015	-0.182	-0.480
	tip 2		0.147	0.163	0.176	0.180	0.170	0.135
0.4	tip 1			0.145	0.097	0.003	-0.164	-0.466
	tip 2			0.145	0.158	0.164	0.156	0.125
0.5	tip 1				0.111	0.018	-0.151	-0.455
	tip 2				0.111	0.118	0.112	0.083
0.6	tip 1					0.025	-0.144	-0.452
	tip 2					0.025	0.020	-0.007
0.7	tip 1						-0.150	-0.460
	tip 2						-0.150	-0.177
0.8	tip 1							-0.488
	tip 2							-0.488

Mode II:

2a1/W		2a2/W 0.2	0.3	0.4	0.5	0.6	0.7	0.8
0.2	tip 1	-0.520	-0.612	-0.717	-0.834	-0.967	-1.108	-1.256
	tip 2	-0.519	-0.593	-0.669	-0.749	-0.837	-0.936	-1.050
0.3	tip 1		-0.685	-0.790	-0.911	-1.050	-1.199	-1.361
	tip 2		-0.683	-0.759	-0.841	-0.932	-1.034	-1.153
0.4	tip 1			-0.868	-0.992	-1.138	-1.298	-1.475
	tip 2			-0.866	-0.951	-1.046	-1.153	-1.279
0.5	tip 1				-1.082	-1.235	-1.405	-1.600
	tip 2				-1.080	-1.180	-1.295	-1.430
0.6	tip 1					-1.344	-1.527	-1.743
	tip 2					-1.342	-1.467	-1.616
0.7	tip 1						-1.668	-1.908
	tip 2						-1.665	-1.834
0.8	tip 1							-2.108
	tip 2							-2.105

Mode III:

2a1/W		2a2/W 0.2	0.3	0.4	0.5	0.6	0.7	0.8
0.2	tip 1	-0.020	-0.031	-0.046	-0.065	-0.081	-0.083	-0.053
	tip 2	0.020	0.023	0.027	0.032	0.037	0.044	0.051
0.3	tip 1		-0.034	-0.049	-0.068	-0.084	-0.086	-0.056
	tip 2		0.034	0.037	0.042	0.047	0.053	0.060
0.4	tip 1			-0.053	-0.071	-0.088	-0.090	-0.061
	tip 2			0.053	0.057	0.062	0.068	0.075
0.5	tip 1				-0.076	-0.093	-0.095	-0.067
	tip 2				0.076	0.082	0.088	0.094
0.6	tip 1					-0.099	-0.103	-0.076
	tip 2					0.099	0.106	0.113
0.7	tip 1						-0.111	-0.086
	tip 2						0.111	0.120
0.8	tip 1							-0.097
	tip 2							0.097

<111/1$\underline{1}$0>, $\theta = 16°$

Mode I:

2a1/W		2a2/W 0.2	0.3	0.4	0.5	0.6	0.7	0.8
0.2	tip 1	0.186	0.199	0.196	0.168	0.098	-0.042	-0.312
	tip 2	0.186	0.214	0.241	0.263	0.279	0.284	0.264
0.3	tip 1		0.228	0.226	0.199	0.131	-0.009	-0.280
	tip 2		0.228	0.255	0.280	0.299	0.306	0.291
0.4	tip 1			0.255	0.230	0.162	0.023	-0.248
	tip 2			0.255	0.282	0.302	0.313	0.302
0.5	tip 1				0.258	0.192	0.054	-0.218
	tip 2				0.258	0.281	0.293	0.286
0.6	tip 1					0.216	0.079	-0.193
	tip 2					0.216	0.231	0.227
0.7	tip 1						0.095	-0.177
	tip 2						0.095	0.092
0.8	tip 1							-0.180
	tip 2							-0.179

Mode II:

2a1/W		2a2/W 0.2	0.3	0.4	0.5	0.6	0.7	0.8
0.2	tip 1	-0.448	-0.535	-0.640	-0.769	-0.928	-1.110	-1.312
	tip 2	-0.446	-0.511	-0.578	-0.650	-0.734	-0.831	-0.947
0.3	tip 1		-0.598	-0.704	-0.836	-1.001	-1.191	-1.407
	tip 2		-0.595	-0.663	-0.737	-0.822	-0.921	-1.041
0.4	tip 1			-0.773	-0.908	-1.079	-1.279	-1.510
	tip 2			-0.770	-0.847	-0.935	-1.039	-1.166
0.5	tip 1				-0.989	-1.167	-1.377	-1.625
	tip 2				-0.987	-1.080	-1.190	-1.325
0.6	tip 1					-1.268	-1.490	-1.758
	tip 2					-1.265	-1.385	-1.533
0.7	tip 1						-1.625	-1.918
	tip 2						-1.623	-1.790
0.8	tip 1							-2.115
	tip 2							-2.114

Mode III:

2a1/W		2a2/W 0.2	0.3	0.4	0.5	0.6	0.7	0.8
0.2	tip 1	0.010	0.003	-0.012	-0.034	-0.063	-0.088	-0.084
	tip 2	-0.010	-0.011	-0.011	-0.009	-0.006	0.000	0.007
0.3	tip 1		0.004	-0.010	-0.033	-0.062	-0.087	-0.083
	tip 2		-0.004	-0.004	-0.002	0.000	0.005	0.011
0.4	tip 1			-0.011	-0.033	-0.062	-0.087	-0.083
	tip 2			0.011	0.012	0.014	0.018	0.024
0.5	tip 1				-0.034	-0.063	-0.088	-0.084
	tip 2				0.034	0.037	0.040	0.046
0.6	tip 1					-0.066	-0.092	-0.089
	tip 2					0.066	0.071	0.076
0.7	tip 1						-0.097	-0.096
	tip 2						0.097	0.104
0.8	tip 1							-0.105
	tip 2							0.106

<111/1$\underline{1}$0>, $\theta = 12°$

Mode I:

2a1/W		2a2/W 0.2	0.3	0.4	0.5	0.6	0.7	0.8
0.2	tip 1	0.237	0.264	0.282	0.281	0.247	0.142	-0.098
	tip 2	0.237	0.274	0.310	0.345	0.376	0.399	0.403
0.3	tip 1		0.302	0.321	0.323	0.290	0.188	-0.050
	tip 2		0.302	0.340	0.377	0.410	0.437	0.446
0.4	tip 1			0.361	0.365	0.335	0.236	0.001
	tip 2			0.361	0.400	0.436	0.466	0.480
0.5	tip 1				0.406	0.379	0.284	0.052
	tip 2				0.406	0.446	0.479	0.496
0.6	tip 1					0.421	0.329	0.099
	tip 2					0.422	0.458	0.479
0.7	tip 1						0.367	0.140
	tip 2						0.367	0.391
0.8	tip 1							0.166
	tip 2							0.166

Mode II:

2a1/W		2a2/W 0.2	0.3	0.4	0.5	0.6	0.7	0.8
0.2	tip 1	-0.356	-0.431	-0.527	-0.656	-0.834	-1.067	-1.353
	tip 2	-0.354	-0.406	-0.460	-0.521	-0.594	-0.684	-0.800
0.3	tip 1		-0.481	-0.579	-0.710	-0.893	-1.134	-1.433
	tip 2		-0.478	-0.533	-0.595	-0.669	-0.760	-0.879
0.4	tip 1			-0.634	-0.768	-0.957	-1.206	-1.521
	tip 2			-0.631	-0.695	-0.772	-0.866	-0.990
0.5	tip 1				-0.836	-1.030	-1.289	-1.619
	tip 2				-0.833	-0.913	-1.014	-1.144
0.6	tip 1					-1.117	-1.387	-1.736
	tip 2					-1.114	-1.223	-1.365
0.7	tip 1						-1.509	-1.881
	tip 2						-1.507	-1.666
0.8	tip 1							-2.070
	tip 2							-2.067

Mode III:

2a1/W		2a2/W 0.2	0.3	0.4	0.5	0.6	0.7	0.8
0.2	tip 1	0.041	0.039	0.031	0.012	-0.021	-0.068	-0.108
	tip 2	-0.041	-0.046	-0.049	-0.052	-0.053	-0.050	-0.044
0.3	tip 1		0.043	0.035	0.017	-0.016	-0.063	-0.102
	tip 2		-0.043	-0.048	-0.050	-0.052	-0.051	-0.046
0.4	tip 1			0.039	0.021	-0.011	-0.058	-0.097
	tip 2			-0.039	-0.043	-0.044	-0.044	-0.040
0.5	tip 1				0.024	-0.008	-0.054	-0.093
	tip 2				-0.024	-0.026	-0.027	-0.023
0.6	tip 1					-0.006	-0.052	-0.092
	tip 2					0.006	0.006	0.009
0.7	tip 1						-0.052	-0.093
	tip 2						0.053	0.057
0.8	tip 1							-0.098
	tip 2							0.098

<111/1$\underline{1}$0>, $\theta = 8°$

Mode I:

2a1/W		2a2/W 0.2	0.3	0.4	0.5	0.6	0.7	0.8
0.2	tip 1	0.278	0.317	0.355	0.386	0.399	0.364	0.192
	tip 2	0.278	0.321	0.365	0.410	0.456	0.500	0.534
0.3	tip 1		0.362	0.401	0.435	0.453	0.423	0.257
	tip 2		0.362	0.408	0.455	0.504	0.551	0.590
0.4	tip 1			0.449	0.486	0.508	0.483	0.324
	tip 2			0.449	0.500	0.551	0.602	0.645
0.5	tip 1				0.540	0.566	0.546	0.394
	tip 2				0.540	0.595	0.649	0.697
0.6	tip 1					0.625	0.610	0.464
	tip 2					0.625	0.684	0.735
0.7	tip 1						0.672	0.533
	tip 2						0.674	0.730
0.8	tip 1							0.593
	tip 2							0.593

Mode II:

2a1/W		2a2/W 0.2	0.3	0.4	0.5	0.6	0.7	0.8
0.2	tip 1	-0.247	-0.302	-0.377	-0.484	-0.650	-0.910	-1.314
	tip 2	-0.245	-0.281	-0.320	-0.364	-0.419	-0.493	-0.598
0.3	tip 1		-0.337	-0.413	-0.522	-0.691	-0.958	-1.374
	tip 2		-0.335	-0.373	-0.418	-0.474	-0.548	-0.654
0.4	tip 1			-0.452	-0.563	-0.737	-1.011	-1.439
	tip 2			-0.449	-0.495	-0.552	-0.628	-0.738
0.5	tip 1				-0.612	-0.790	-1.071	-1.512
	tip 2				-0.608	-0.668	-0.749	-0.863
0.6	tip 1					-0.855	-1.145	-1.602
	tip 2					-0.851	-0.937	-1.061
0.7	tip 1						-1.242	-1.719
	tip 2						-1.237	-1.374
0.8	tip 1							-1.881
	tip 2							-1.880

Mode III:

2a1/W		2a2/W 0.2	0.3	0.4	0.5	0.6	0.7	0.8
0.2	tip 1	0.067	0.072	0.072	0.065	0.045	-0.002	-0.089
	tip 2	-0.067	-0.075	-0.082	-0.089	-0.095	-0.099	-0.098
0.3	tip 1		0.079	0.080	0.074	0.054	0.007	-0.079
	tip 2		-0.079	-0.087	-0.094	-0.101	-0.106	-0.106
0.4	tip 1			0.088	0.082	0.062	0.017	-0.068
	tip 2			-0.088	-0.096	-0.103	-0.109	-0.110
0.5	tip 1				0.090	0.071	0.027	-0.056
	tip 2				-0.090	-0.098	-0.104	-0.107
0.6	tip 1					0.080	0.035	-0.047
	tip 2					-0.080	-0.087	-0.090
0.7	tip 1						0.043	-0.040
	tip 2						-0.044	-0.047
0.8	tip 1							-0.036
	tip 2							0.037

<111/11$\underline{2}$0>, $\theta = 4°$

Mode I:

2a1/W		2a2/W 0.2	0.3	0.4	0.5	0.6	0.7	0.8
0.2	tip 1	0.304	0.352	0.404	0.460	0.522	0.583	0.595
	tip 2	0.304	0.351	0.401	0.453	0.510	0.573	0.642
0.3	tip 1		0.401	0.455	0.515	0.582	0.650	0.674
	tip 2		0.401	0.452	0.507	0.566	0.632	0.706
0.4	tip 1			0.509	0.573	0.645	0.720	0.754
	tip 2			0.509	0.567	0.629	0.699	0.776
0.5	tip 1				0.634	0.711	0.793	0.838
	tip 2				0.634	0.701	0.774	0.855
0.6	tip 1					0.783	0.871	0.927
	tip 2					0.783	0.861	0.947
0.7	tip 1						0.955	1.019
	tip 2						0.955	1.046
0.8	tip 1							1.118
	tip 2							1.120

Mode II:

2a1/W		2a2/W 0.2	0.3	0.4	0.5	0.6	0.7	0.8
0.2	tip 1	-0.127	-0.157	-0.198	-0.259	-0.362	-0.550	-0.956
	tip 2	-0.125	-0.144	-0.164	-0.187	-0.217	-0.260	-0.329
0.3	tip 1		-0.175	-0.216	-0.279	-0.383	-0.575	-0.989
	tip 2		-0.172	-0.192	-0.215	-0.246	-0.288	-0.358
0.4	tip 1			-0.236	-0.300	-0.407	-0.602	-1.025
	tip 2			-0.233	-0.257	-0.288	-0.331	-0.403
0.5	tip 1				-0.325	-0.435	-0.635	-1.065
	tip 2				-0.321	-0.353	-0.399	-0.473
0.6	tip 1					-0.470	-0.675	-1.113
	tip 2					-0.465	-0.514	-0.592
0.7	tip 1						-0.729	-1.179
	tip 2						-0.723	-0.810
0.8	tip 1							-1.283
	tip 2							-1.274

Mode III:

2a1/W		2a2/W 0.2	0.3	0.4	0.5	0.6	0.7	0.8
0.2	tip 1	0.084	0.094	0.103	0.110	0.113	0.103	0.048
	tip 2	-0.084	-0.095	-0.105	-0.115	-0.126	-0.137	-0.148
0.3	tip 1		0.104	0.114	0.121	0.125	0.116	0.064
	tip 2		-0.104	-0.115	-0.125	-0.137	-0.149	-0.161
0.4	tip 1			0.124	0.132	0.137	0.130	0.079
	tip 2			-0.124	-0.135	-0.147	-0.160	-0.172
0.5	tip 1				0.143	0.149	0.144	0.097
	tip 2				-0.143	-0.156	-0.170	-0.184
0.6	tip 1					0.163	0.159	0.113
	tip 2					-0.163	-0.177	-0.192
0.7	tip 1						0.176	0.133
	tip 2						-0.176	-0.193
0.8	tip 1							0.151
	tip 2							-0.153

<111/1$\underline{1}$0>, $\theta = 0°$

Mode I:

2a1/W		2a2/W 0.2	0.3	0.4	0.5	0.6	0.7	0.8
0.2	tip 1	0.312	0.364	0.421	0.488	0.570	0.681	0.852
	tip 2	0.312	0.362	0.413	0.468	0.529	0.600	0.688
0.3	tip 1		0.415	0.474	0.544	0.632	0.750	0.936
	tip 2		0.415	0.468	0.525	0.589	0.662	0.754
0.4	tip 1			0.530	0.604	0.698	0.824	1.022
	tip 2			0.530	0.590	0.657	0.734	0.829
0.5	tip 1				0.668	0.767	0.901	1.112
	tip 2				0.668	0.739	0.820	0.919
0.6	tip 1					0.844	0.986	1.208
	tip 2					0.844	0.930	1.033
0.7	tip 1						1.078	1.310
	tip 2						1.077	1.185
0.8	tip 1							1.425
	tip 2							1.426

Mode II:

2a1/W		2a2/W 0.2	0.3	0.4	0.5	0.6	0.7	0.8
0.2	tip 1	-0.001	-0.002	-0.002	-0.003	-0.004	-0.004	-0.012
	tip 2	0.001	0.000	0.000	0.000	-0.001	0.000	-0.001
0.3	tip 1		-0.002	-0.002	-0.003	-0.004	-0.004	-0.010
	tip 2		0.001	0.001	0.001	0.000	0.000	-0.001
0.4	tip 1			-0.002	-0.003	-0.003	-0.004	-0.010
	tip 2			0.001	0.001	0.001	0.001	0.000
0.5	tip 1				-0.002	-0.003	-0.004	-0.009
	tip 2				0.002	0.001	0.002	-0.001
0.6	tip 1					-0.004	-0.005	-0.012
	tip 2					0.001	0.001	0.001
0.7	tip 1						-0.005	-0.009
	tip 2						0.001	0.001
0.8	tip 1							-0.009
	tip 2							0.001

Mode III:

2a1/W		2a2/W 0.2	0.3	0.4	0.5	0.6	0.7	0.8
0.2	tip 1	0.090	0.103	0.115	0.128	0.143	0.162	0.193
	tip 2	-0.090	-0.102	-0.113	-0.125	-0.137	-0.152	-0.171
0.3	tip 1		0.113	0.126	0.139	0.156	0.177	0.211
	tip 2		-0.113	-0.125	-0.136	-0.150	-0.166	-0.185
0.4	tip 1			0.137	0.151	0.168	0.191	0.228
	tip 2			-0.137	-0.150	-0.163	-0.180	-0.200
0.5	tip 1				0.165	0.183	0.207	0.247
	tip 2				-0.165	-0.179	-0.196	-0.218
0.6	tip 1					0.199	0.225	0.268
	tip 2					-0.199	-0.216	-0.239
0.7	tip 1						0.247	0.293
	tip 2						-0.247	-0.271
0.8	tip 1							0.320
	tip 2							-0.320

<111/11$\underline{2}$>, $\theta = 20°$

Mode I:

2a1/W		2a2/W 0.2	0.3	0.4	0.5	0.6	0.7	0.8
0.2	tip 1	0.044	0.029	-0.007	-0.072	-0.180	-0.349	-0.610
	tip 2	0.044	0.050	0.053	0.048	0.035	0.006	-0.047
0.3	tip 1		0.035	-0.001	-0.068	-0.178	-0.352	-0.619
	tip 2		0.035	0.037	0.034	0.021	-0.007	-0.059
0.4	tip 1			0.001	-0.067	-0.180	-0.358	-0.633
	tip 2			0.001	-0.003	-0.017	-0.046	-0.098
0.5	tip 1				-0.072	-0.188	-0.371	-0.654
	tip 2				-0.072	-0.088	-0.117	-0.171
0.6	tip 1					-0.207	-0.394	-0.687
	tip 2					-0.207	-0.240	-0.297
0.7	tip 1						-0.433	-0.735
	tip 2						-0.434	-0.497
0.8	tip 1							-0.807
	tip 2							-0.807

Mode II:

2a1/W		2a2/W 0.2	0.3	0.4	0.5	0.6	0.7	0.8
0.2	tip 1	-0.548	-0.648	-0.759	-0.882	-1.014	-1.142	-1.260
	tip 2	-0.548	-0.628	-0.709	-0.795	-0.889	-0.993	-1.109
0.3	tip 1		-0.726	-0.839	-0.964	-1.102	-1.240	-1.373
	tip 2		-0.726	-0.808	-0.896	-0.992	-1.099	-1.221
0.4	tip 1			-0.923	-1.052	-1.197	-1.345	-1.495
	tip 2			-0.923	-1.014	-1.115	-1.227	-1.358
0.5	tip 1				-1.148	-1.301	-1.461	-1.629
	tip 2				-1.149	-1.255	-1.376	-1.517
0.6	tip 1					-1.418	-1.590	-1.781
	tip 2					-1.418	-1.550	-1.705
0.7	tip 1						-1.739	-1.956
	tip 2						-1.739	-1.916
0.8	tip 1							-2.166
	tip 2							-2.166

Mode III: all zero

<111/11$\underline{2}$>, $\theta = 16°$

Mode I:

2a1/W		2a2/W 0.2	0.3	0.4	0.5	0.6	0.7	0.8
0.2	tip 1	0.123	0.124	0.107	0.061	-0.031	-0.191	-0.460
	tip 2	0.123	0.142	0.157	0.168	0.171	0.160	0.125
0.3	tip 1		0.143	0.126	0.080	-0.012	-0.175	-0.449
	tip 2		0.143	0.160	0.171	0.175	0.166	0.133
0.4	tip 1			0.143	0.097	0.004	-0.161	-0.440
	tip 2			0.143	0.155	0.160	0.151	0.119
0.5	tip 1				0.109	0.015	-0.153	-0.436
	tip 2				0.109	0.113	0.104	0.072
0.6	tip 1					0.017	-0.154	-0.443
	tip 2					0.017	0.006	-0.028
0.7	tip 1						-0.169	-0.465
	tip 2						-0.169	-0.208
0.8	tip 1							-0.512
	tip 2							-0.511

Mode II:

2a1/W		2a2/W 0.2	0.3	0.4	0.5	0.6	0.7	0.8
0.2	tip 1	-0.453	-0.548	-0.664	-0.806	-0.976	-1.158	-1.339
	tip 2	-0.453	-0.520	-0.590	-0.668	-0.756	-0.858	-0.979
0.3	tip 1		-0.614	-0.731	-0.876	-1.051	-1.243	-1.439
	tip 2		-0.614	-0.684	-0.762	-0.852	-0.957	-1.082
0.4	tip 1			-0.804	-0.951	-1.134	-1.336	-1.548
	tip 2			-0.804	-0.885	-0.978	-1.086	-1.218
0.5	tip 1				-1.037	-1.226	-1.439	-1.669
	tip 2				-1.038	-1.136	-1.251	-1.392
0.6	tip 1					-1.333	-1.558	-1.810
	tip 2					-1.334	-1.459	-1.613
0.7	tip 1						-1.700	-1.978
	tip 2						-1.701	-1.875
0.8	tip 1							-2.185
	tip 2							-2.186

Mode III: all zero

<111/11$\underline{2}$>, $\theta = 12°$

Mode I:

2a1/W		2a2/W 0.2	0.3	0.4	0.5	0.6	0.7	0.8
0.2	tip 1	0.196	0.215	0.223	0.207	0.149	0.012	-0.261
	tip 2	0.196	0.226	0.255	0.282	0.304	0.314	0.303
0.3	tip 1		0.247	0.255	0.240	0.183	0.046	-0.228
	tip 2		0.247	0.277	0.305	0.329	0.341	0.333
0.4	tip 1			0.286	0.273	0.217	0.081	-0.195
	tip 2			0.286	0.316	0.341	0.355	0.349
0.5	tip 1				0.304	0.248	0.112	-0.164
	tip 2				0.304	0.330	0.345	0.340
0.6	tip 1					0.274	0.137	-0.142
	tip 2					0.274	0.289	0.283
0.7	tip 1						0.151	-0.133
	tip 2						0.150	0.142
0.8	tip 1							-0.146
	tip 2							-0.146

Mode II:

2a1/W		2a2/W 0.2	0.3	0.4	0.5	0.6	0.7	0.8
0.2	tip 1	-0.329	-0.409	-0.517	-0.664	-0.866	-1.121	-1.410
	tip 2	-0.329	-0.379	-0.433	-0.496	-0.572	-0.667	-0.789
0.3	tip 1		-0.458	-0.567	-0.716	-0.924	-1.188	-1.491
	tip 2		-0.458	-0.512	-0.575	-0.651	-0.747	-0.871
0.4	tip 1			-0.622	-0.774	-0.987	-1.260	-1.580
	tip 2			-0.622	-0.686	-0.765	-0.863	-0.992
0.5	tip 1				-0.842	-1.061	-1.343	-1.680
	tip 2				-0.843	-0.924	-1.028	-1.164
0.6	tip 1					-1.150	-1.444	-1.800
	tip 2					-1.151	-1.263	-1.409
0.7	tip 1						-1.570	-1.950
	tip 2						-1.572	-1.737
0.8	tip 1							-2.147
	tip 2							-2.147

Mode III: all zero

<111/11$\underline{2}$>, $\theta = 8°$

Mode I:

2a1/W		2a2/W 0.2	0.3	0.4	0.5	0.6	0.7	0.8
0.2	tip 1	0.255	0.292	0.325	0.349	0.347	0.280	0.048
	tip 2	0.255	0.295	0.336	0.377	0.418	0.455	0.477
0.3	tip 1		0.333	0.368	0.394	0.396	0.332	0.104
	tip 2		0.333	0.375	0.419	0.462	0.501	0.527
0.4	tip 1			0.412	0.441	0.445	0.385	0.161
	tip 2			0.412	0.458	0.503	0.545	0.573
0.5	tip 1				0.488	0.496	0.438	0.218
	tip 2				0.489	0.536	0.580	0.610
0.6	tip 1					0.546	0.491	0.273
	tip 2					0.546	0.591	0.623
0.7	tip 1						0.537	0.321
	tip 2						0.539	0.571
0.8	tip 1							0.350
	tip 2							0.351

Mode II:

2a1/W		2a2/W 0.2	0.3	0.4	0.5	0.6	0.7	0.8
0.2	tip 1	-0.187	-0.240	-0.319	-0.439	-0.631	-0.936	-1.391
	tip 2	-0.187	-0.217	-0.250	-0.291	-0.344	-0.419	-0.530
0.3	tip 1		-0.270	-0.349	-0.470	-0.666	-0.978	-1.447
	tip 2		-0.270	-0.303	-0.343	-0.396	-0.470	-0.582
0.4	tip 1			-0.383	-0.506	-0.706	-1.024	-1.506
	tip 2			-0.383	-0.424	-0.477	-0.552	-0.666
0.5	tip 1				-0.549	-0.753	-1.079	-1.573
	tip 2				-0.549	-0.604	-0.682	-0.799
0.6	tip 1					-0.813	-1.147	-1.657
	tip 2					-0.812	-0.896	-1.021
0.7	tip 1						-1.240	-1.773
	tip 2						-1.240	-1.378
0.8	tip 1							-1.935
	tip 2							-1.939

Mode III: all zero

<111/11$\underline{2}$>, $\theta = 4°$

Mode I:

2a1/W		2a2/W 0.2	0.3	0.4	0.5	0.6	0.7	0.8
0.2	tip 1	0.296	0.345	0.397	0.454	0.514	0.565	0.540
	tip 2	0.296	0.342	0.391	0.442	0.499	0.560	0.626
0.3	tip 1		0.392	0.447	0.507	0.572	0.630	0.616
	tip 2		0.392	0.443	0.497	0.555	0.620	0.689
0.4	tip 1			0.500	0.564	0.633	0.698	0.693
	tip 2			0.500	0.557	0.618	0.686	0.758
0.5	tip 1				0.624	0.698	0.769	0.773
	tip 2				0.624	0.689	0.759	0.834
0.6	tip 1					0.767	0.843	0.856
	tip 2					0.768	0.842	0.919
0.7	tip 1						0.922	0.941
	tip 2						0.923	1.004
0.8	tip 1							1.026
	tip 2							1.030

Mode II:

2a1/W		2a2/W 0.2	0.3	0.4	0.5	0.6	0.7	0.8
0.2	tip 1	-0.041	-0.061	-0.096	-0.154	-0.260	-0.471	-0.948
	tip 2	-0.041	-0.050	-0.060	-0.075	-0.096	-0.131	-0.198
0.3	tip 1		-0.070	-0.104	-0.163	-0.271	-0.485	-0.971
	tip 2		-0.070	-0.080	-0.094	-0.115	-0.149	-0.213
0.4	tip 1			-0.115	-0.174	-0.283	-0.500	-0.993
	tip 2			-0.115	-0.128	-0.148	-0.182	-0.246
0.5	tip 1				-0.188	-0.299	-0.518	-1.019
	tip 2				-0.188	-0.208	-0.242	-0.307
0.6	tip 1					-0.320	-0.543	-1.049
	tip 2					-0.319	-0.354	-0.422
0.7	tip 1						-0.582	-1.097
	tip 2						-0.578	-0.652
0.8	tip 1							-1.186
	tip 2							-1.178

Mode III: all zero

<111/11$\underline{2}$>, $\theta = 0°$

Mode I:

2a1/W		2a2/W 0.2	0.3	0.4	0.5	0.6	0.7	0.8
0.2	tip 1	0.316	0.370	0.429	0.499	0.585	0.698	0.871
	tip 2	0.316	0.366	0.418	0.474	0.537	0.609	0.699
0.3	tip 1		0.421	0.483	0.556	0.648	0.769	0.956
	tip 2		0.421	0.475	0.534	0.599	0.675	0.769
0.4	tip 1			0.540	0.617	0.715	0.844	1.045
	tip 2			0.540	0.602	0.671	0.750	0.848
0.5	tip 1				0.683	0.786	0.924	1.138
	tip 2				0.684	0.757	0.840	0.942
0.6	tip 1					0.865	1.011	1.236
	tip 2					0.865	0.954	1.059
0.7	tip 1						1.106	1.342
	tip 2						1.106	1.217
0.8	tip 1							1.461
	tip 2							1.461

Mode II:

2a1/W		2a2/W 0.2	0.3	0.4	0.5	0.6	0.7	0.8
0.2	tip 1	0.095	0.107	0.117	0.128	0.141	0.157	0.179
	tip 2	0.095	0.107	0.118	0.129	0.140	0.153	0.168
0.3	tip 1		0.118	0.129	0.140	0.154	0.171	0.197
	tip 2		0.118	0.129	0.141	0.154	0.168	0.184
0.4	tip 1			0.141	0.153	0.168	0.186	0.214
	tip 2			0.141	0.154	0.168	0.184	0.202
0.5	tip 1				0.167	0.184	0.204	0.235
	tip 2				0.168	0.183	0.201	0.222
0.6	tip 1					0.201	0.224	0.255
	tip 2					0.202	0.222	0.246
0.7	tip 1						0.247	0.287
	tip 2						0.248	0.276
0.8	tip 1							0.319
	tip 2							0.324

Mode III: all zero

<111/112>, $\theta = -4°$

Mode I:

2a1/W		2a2/W 0.2	0.3	0.4	0.5	0.6	0.7	0.8
0.2	tip 1	0.319	0.371	0.427	0.489	0.559	0.634	0.693
	tip 2	0.319	0.369	0.421	0.476	0.537	0.604	0.681
0.3	tip 1		0.422	0.481	0.547	0.622	0.705	0.777
	tip 2		0.422	0.476	0.535	0.598	0.670	0.751
0.4	tip 1			0.538	0.608	0.689	0.781	0.865
	tip 2			0.538	0.600	0.668	0.743	0.830
0.5	tip 1				0.674	0.761	0.861	0.960
	tip 2				0.674	0.747	0.827	0.920
0.6	tip 1					0.840	0.948	1.057
	tip 2					0.840	0.926	1.025
0.7	tip 1						1.042	1.164
	tip 2						1.042	1.149
0.8	tip 1							1.281
	tip 2							1.280

Mode II:

2a1/W		2a2/W 0.2	0.3	0.4	0.5	0.6	0.7	0.8
0.2	tip 1	0.213	0.250	0.296	0.359	0.455	0.615	0.937
	tip 2	0.213	0.241	0.271	0.303	0.342	0.391	0.463
0.3	tip 1		0.278	0.325	0.389	0.487	0.652	0.983
	tip 2		0.278	0.308	0.341	0.381	0.432	0.506
0.4	tip 1			0.356	0.421	0.524	0.694	1.032
	tip 2			0.356	0.391	0.433	0.486	0.563
0.5	tip 1				0.459	0.564	0.740	1.092
	tip 2				0.459	0.504	0.561	0.643
0.6	tip 1					0.614	0.797	1.156
	tip 2					0.614	0.676	0.766
0.7	tip 1						0.867	1.241
	tip 2						0.868	0.968
0.8	tip 1							1.361
	tip 2							1.361

Mode III: all zero

<111/11$\underline{2}$>, $\theta = -8°$

Mode I:

2a1/W		2a2/W 0.2	0.3	0.4	0.5	0.6	0.7	0.8
0.2	tip 1	0.308	0.354	0.400	0.444	0.479	0.485	0.386
	tip 2	0.308	0.356	0.405	0.456	0.509	0.564	0.615
0.3	tip 1		0.404	0.452	0.499	0.539	0.552	0.464
	tip 2		0.404	0.455	0.509	0.566	0.625	0.682
0.4	tip 1			0.506	0.557	0.603	0.623	0.544
	tip 2			0.506	0.564	0.625	0.689	0.752
0.5	tip 1				0.619	0.671	0.698	0.630
	tip 2				0.619	0.685	0.754	0.825
0.6	tip 1					0.743	0.777	0.720
	tip 2					0.742	0.818	0.895
0.7	tip 1						0.861	0.815
	tip 2						0.861	0.946
0.8	tip 1							0.910
	tip 2							0.909

Mode II:

2a1/W		2a2/W 0.2	0.3	0.4	0.5	0.6	0.7	0.8
0.2	tip 1	0.309	0.365	0.434	0.526	0.661	0.868	1.220
	tip 2	0.309	0.352	0.396	0.444	0.501	0.573	0.671
0.3	tip 1		0.407	0.477	0.571	0.710	0.923	1.286
	tip 2		0.407	0.451	0.501	0.559	0.633	0.733
0.4	tip 1			0.523	0.619	0.763	0.984	1.359
	tip 2			0.523	0.575	0.636	0.712	0.818
0.5	tip 1				0.674	0.823	1.052	1.441
	tip 2				0.675	0.740	0.822	0.934
0.6	tip 1					0.895	1.133	1.536
	tip 2					0.895	0.984	1.106
0.7	tip 1						1.234	1.656
	tip 2						1.234	1.371
0.8	tip 1							1.820
	tip 2							1.820

Mode III: all zero

<111/11$\underline{2}$>, $\theta = -12°$

Mode I:

2a1/W		2a2/W 0.2	0.3	0.4	0.5	0.6	0.7	0.8
0.2	tip 1	0.287	0.325	0.358	0.378	0.375	0.311	0.086
	tip 2	0.287	0.331	0.376	0.420	0.464	0.504	0.527
0.3	tip 1		0.371	0.405	0.429	0.430	0.371	0.151
	tip 2		0.371	0.417	0.465	0.512	0.556	0.587
0.4	tip 1			0.455	0.482	0.488	0.435	0.223
	tip 2			0.455	0.506	0.557	0.607	0.644
0.5	tip 1				0.537	0.548	0.501	0.297
	tip 2				0.537	0.594	0.648	0.693
0.6	tip 1					0.610	0.569	0.373
	tip 2					0.610	0.671	0.723
0.7	tip 1						0.637	0.449
	tip 2						0.638	0.698
0.8	tip 1							0.520
	tip 2							0.520

Mode II:

2a1/W		2a2/W 0.2	0.3	0.4	0.5	0.6	0.7	0.8
0.2	tip 1	0.386	0.455	0.538	0.644	0.793	1.005	1.319
	tip 2	0.386	0.439	0.495	0.555	0.624	0.709	0.819
0.3	tip 1		0.507	0.592	0.701	0.854	1.073	1.400
	tip 2		0.507	0.563	0.624	0.696	0.783	0.896
0.4	tip 1			0.649	0.761	0.920	1.148	1.488
	tip 2			0.649	0.713	0.787	0.878	0.997
0.5	tip 1				0.829	0.994	1.231	1.587
	tip 2				0.830	0.909	1.005	1.131
0.6	tip 1					1.081	1.328	1.704
	tip 2					1.081	1.186	1.324
0.7	tip 1						1.447	1.845
	tip 2						1.447	1.602
0.8	tip 1							2.030
	tip 2							2.029

Mode III: all zero

<111/11$\underline{2}$>, $\theta = -16°$

Mode I:

2a1/W		2a2/W 0.2	0.3	0.4	0.5	0.6	0.7	0.8
0.2	tip 1	0.259	0.288	0.304	0.301	0.258	0.128	-0.194
	tip 2	0.259	0.299	0.337	0.374	0.406	0.429	0.426
0.3	tip 1		0.328	0.347	0.346	0.306	0.180	-0.139
	tip 2		0.328	0.369	0.408	0.444	0.472	0.476
0.4	tip 1			0.390	0.392	0.355	0.234	-0.080
	tip 2			0.390	0.433	0.473	0.506	0.518
0.5	tip 1				0.438	0.406	0.289	-0.020
	tip 2				0.438	0.483	0.521	0.541
0.6	tip 1					0.456	0.345	0.042
	tip 2					0.456	0.500	0.527
0.7	tip 1						0.394	0.098
	tip 2						0.394	0.428
0.8	tip 1							0.139
	tip 2							0.138

Mode II:

2a1/W		2a2/W 0.2	0.3	0.4	0.5	0.6	0.7	0.8
0.2	tip 1	0.446	0.523	0.615	0.728	0.878	1.078	1.340
	tip 2	0.446	0.508	0.572	0.641	0.719	0.811	0.926
0.3	tip 1		0.584	0.677	0.793	0.949	1.157	1.432
	tip 2		0.585	0.649	0.719	0.799	0.894	1.012
0.4	tip 1			0.743	0.862	1.024	1.241	1.532
	tip 2			0.744	0.816	0.900	0.999	1.124
0.5	tip 1				0.940	1.108	1.336	1.643
	tip 2				0.941	1.029	1.135	1.268
0.6	tip 1					1.205	1.445	1.772
	tip 2					1.205	1.321	1.467
0.7	tip 1						1.574	1.926
	tip 2						1.574	1.739
0.8	tip 1							2.121
	tip 2							2.120

Mode III: all zero

<111/112>, $\theta = -20°$

Mode I:

2a1/W		2a2/W 0.2	0.3	0.4	0.5	0.6	0.7	0.8
0.2	tip 1	0.225	0.243	0.243	0.213	0.129	-0.063	-0.447
	tip 2	0.225	0.259	0.290	0.318	0.338	0.343	0.314
0.3	tip 1		0.277	0.279	0.251	0.168	-0.022	-0.405
	tip 2		0.277	0.311	0.341	0.365	0.374	0.353
0.4	tip 1			0.315	0.289	0.209	0.022	-0.360
	tip 2			0.315	0.348	0.376	0.390	0.376
0.5	tip 1				0.325	0.249	0.065	-0.315
	tip 2				0.326	0.357	0.377	0.371
0.6	tip 1					0.285	0.105	-0.272
	tip 2					0.285	0.310	0.311
0.7	tip 1						0.134	-0.238
	tip 2						0.134	0.142
0.8	tip 1							-0.225
	tip 2							-0.225

Mode II:

2a1/W		2a2/W 0.2	0.3	0.4	0.5	0.6	0.7	0.8
0.2	tip 1	0.493	0.576	0.672	0.787	0.934	1.115	1.316
	tip 2	0.493	0.562	0.632	0.708	0.791	0.888	1.004
0.3	tip 1		0.644	0.741	0.859	1.012	1.201	1.417
	tip 2		0.644	0.715	0.792	0.878	0.978	1.097
0.4	tip 1			0.814	0.936	1.095	1.293	1.525
	tip 2			0.815	0.894	0.984	1.088	1.215
0.5	tip 1				1.020	1.186	1.396	1.644
	tip 2				1.021	1.116	1.228	1.363
0.6	tip 1					1.290	1.512	1.781
	tip 2					1.290	1.412	1.560
0.7	tip 1						1.649	1.943
	tip 2						1.649	1.817
0.8	tip 1							2.143
	tip 2							2.142

Mode III: all zero

Isotropic, $\theta = 20°$

Mode I:

2a1/W		0.2	0.3	0.4	0.5	0.6	0.7	0.8
0.2	tip 1	0.175	0.173	0.144	0.071	-0.070	-0.304	-0.626
	tip 2	0.175	0.200	0.220	0.234	0.235	0.214	0.161
0.3	tip 1		0.199	0.171	0.098	-0.043	-0.279	-0.607
	tip 2		0.199	0.221	0.236	0.240	0.224	0.176
0.4	tip 1			0.194	0.122	-0.019	-0.256	-0.588
	tip 2			0.194	0.211	0.217	0.204	0.161
0.5	tip 1				0.141	0.000	-0.239	-0.574
	tip 2				0.141	0.148	0.138	0.098
0.6	tip 1					0.008	-0.231	-0.570
	tip 2					0.008	-0.001	-0.038
0.7	tip 1						-0.242	-0.584
	tip 2						-0.242	-0.279
0.8	tip 1							-0.623
	tip 2							-0.623

Mode II:

2a1/W		0.2	0.3	0.4	0.5	0.6	0.7	0.8
0.2	tip 1	-0.475	-0.570	-0.689	-0.835	-1.011	-1.192	-1.338
	tip 2	-0.475	-0.543	-0.616	-0.696	-0.788	-0.896	-1.020
0.3	tip 1		-0.638	-0.758	-0.908	-1.091	-1.281	-1.443
	tip 2		-0.638	-0.711	-0.793	-0.887	-0.997	-1.125
0.4	tip 1			-0.834	-0.987	-1.177	-1.378	-1.557
	tip 2			-0.834	-0.918	-1.016	-1.130	-1.265
0.5	tip 1				-1.077	-1.274	-1.486	-1.684
	tip 2				-1.077	-1.180	-1.301	-1.446
0.6	tip 1					-1.386	-1.611	-1.830
	tip 2					-1.386	-1.518	-1.676
0.7	tip 1						-1.759	-2.005
	tip 2						-1.760	-1.938
0.8	tip 1							-2.217
	tip 2							-2.217

Mode III: all zero

Isotropic, $\theta = 16°$

Mode I:

2a1/W		0.2	0.3	0.4	0.5	0.6	0.7	0.8
0.2	tip 1	0.239	0.256	0.253	0.215	0.115	-0.092	-0.451
	tip 2	0.239	0.275	0.307	0.336	0.355	0.358	0.328
0.3	tip 1		0.292	0.290	0.254	0.156	-0.051	-0.410
	tip 2		0.292	0.327	0.357	0.380	0.387	0.363
0.4	tip 1			0.327	0.293	0.196	-0.009	-0.370
	tip 2			0.327	0.360	0.386	0.397	0.378
0.5	tip 1				0.328	0.234	0.030	-0.331
	tip 2				0.328	0.357	0.371	0.357
0.6	tip 1					0.265	0.061	-0.299
	tip 2					0.265	0.282	0.272
0.7	tip 1						0.080	-0.282
	tip 2						0.079	0.071
0.8	tip 1							-0.290
	tip 2							-0.290

Mode II:

2a1/W		0.2	0.3	0.4	0.5	0.6	0.7	0.8
0.2	tip 1	-0.394	-0.479	-0.589	-0.735	-0.933	-1.176	-1.422
	tip 2	-0.394	-0.451	-0.513	-0.583	-0.665	-0.768	-0.895
0.3	tip 1		-0.535	-0.647	-0.796	-1.000	-1.252	-1.514
	tip 2		-0.535	-0.597	-0.667	-0.752	-0.856	-0.986
0.4	tip 1			-0.710	-0.863	-1.073	-1.336	-1.614
	tip 2			-0.710	-0.783	-0.870	-0.978	-1.113
0.5	tip 1				-0.940	-1.157	-1.430	-1.726
	tip 2				-0.941	-1.032	-1.146	-1.289
0.6	tip 1					-1.257	-1.542	-1.858
	tip 2					-1.257	-1.380	-1.535
0.7	tip 1						-1.679	-2.021
	tip 2						-1.680	-1.855
0.8	tip 1							-2.230
	tip 2							-2.232

Mode III: all zero

Isotropic, $\theta = 12°$

Mode I:

2a1/W		0.2	0.3	0.4	0.5	0.6	0.7	0.8
0.2	tip 1	0.291	0.324	0.346	0.346	0.302	0.159	-0.184
	tip 2	0.292	0.335	0.378	0.420	0.457	0.484	0.485
0.3	tip 1		0.369	0.392	0.395	0.354	0.214	-0.127
	tip 2		0.369	0.414	0.458	0.499	0.531	0.538
0.4	tip 1			0.440	0.446	0.408	0.273	-0.065
	tip 2			0.440	0.487	0.532	0.568	0.581
0.5	tip 1				0.496	0.462	0.331	-0.003
	tip 2				0.496	0.544	0.585	0.603
0.6	tip 1					0.514	0.386	0.055
	tip 2					0.515	0.559	0.582
0.7	tip 1						0.434	0.104
	tip 2						0.433	0.460
0.8	tip 1							0.133
	tip 2							0.134

Mode II:

2a1/W		0.2	0.3	0.4	0.5	0.6	0.7	0.8
0.2	tip 1	-0.304	-0.373	-0.465	-0.597	-0.793	-1.079	-1.455
	tip 2	-0.304	-0.349	-0.397	-0.453	-0.521	-0.611	-0.735
0.3	tip 1		-0.417	-0.510	-0.645	-0.846	-1.140	-1.531
	tip 2		-0.417	-0.465	-0.521	-0.591	-0.682	-0.807
0.4	tip 1			-0.560	-0.697	-0.903	-1.205	-1.612
	tip 2			-0.560	-0.618	-0.690	-0.783	-0.912
0.5	tip 1				-0.759	-0.970	-1.282	-1.706
	tip 2				-0.759	-0.834	-0.932	-1.067
0.6	tip 1					-1.052	-1.374	-1.817
	tip 2					-1.052	-1.158	-1.303
0.7	tip 1						-1.493	-1.959
	tip 2						-1.494	-1.656
0.8	tip 1							-2.153
	tip 2							-2.152

Mode III: all zero

Isotropic, $\theta = 8°$

Mode I:

2a1/W		0.2	0.3	0.4	0.5	0.6	0.7	0.8
0.2	tip 1	0.330	0.375	0.417	0.451	0.467	0.426	0.204
	tip 2	0.330	0.380	0.431	0.482	0.535	0.586	0.625
0.3	tip 1		0.427	0.471	0.508	0.529	0.494	0.281
	tip 2		0.427	0.479	0.534	0.590	0.646	0.691
0.4	tip 1			0.526	0.568	0.593	0.565	0.359
	tip 2			0.526	0.585	0.645	0.705	0.755
0.5	tip 1				0.630	0.661	0.638	0.441
	tip 2				0.630	0.695	0.759	0.814
0.6	tip 1					0.730	0.713	0.525
	tip 2					0.730	0.799	0.860
0.7	tip 1						0.787	0.605
	tip 2						0.788	0.854
0.8	tip 1							0.675
	tip 2							0.675

Mode II:

2a1/W		0.2	0.3	0.4	0.5	0.6	0.7	0.8
0.2	tip 1	-0.207	-0.255	-0.322	-0.422	-0.583	-0.855	-1.333
	tip 2	-0.207	-0.237	-0.271	-0.310	-0.359	-0.428	-0.533
0.3	tip 1		-0.285	-0.353	-0.455	-0.619	-0.898	-1.388
	tip 2		-0.285	-0.318	-0.358	-0.408	-0.477	-0.582
0.4	tip 1			-0.388	-0.491	-0.660	-0.944	-1.447
	tip 2			-0.388	-0.428	-0.479	-0.550	-0.658
0.5	tip 1				-0.534	-0.706	-0.998	-1.513
	tip 2				-0.534	-0.588	-0.662	-0.774
0.6	tip 1					-0.765	-1.066	-1.593
	tip 2					-0.765	-0.844	-0.964
0.7	tip 1						-1.154	-1.704
	tip 2						-1.152	-1.285
0.8	tip 1							-1.859
	tip 2							-1.863

Mode III: all zero

Isotropic, $\theta = 4°$

Mode I:

2a1/W		0.2	0.3	0.4	0.5	0.6	0.7	0.8
0.2	tip 1	0.353	0.407	0.462	0.520	0.583	0.645	0.663
	tip 2	0.354	0.408	0.463	0.521	0.584	0.653	0.730
0.3	tip 1		0.462	0.520	0.582	0.651	0.721	0.752
	tip 2		0.462	0.520	0.581	0.648	0.721	0.803
0.4	tip 1			0.581	0.648	0.722	0.800	0.844
	tip 2			0.581	0.646	0.717	0.794	0.881
0.5	tip 1				0.717	0.798	0.884	0.939
	tip 2				0.717	0.793	0.875	0.966
0.6	tip 1					0.879	0.972	1.039
	tip 2					0.879	0.967	1.063
0.7	tip 1						1.066	1.140
	tip 2						1.065	1.167
0.8	tip 1							1.251
	tip 2							1.251

Mode II:

2a1/W		0.2	0.3	0.4	0.5	0.6	0.7	0.8
0.2	tip 1	-0.105	-0.130	-0.165	-0.220	-0.312	-0.484	-0.875
	tip 2	-0.105	-0.120	-0.137	-0.157	-0.184	-0.221	-0.285
0.3	tip 1		-0.145	-0.181	-0.236	-0.330	-0.506	-0.904
	tip 2		-0.145	-0.162	-0.182	-0.209	-0.246	-0.310
0.4	tip 1			-0.199	-0.255	-0.350	-0.530	-0.935
	tip 2			-0.198	-0.219	-0.246	-0.285	-0.349
0.5	tip 1				-0.277	-0.375	-0.558	-0.970
	tip 2				-0.277	-0.305	-0.345	-0.411
0.6	tip 1					-0.405	-0.593	-1.014
	tip 2					-0.405	-0.448	-0.518
0.7	tip 1						-0.641	-1.071
	tip 2						-0.639	-0.718
0.8	tip 1							-1.164
	tip 2							-1.161

Mode III: all zero

Isotropic, $\theta = 0°$

Mode I:

2a1/W		0.2	0.3	0.4	0.5	0.6	0.7	0.8
0.2	tip 1	0.361	0.418	0.477	0.545	0.626	0.732	0.898
	tip 2	0.361	0.417	0.474	0.534	0.601	0.677	0.770
0.3	tip 1		0.474	0.537	0.608	0.695	0.810	0.992
	tip 2		0.474	0.534	0.597	0.667	0.748	0.845
0.4	tip 1			0.599	0.675	0.769	0.893	1.088
	tip 2			0.599	0.667	0.741	0.826	0.928
0.5	tip 1				0.748	0.847	0.980	1.189
	tip 2				0.748	0.827	0.916	1.023
0.6	tip 1					0.933	1.074	1.295
	tip 2					0.933	1.027	1.138
0.7	tip 1						1.175	1.406
	tip 2						1.174	1.291
0.8	tip 1							1.529
	tip 2							1.530

Mode II:

2a1/W		0.2	0.3	0.4	0.5	0.6	0.7	0.8
0.2	tip 1	0.000	0.000	0.000	-0.001	-0.001	-0.001	-0.007
	tip 2	0.000	0.000	0.000	0.000	0.000	-0.001	-0.001
0.3	tip 1		0.000	0.000	-0.001	-0.001	-0.001	-0.006
	tip 2		0.000	0.000	0.000	0.000	0.000	-0.001
0.4	tip 1			0.000	-0.001	-0.001	-0.001	-0.007
	tip 2			0.000	0.000	0.000	0.000	-0.001
0.5	tip 1				-0.001	-0.001	-0.001	-0.003
	tip 2				0.000	0.000	0.000	-0.001
0.6	tip 1					-0.001	-0.002	-0.008
	tip 2					-0.001	0.000	-0.001
0.7	tip 1						-0.002	-0.004
	tip 2						-0.001	-0.001
0.8	tip 1							-0.005
	tip 2							-0.002

Mode III: all zero

<111/11̲0>, $\theta = 20°$

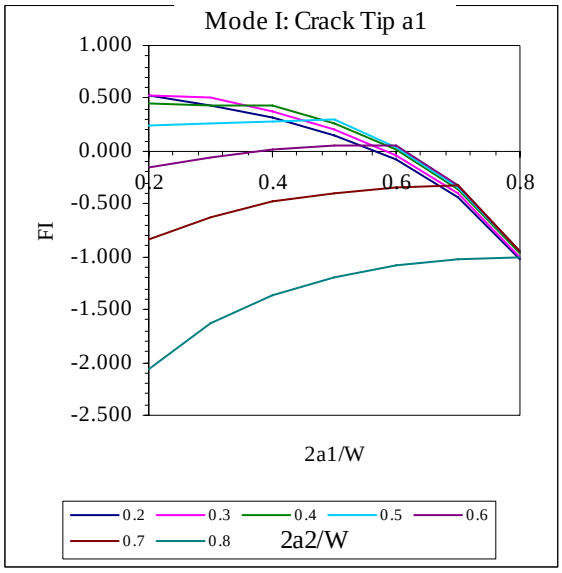

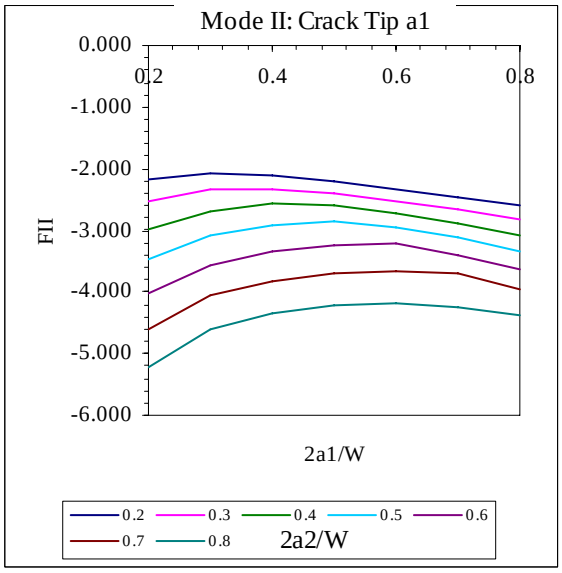

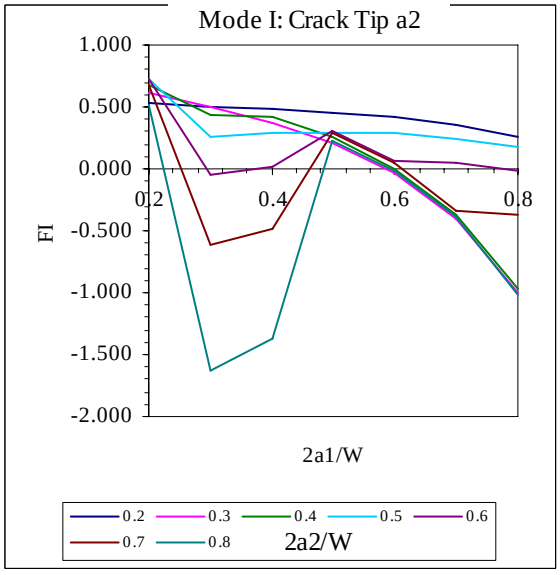

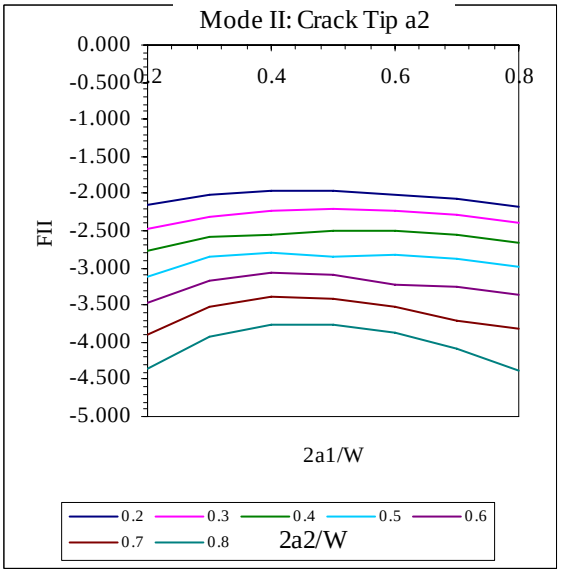

<111/1$\underline{1}$0>, $\theta = 16°$

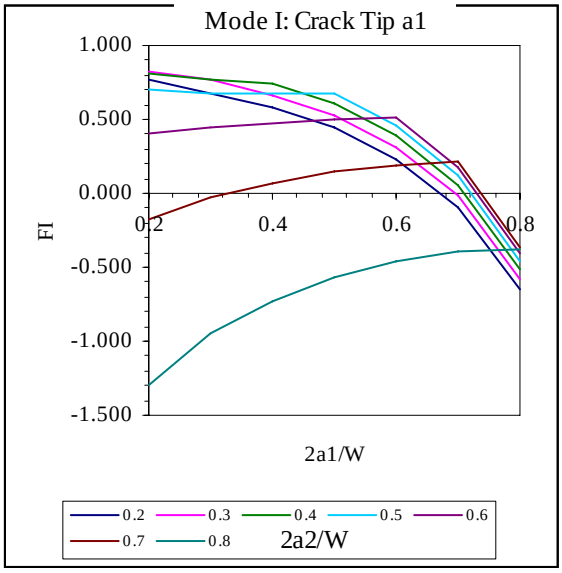

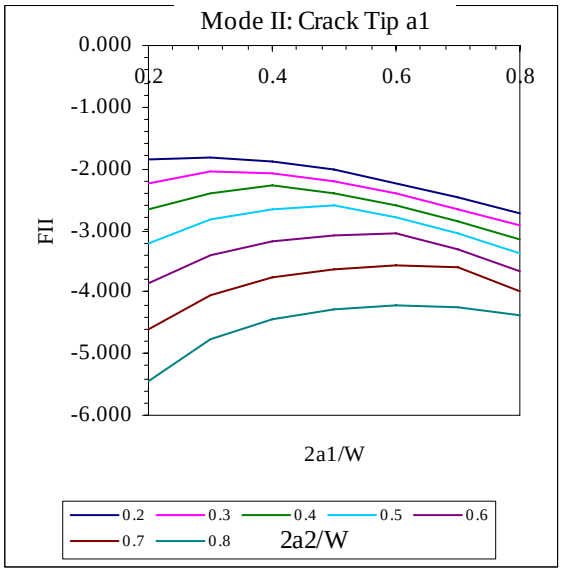

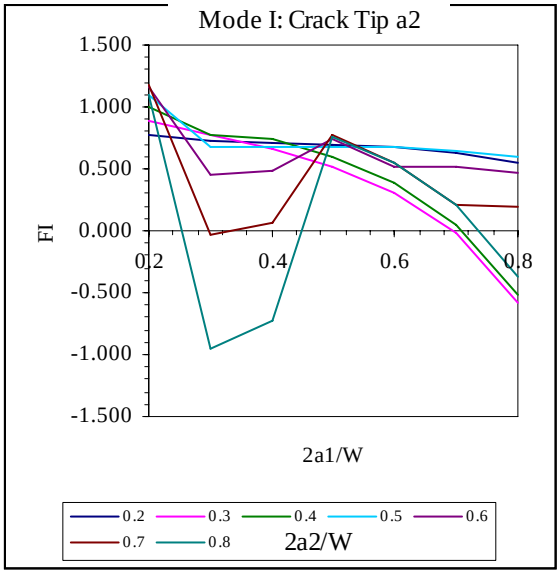

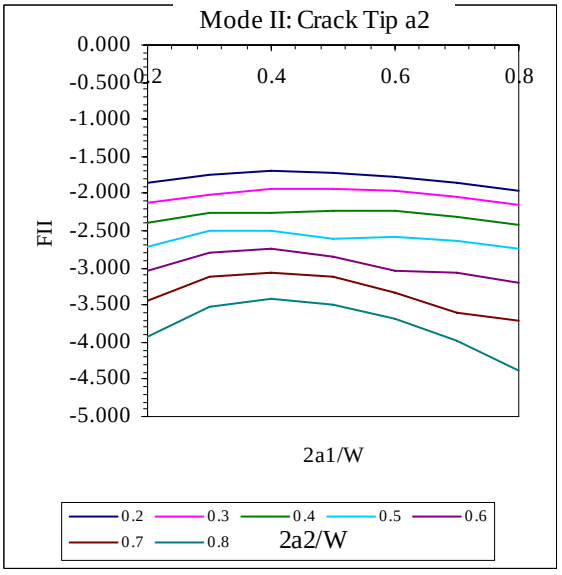

<111/1$\underline{1}$0>, $\theta = 12°$

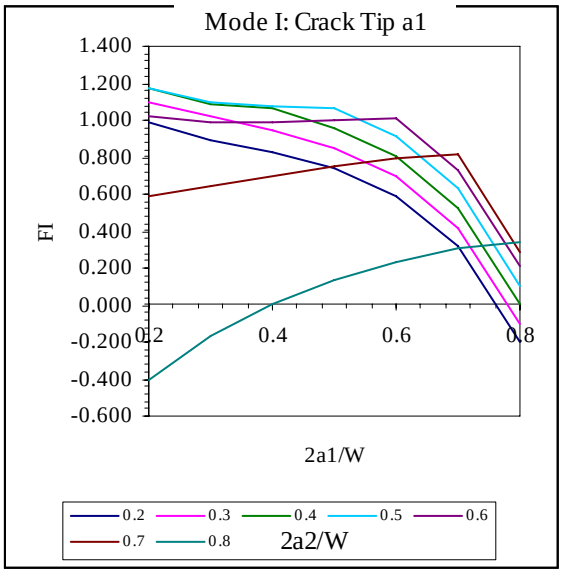

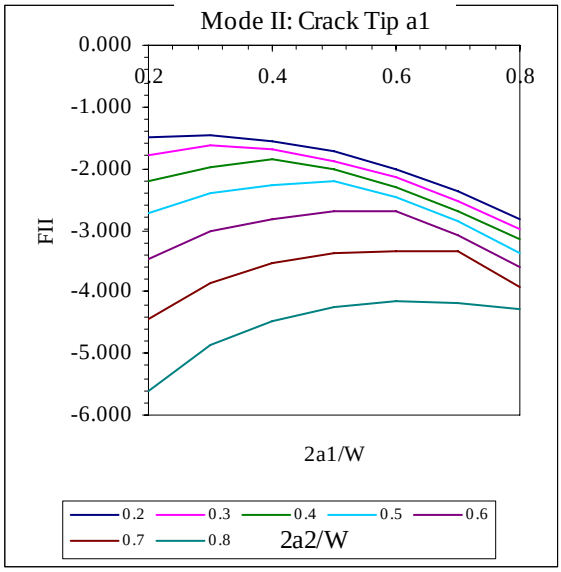

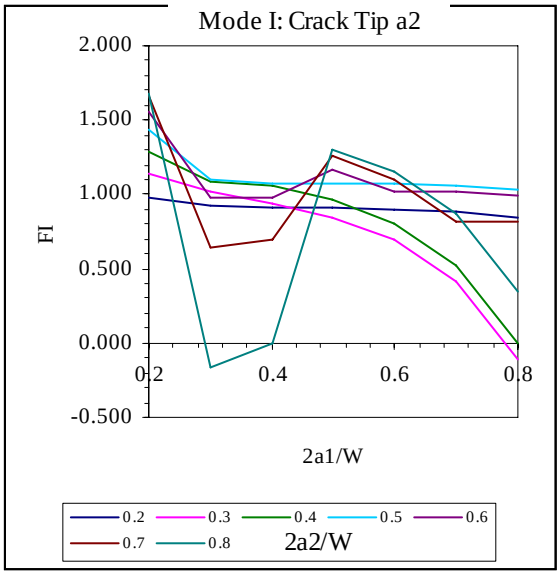

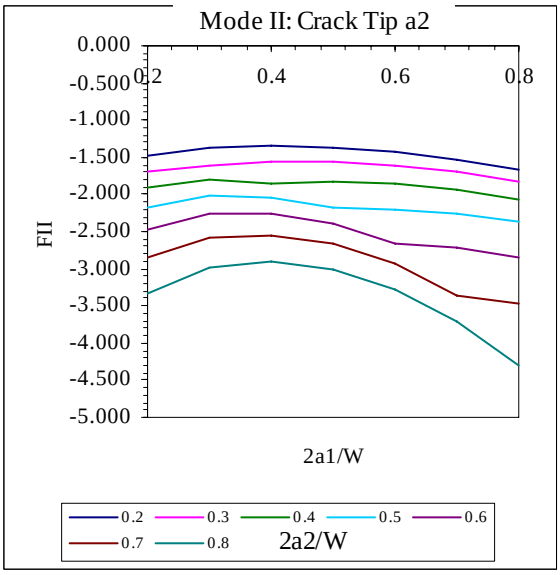

<111/1$\underline{1}$0>, $\theta = 8°$

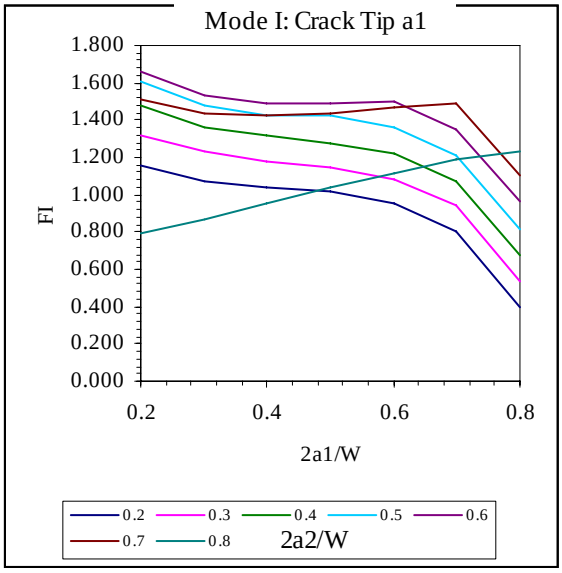

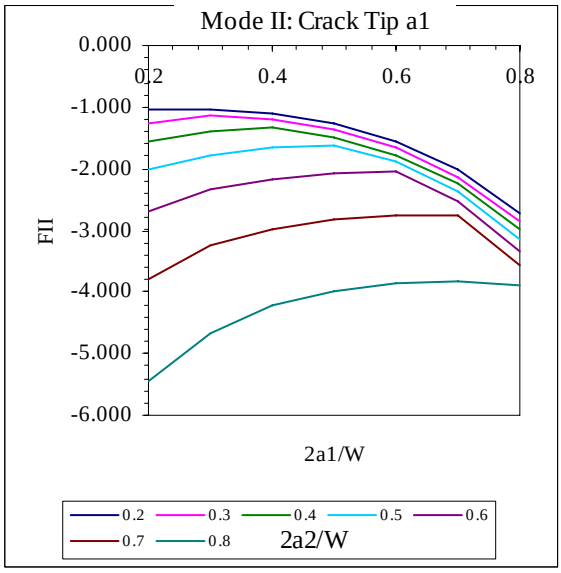

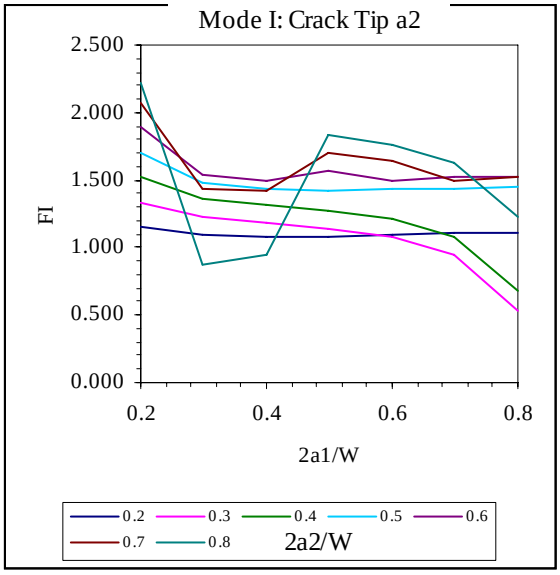

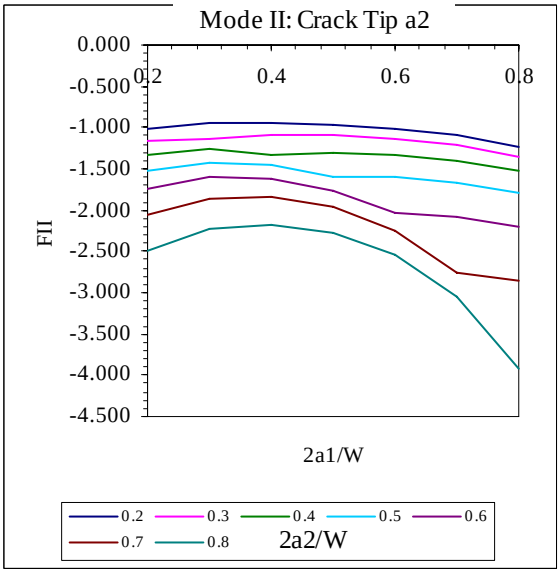

<111/1$\underline{1}$0>, $\theta = 4°$

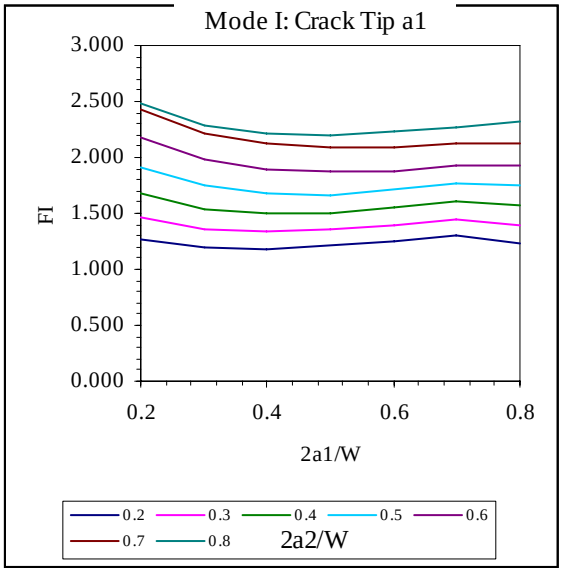

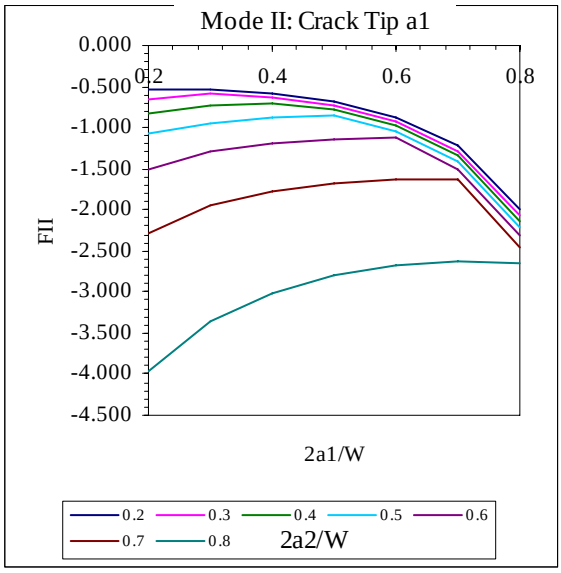

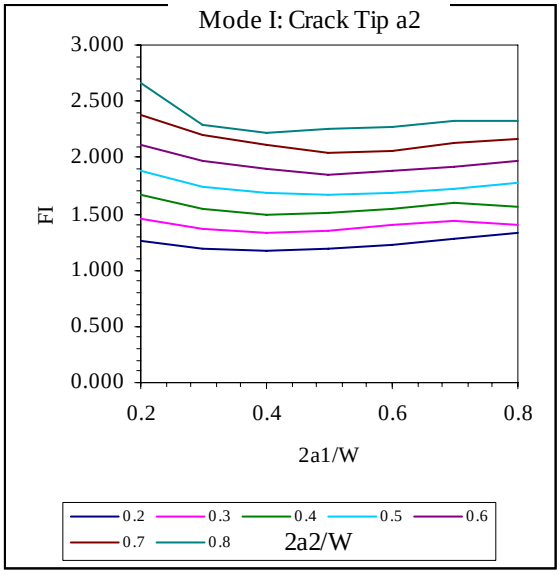

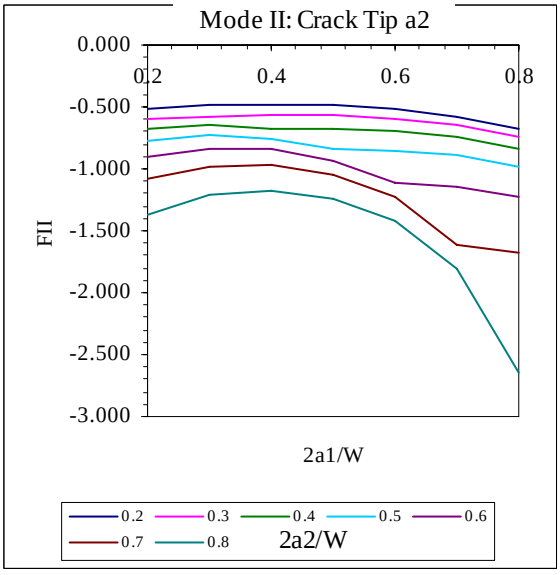

<111/1$\underline{1}$0>, θ=0°

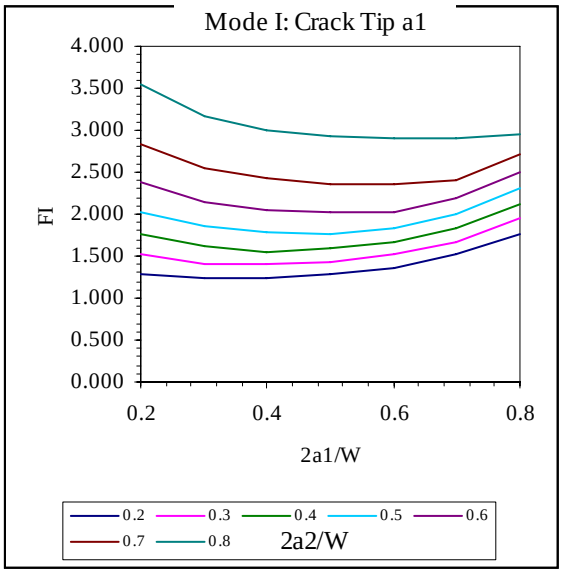

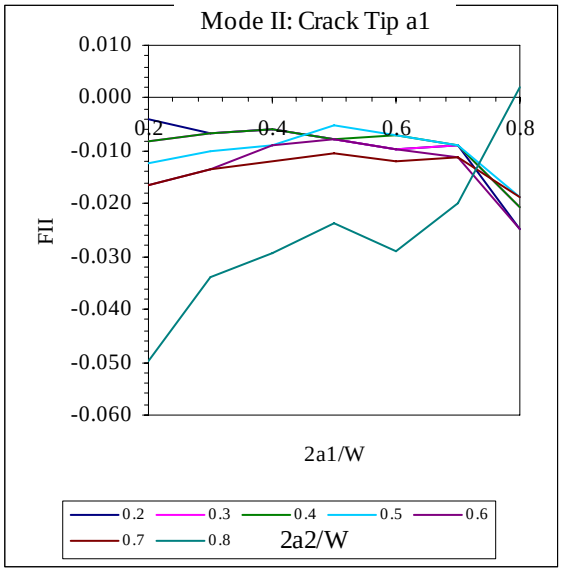

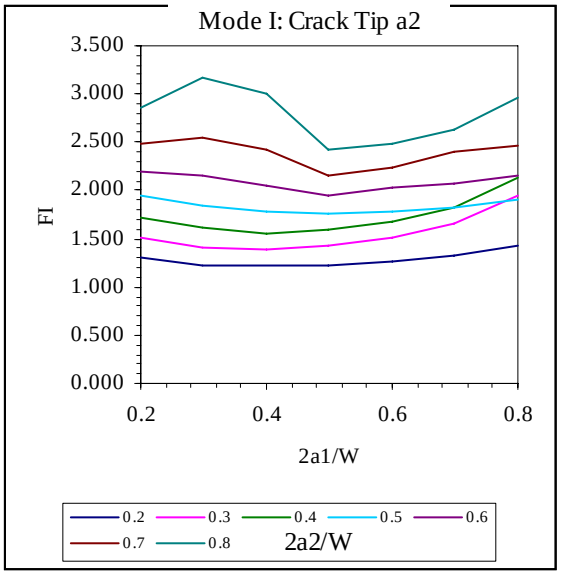

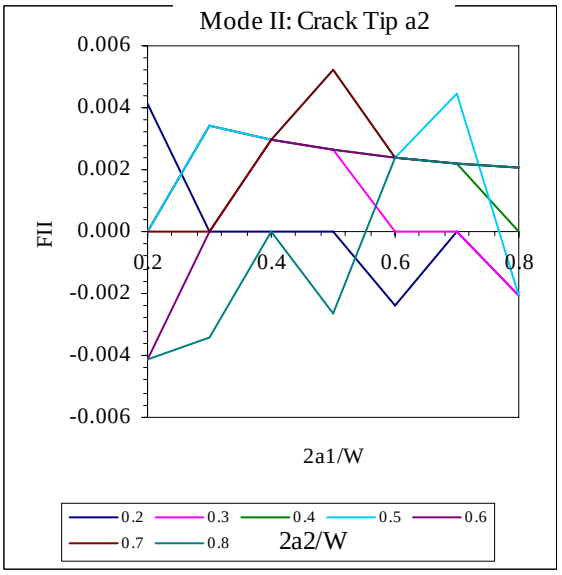

<111/112>, $\theta = 20°$

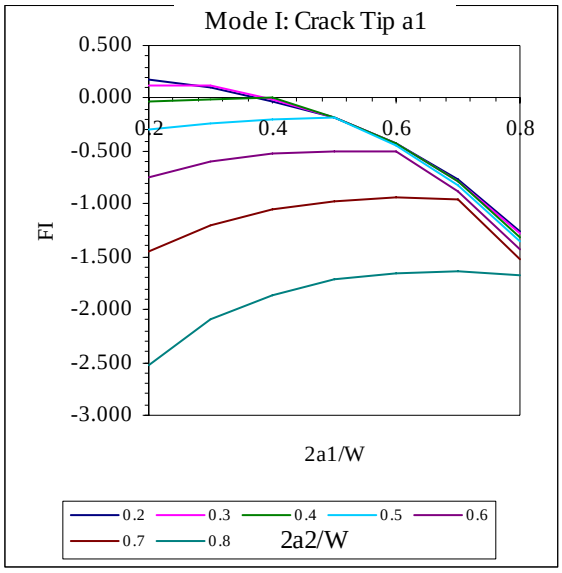

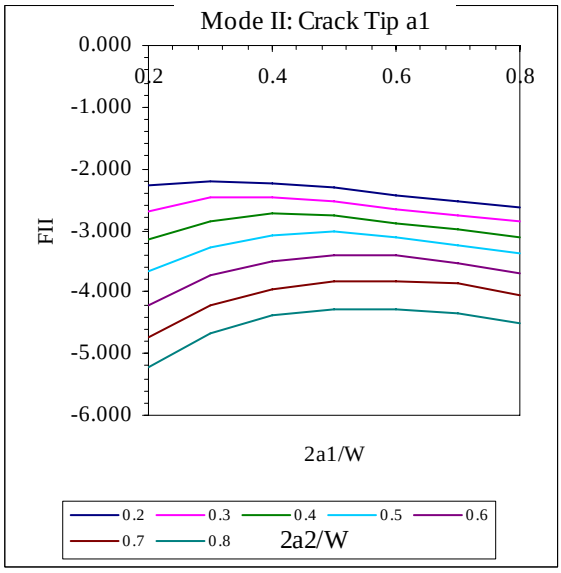

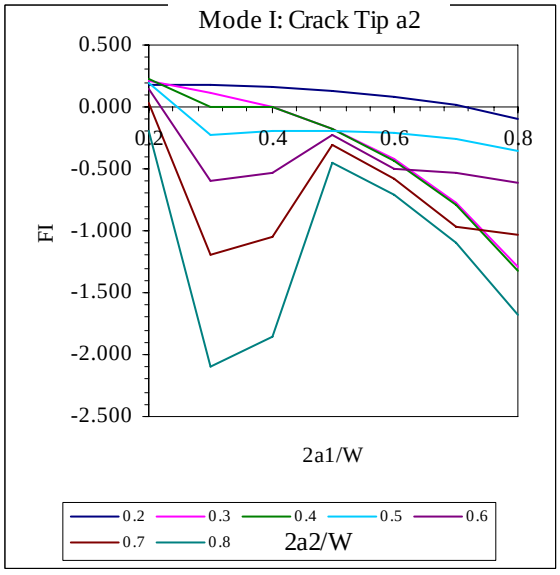

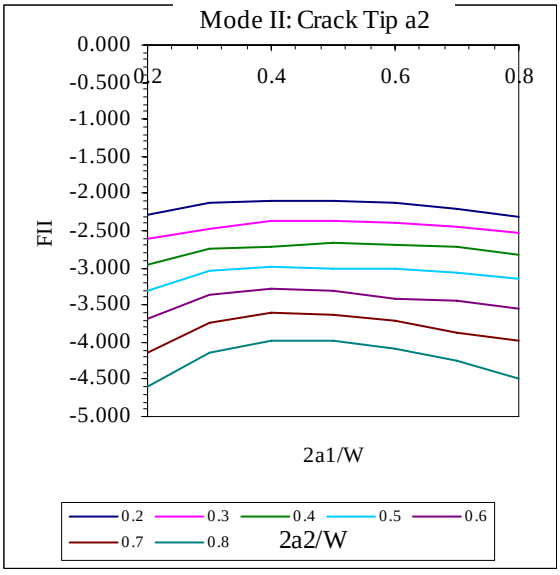

<111/112>, $\theta = 16°$

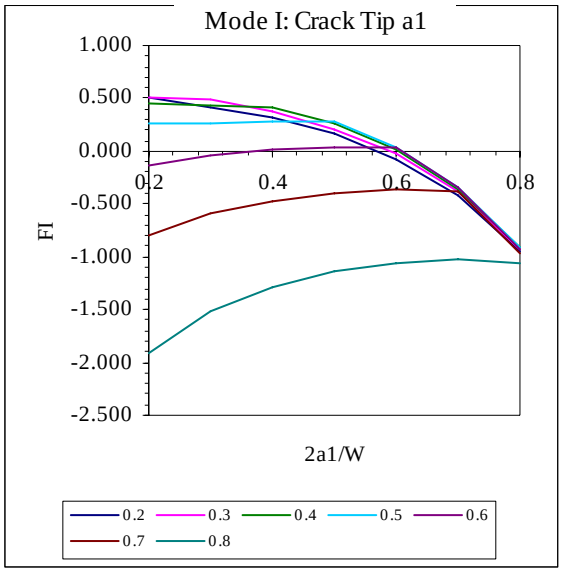

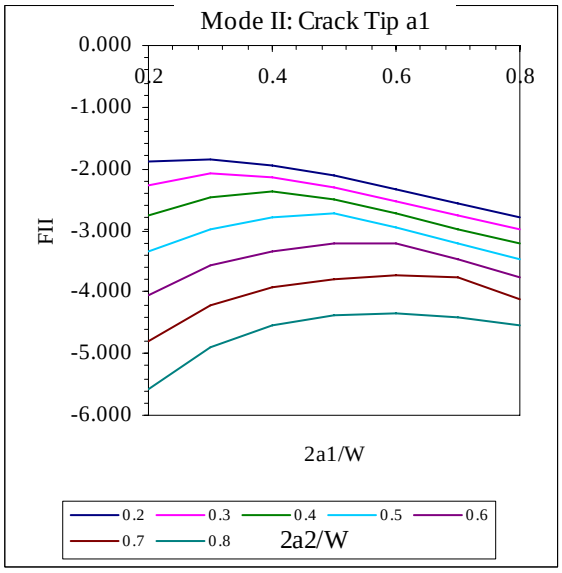

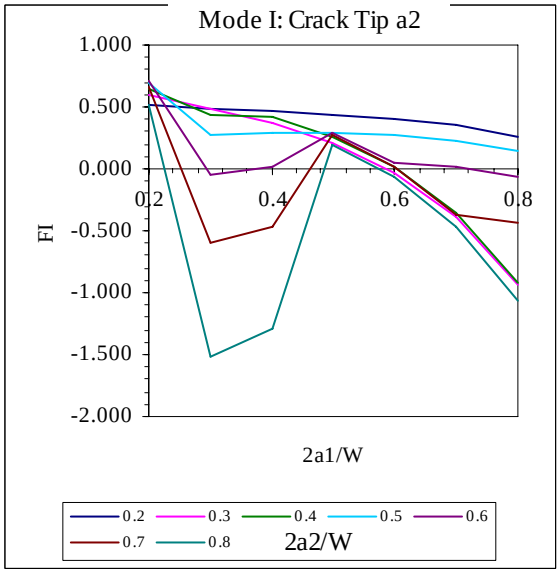

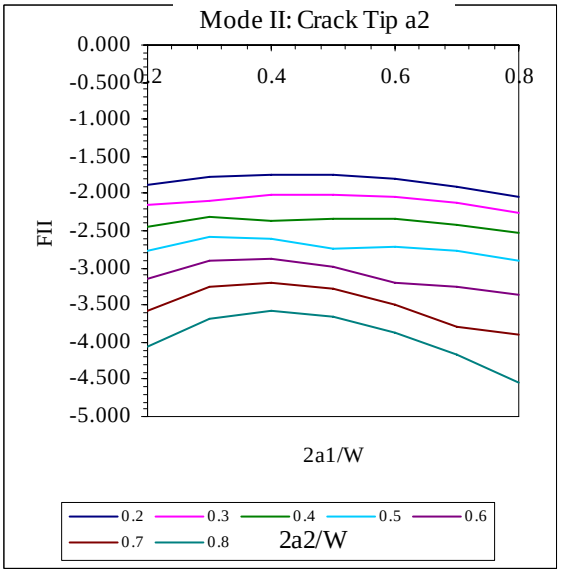

<111/112>, θ=12°

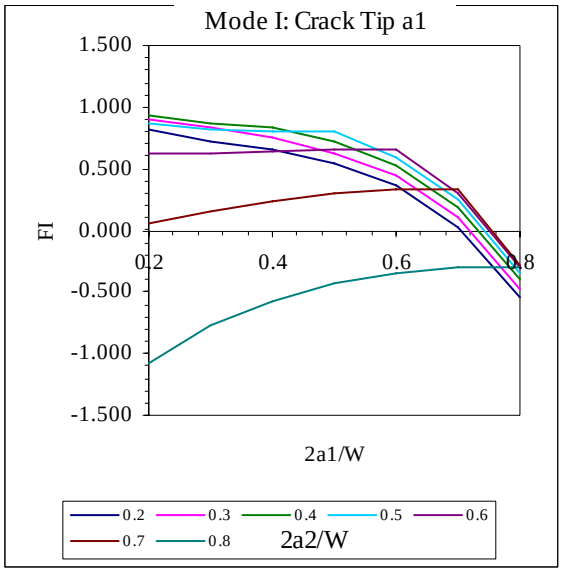

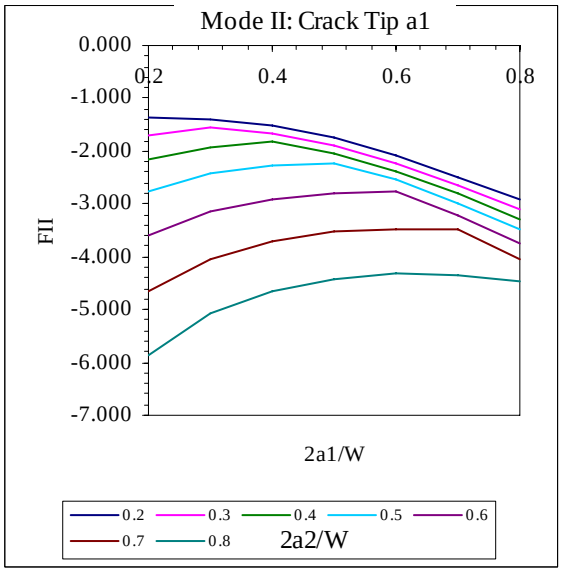

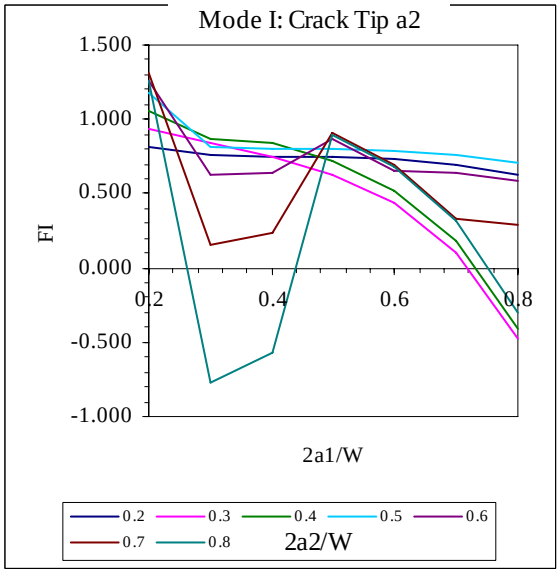

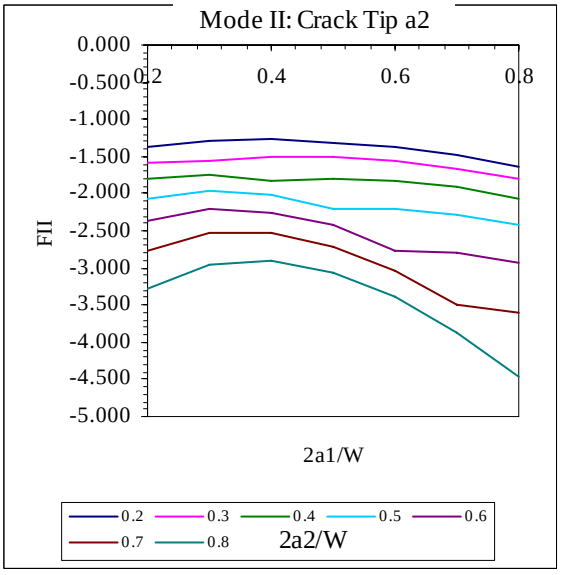

<111/112>, θ=8°

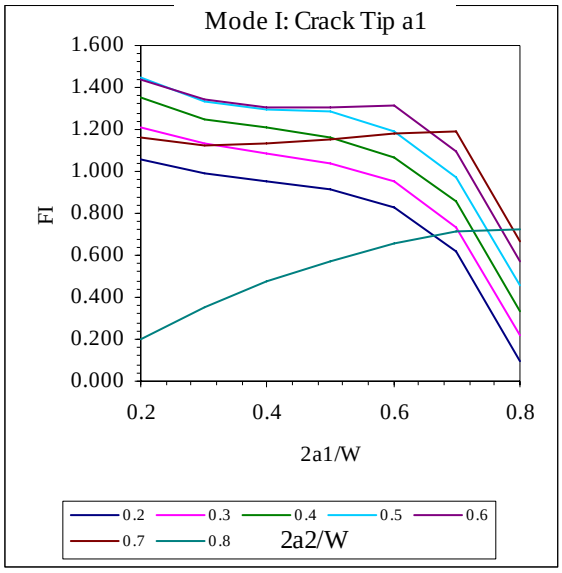

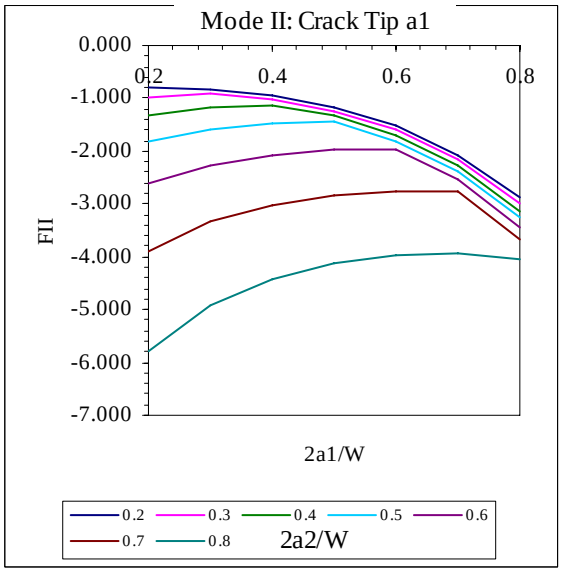

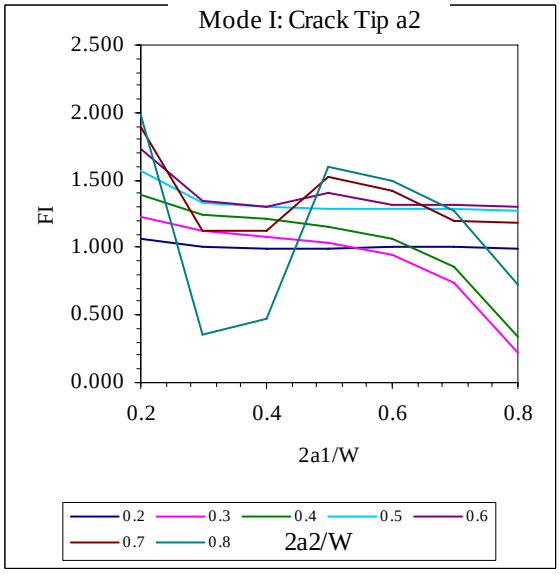

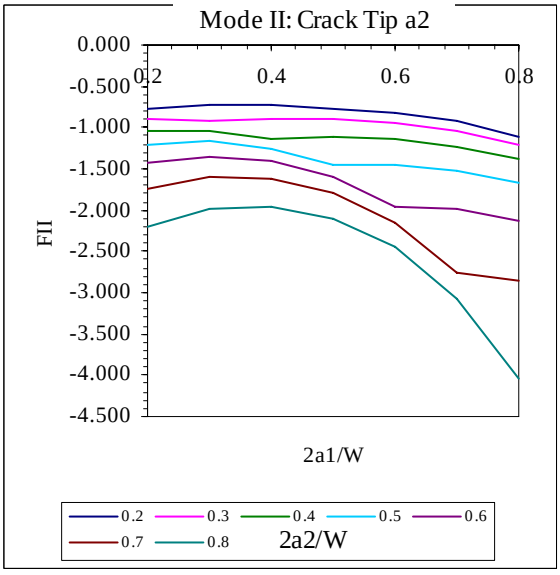

<111/112>, $\theta = 4°$

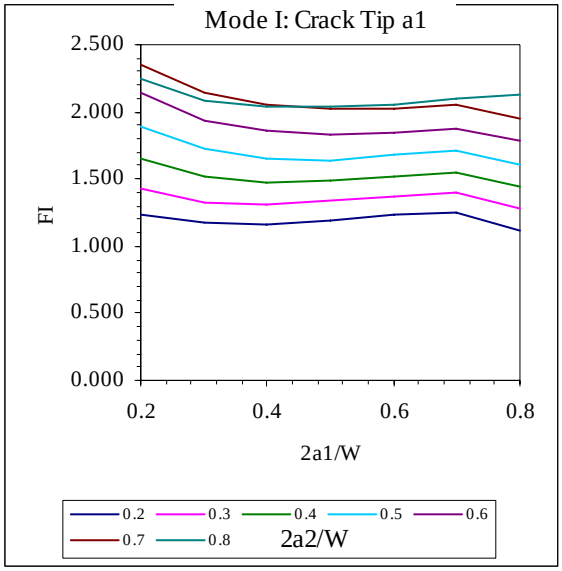

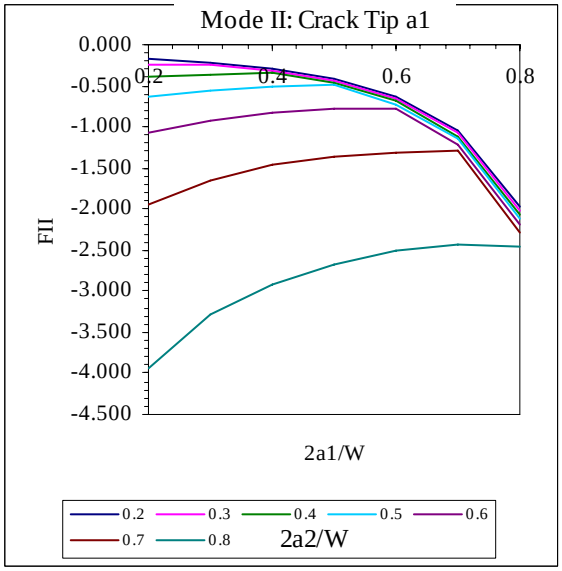

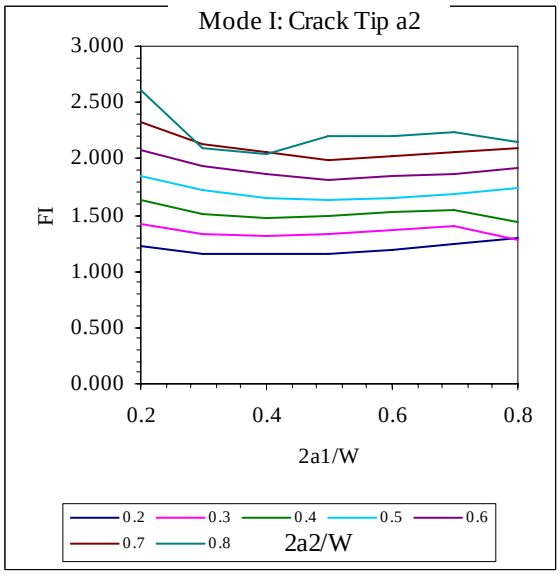

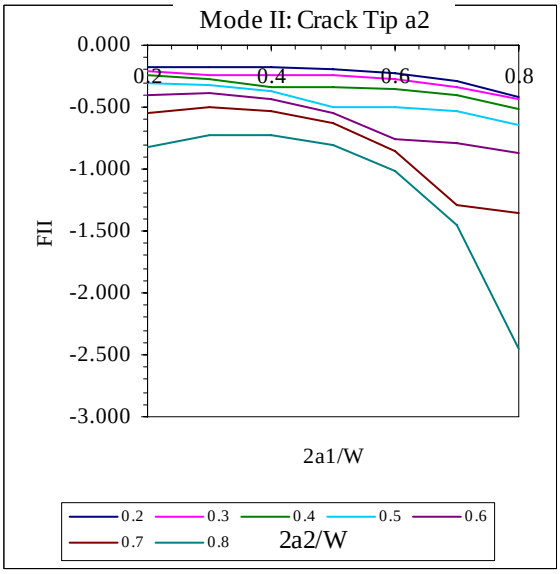

<111/112>, $\theta = 0°$

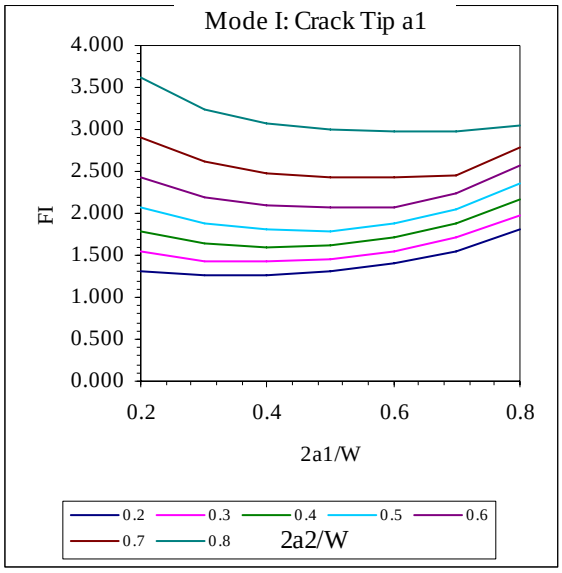

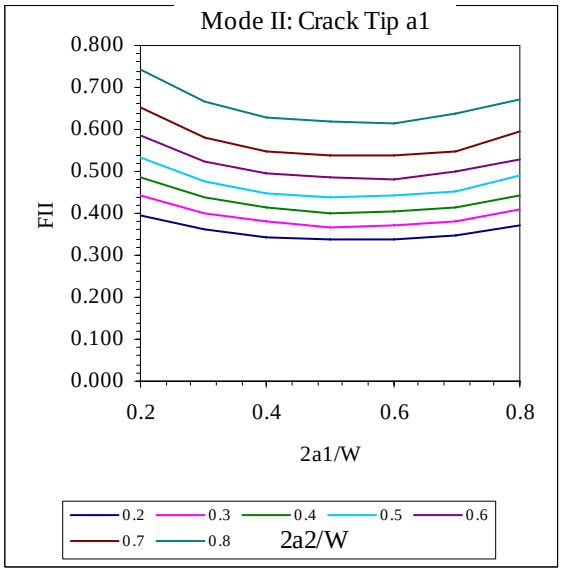

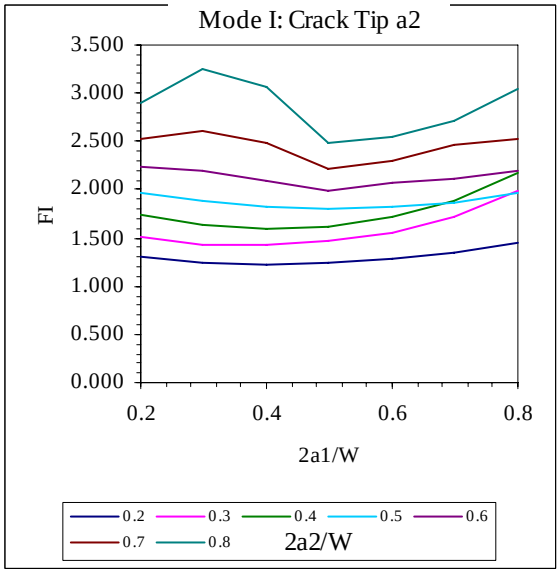

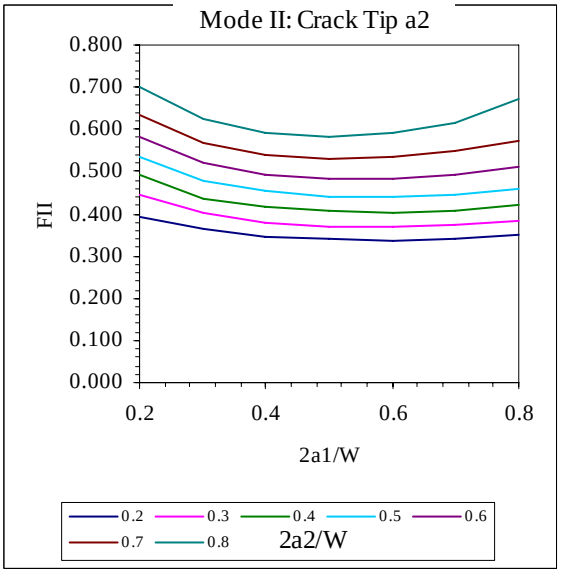

<111/112>, $\theta = -4°$

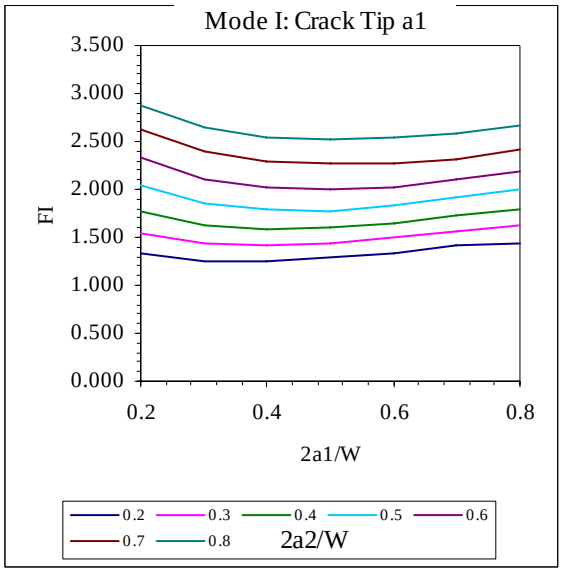

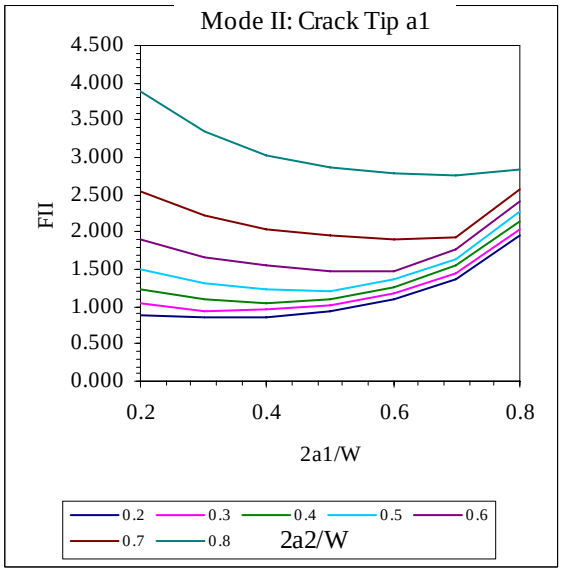

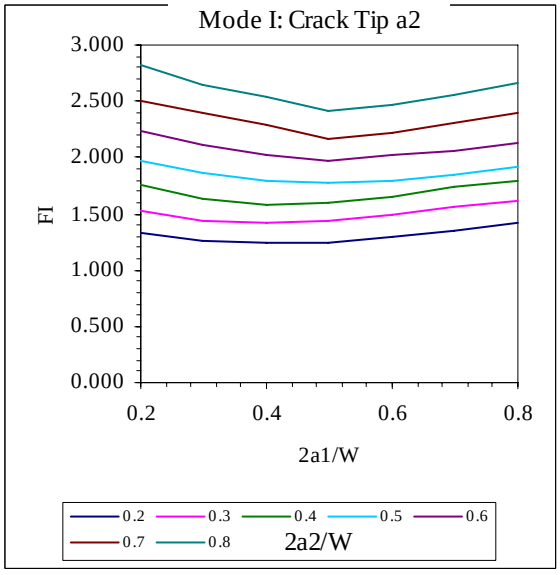

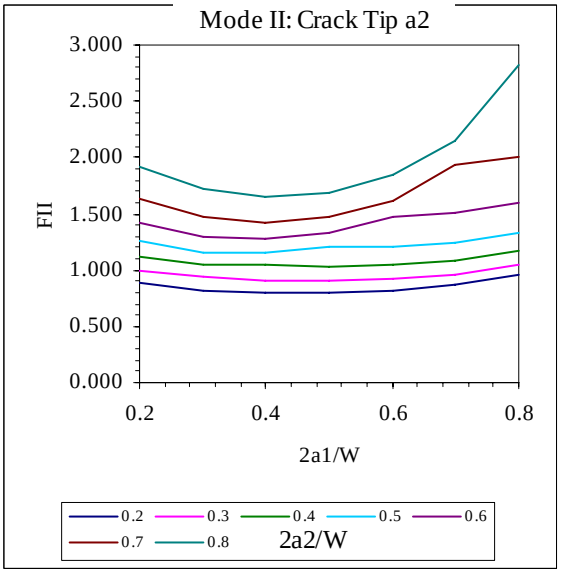

<111/112>, $\theta = -8°$

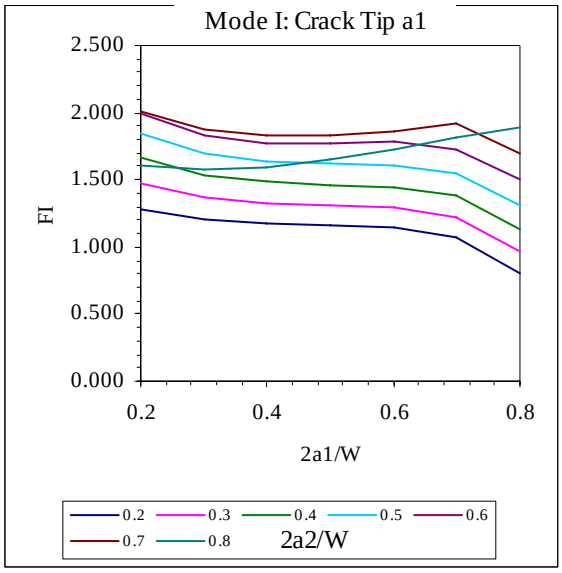

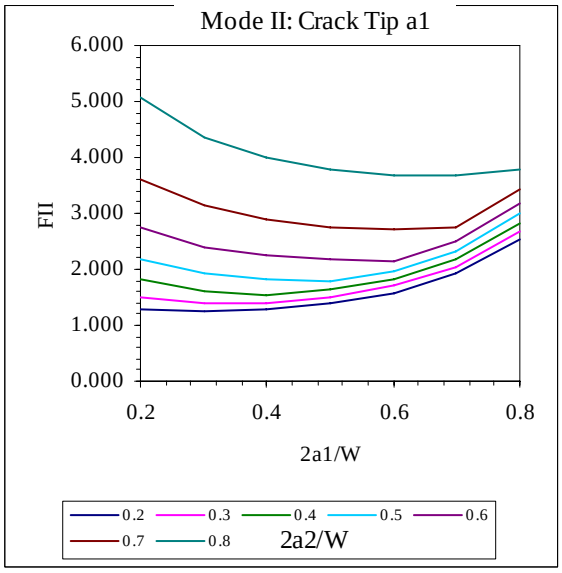

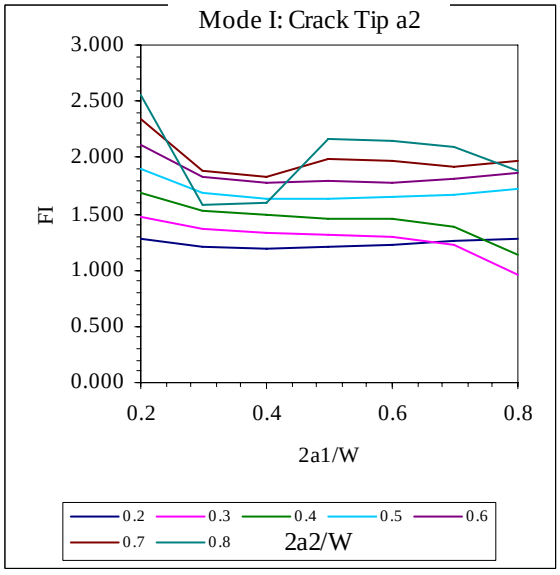

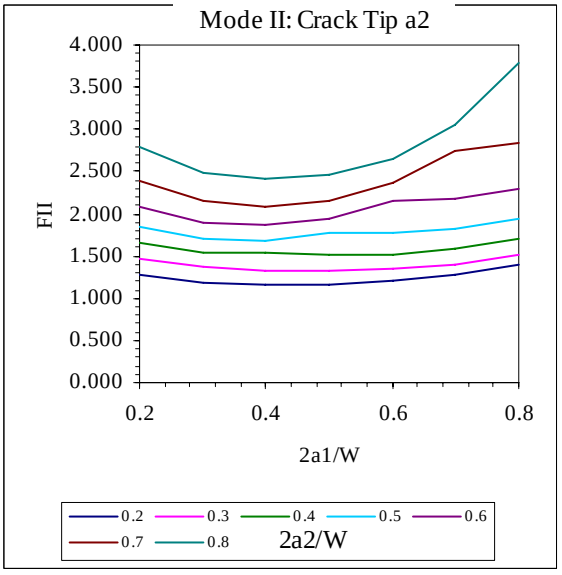

<111/112>, $\theta = -12°$

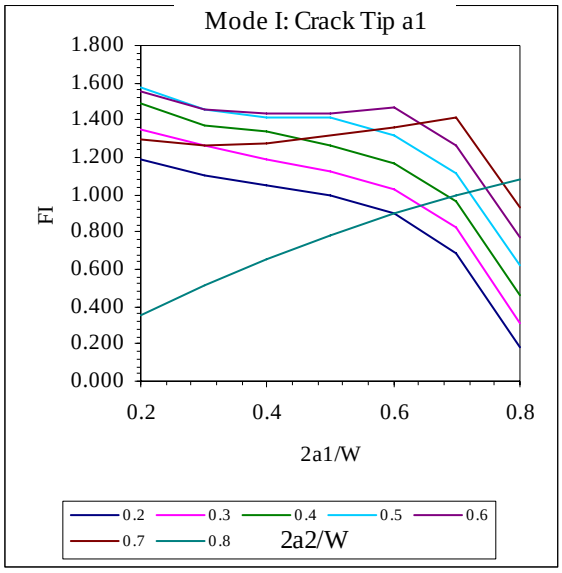

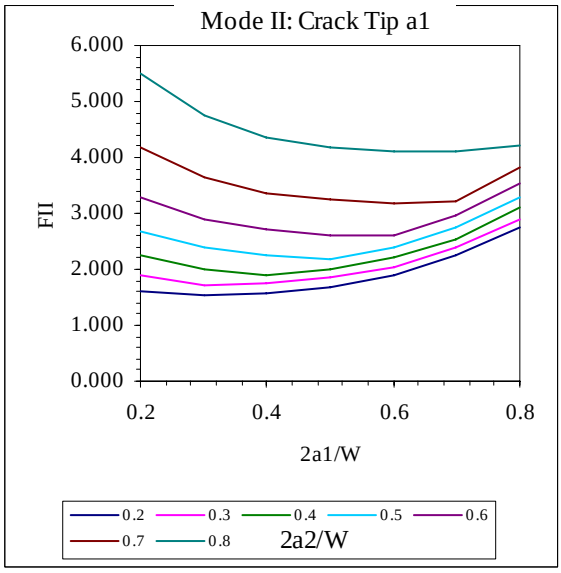

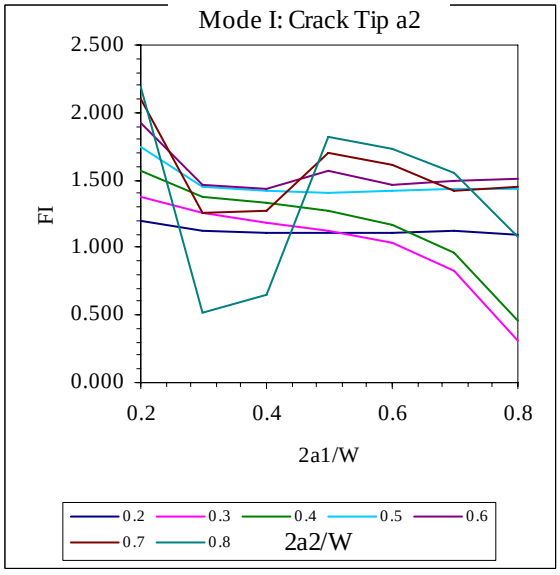

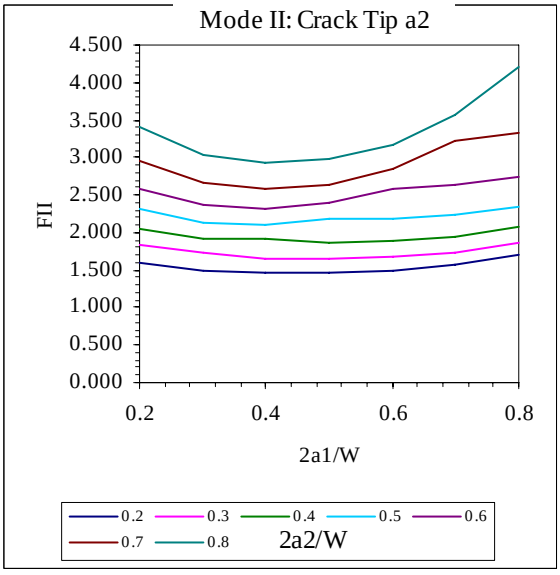

<111/112>, $\theta = -16°$

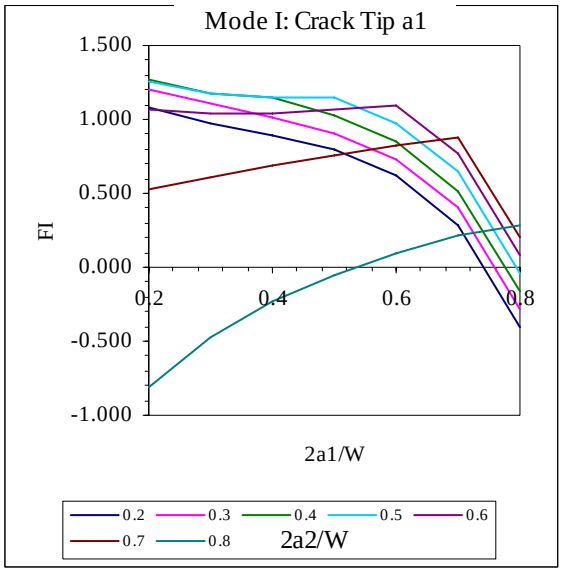

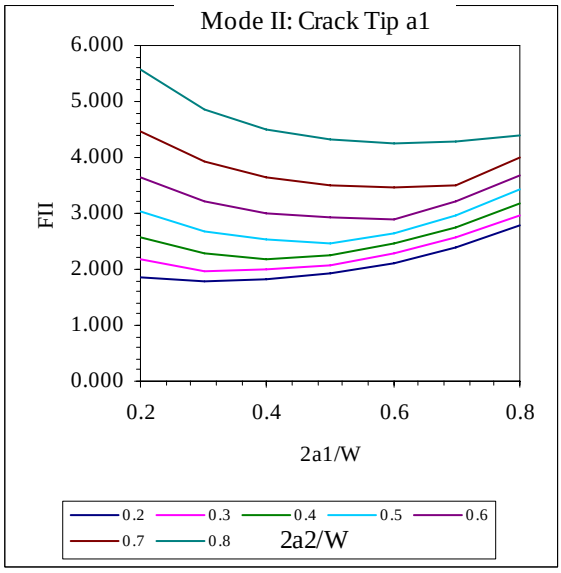

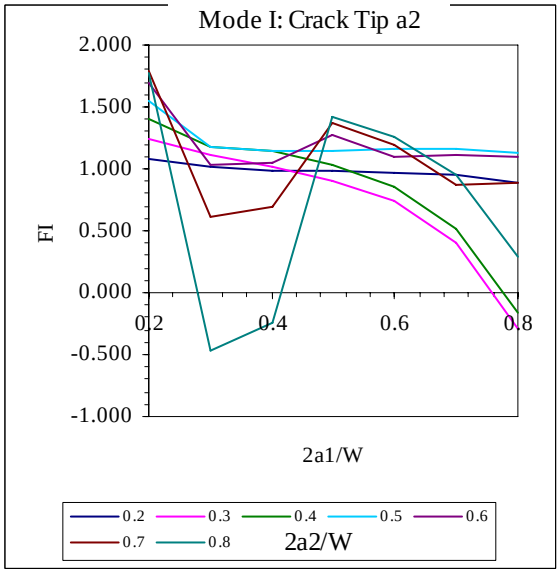

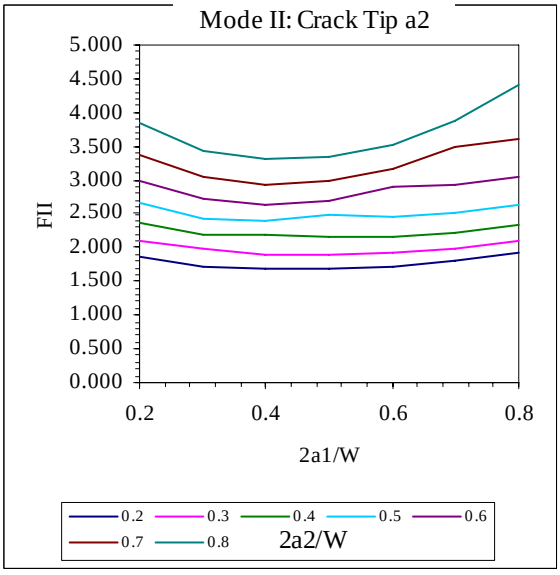

<111/112>, $\theta = -20°$

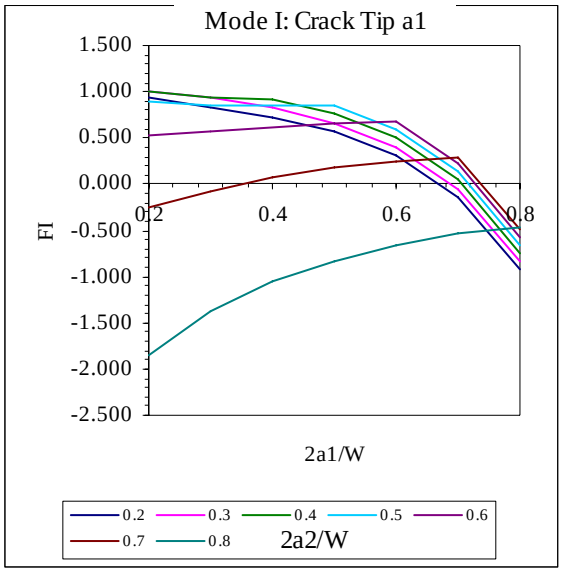

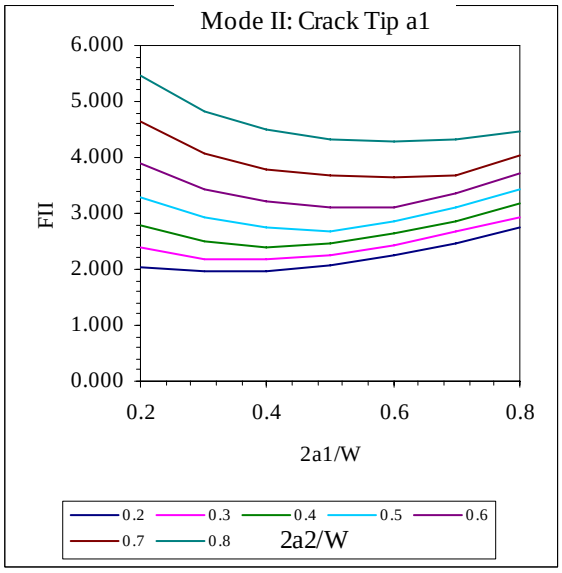

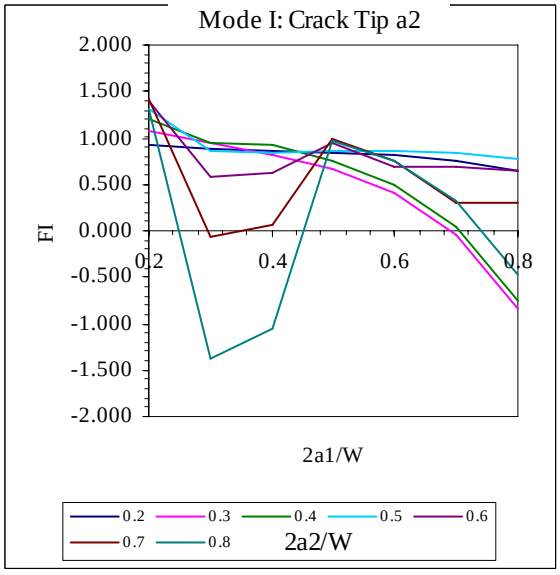

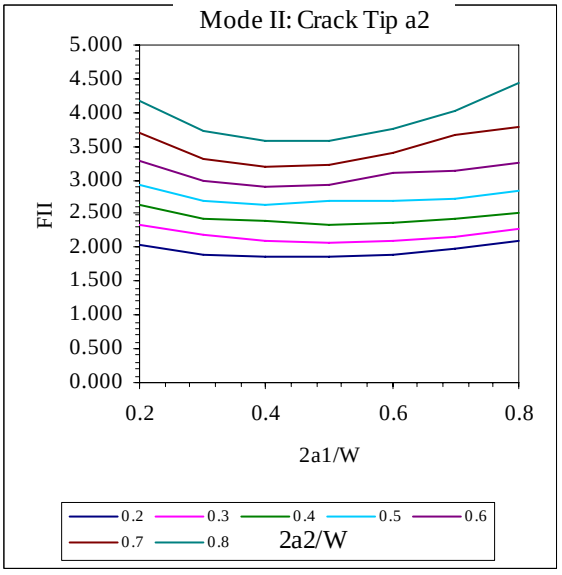

Isotropic, $\theta = 20°$

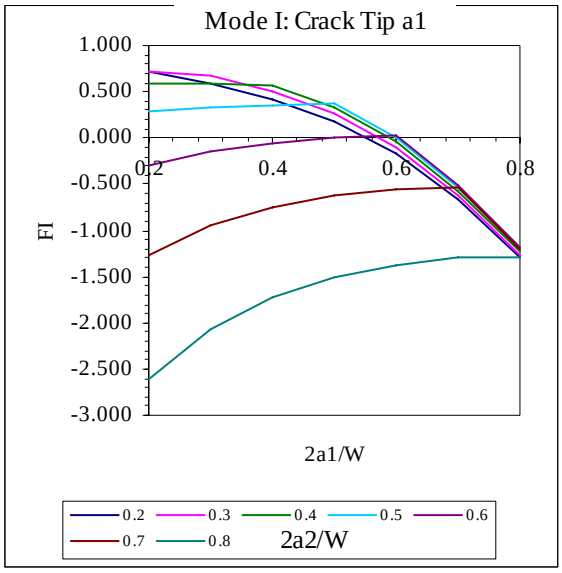

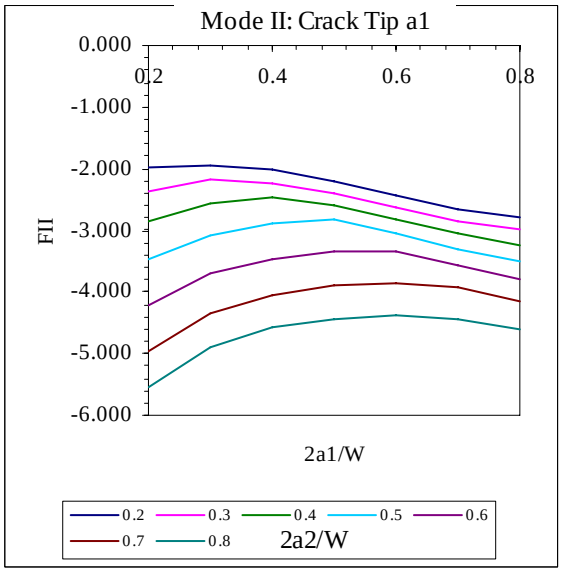

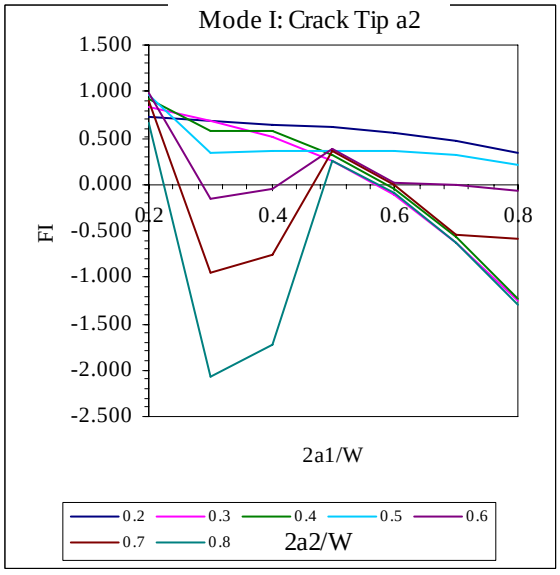

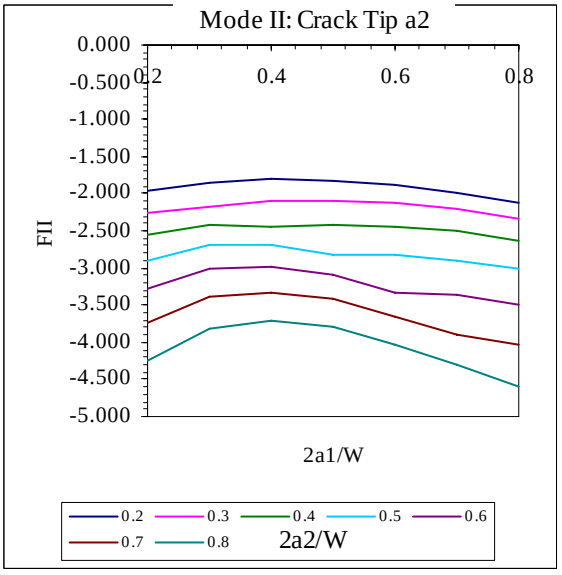

Isotropic, $\theta = 16°$

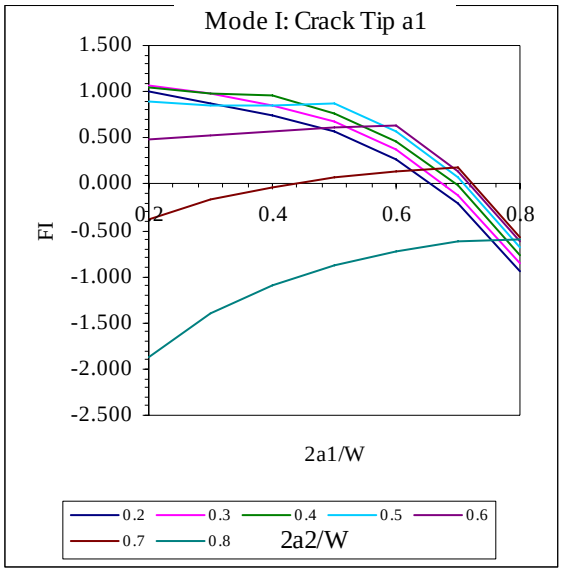

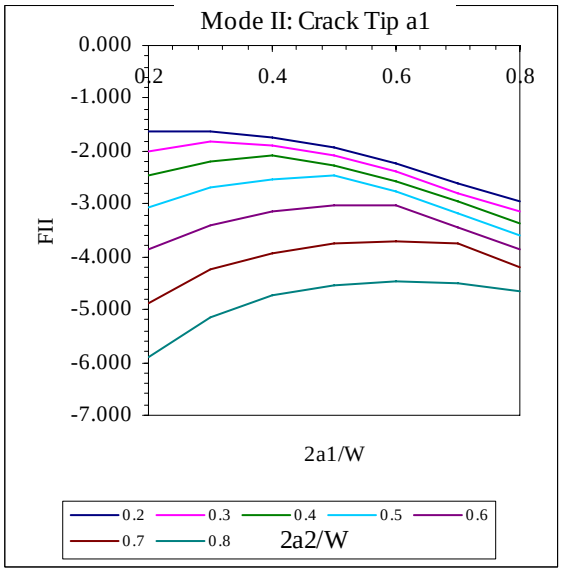

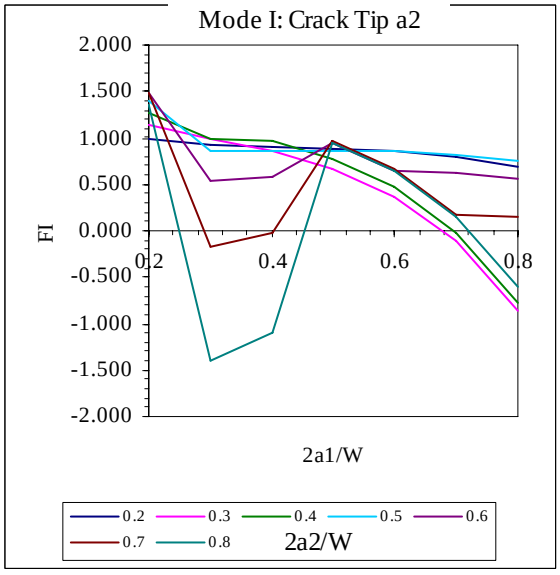

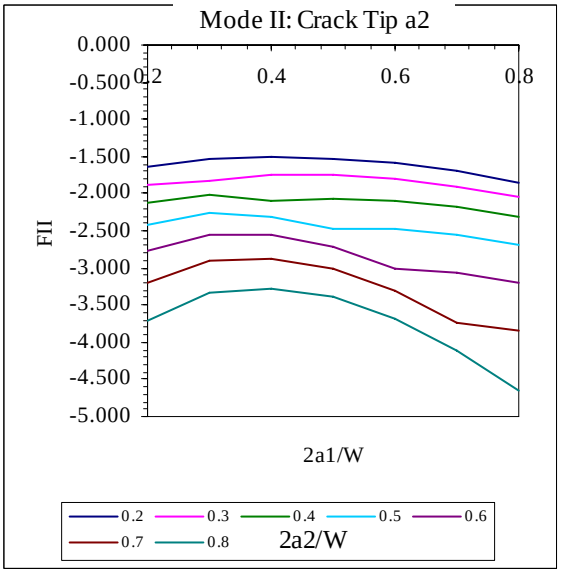

Isotropic, $\theta = 12°$

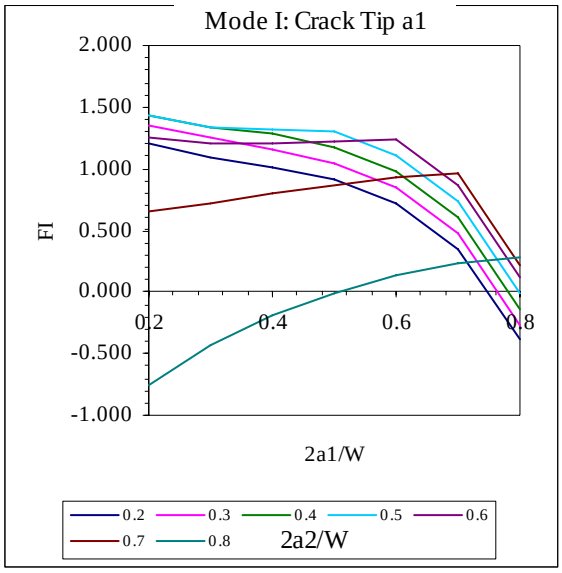

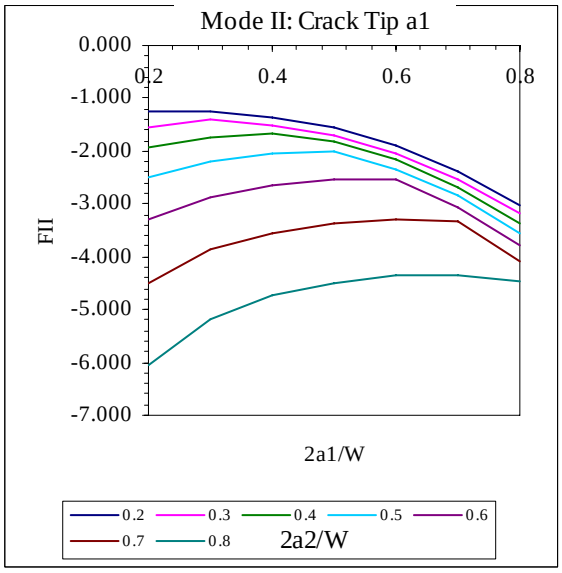

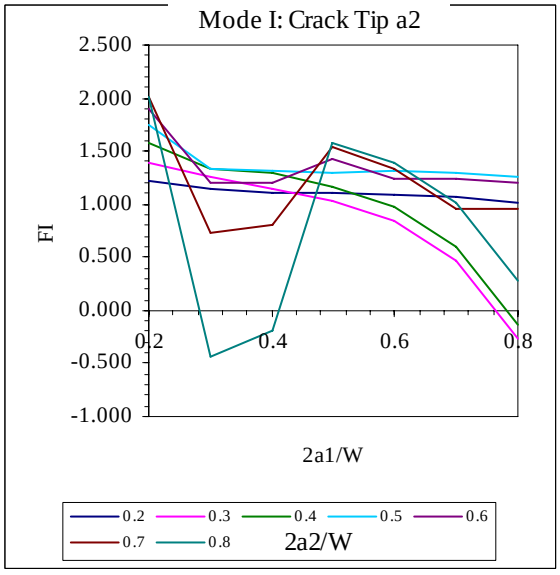

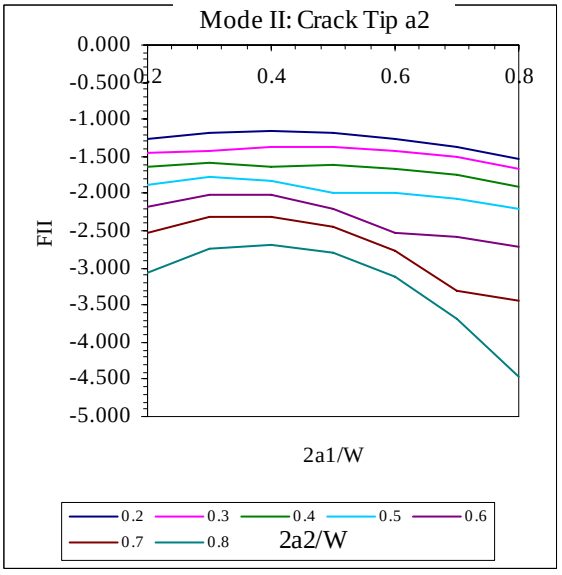

Isotropic, $\theta = 8°$

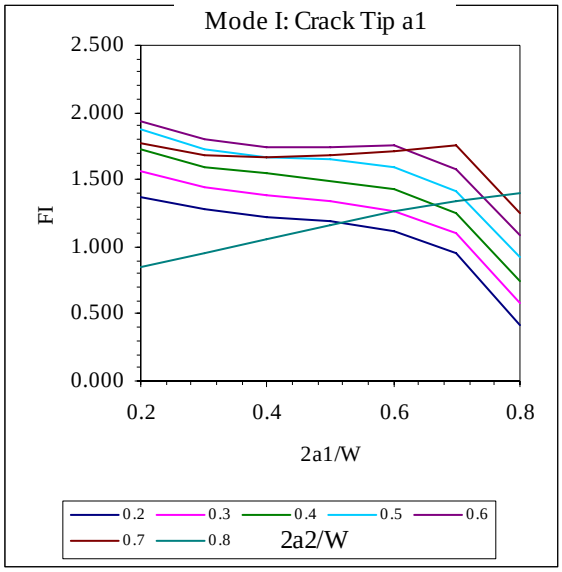

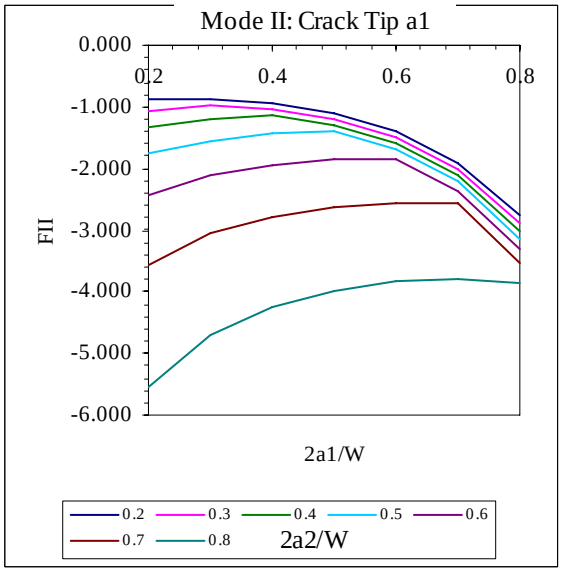

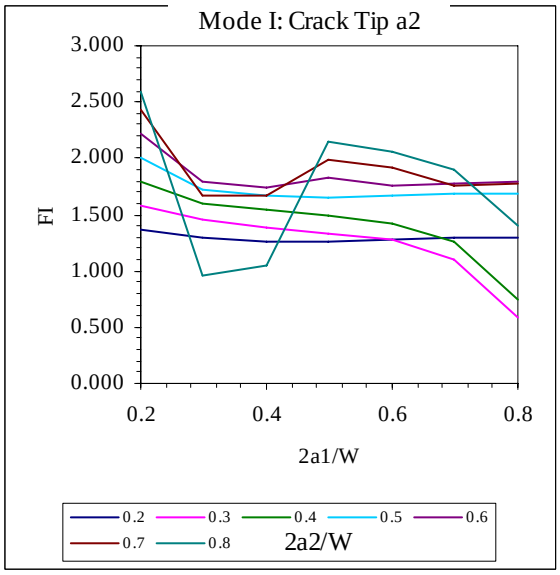

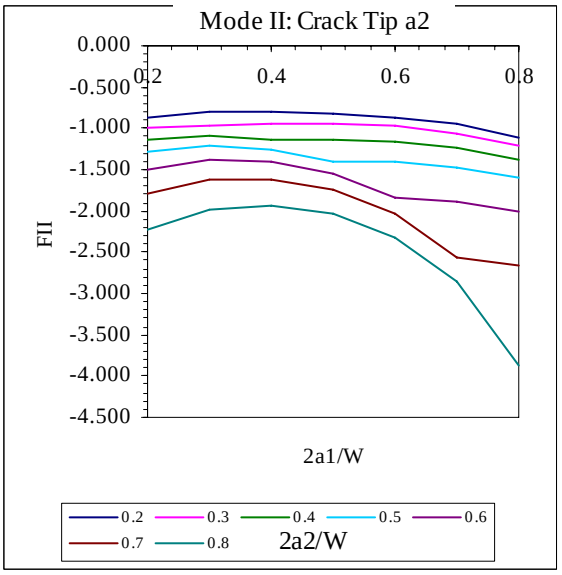

Isotropic, $\theta = 4°$

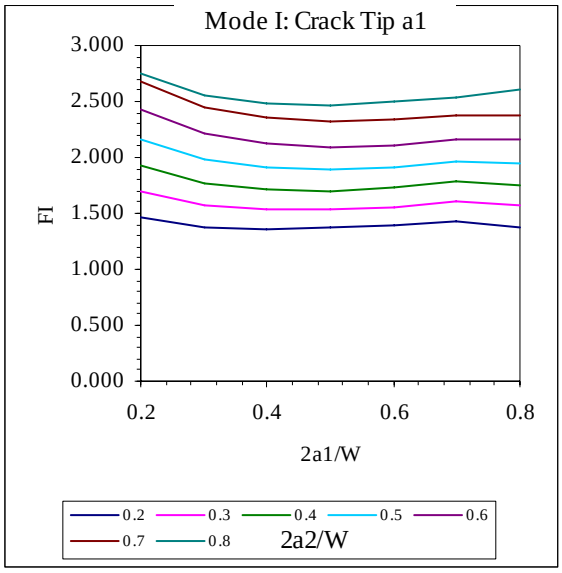

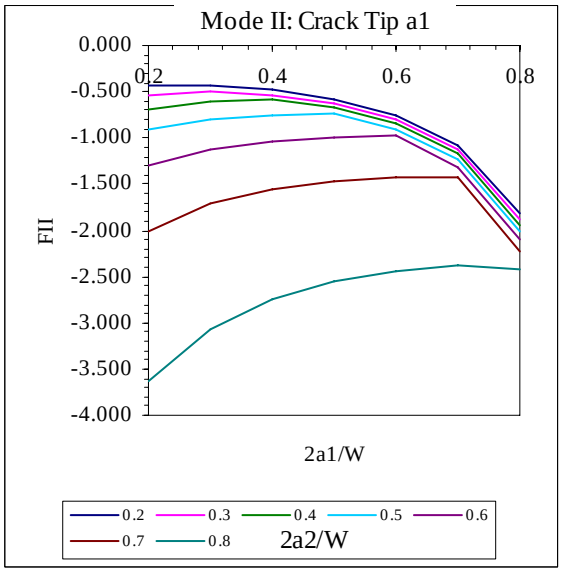

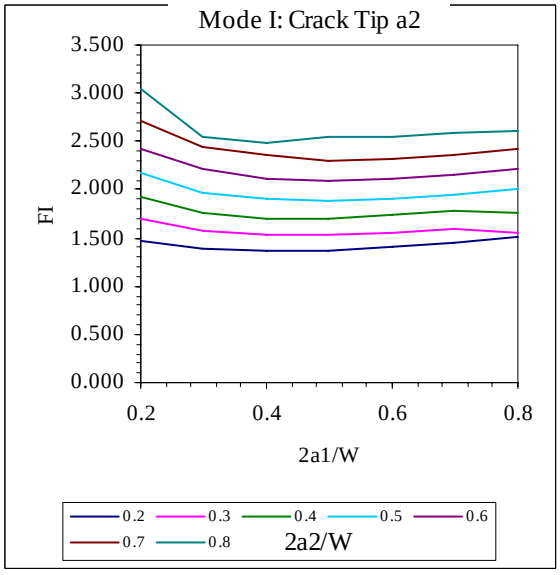

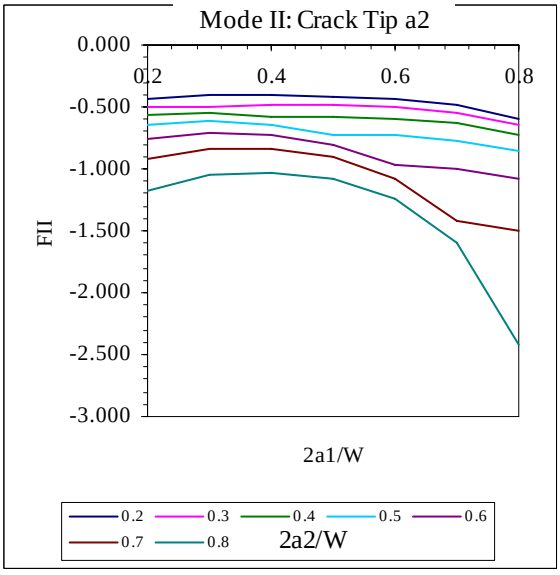

Isotropic, $\theta = 0°$

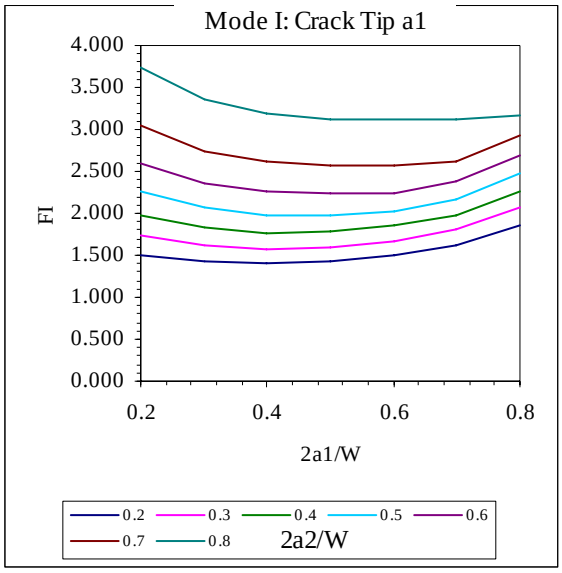

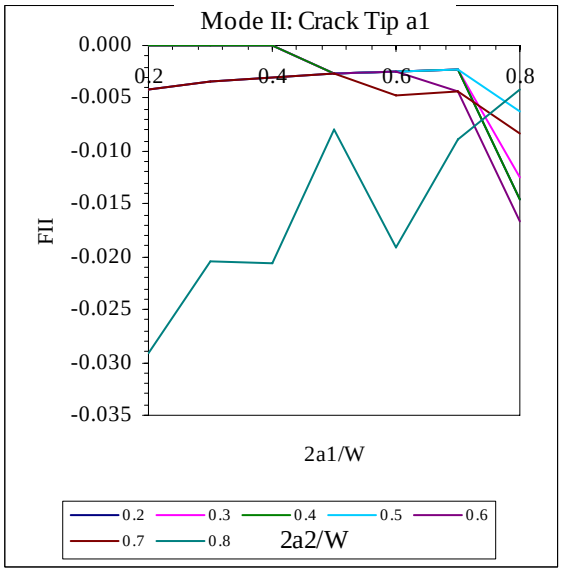

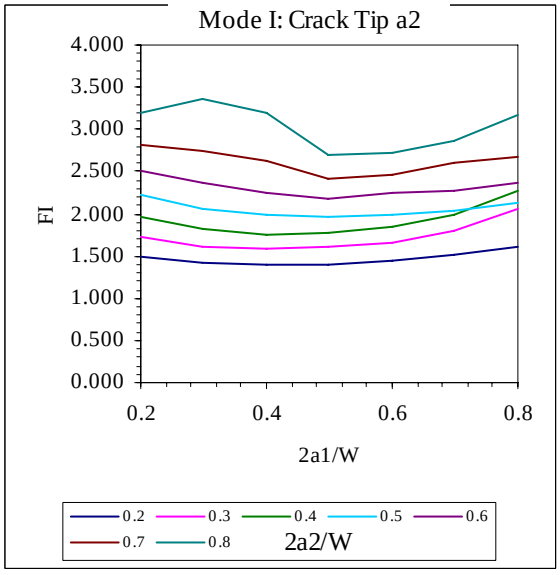

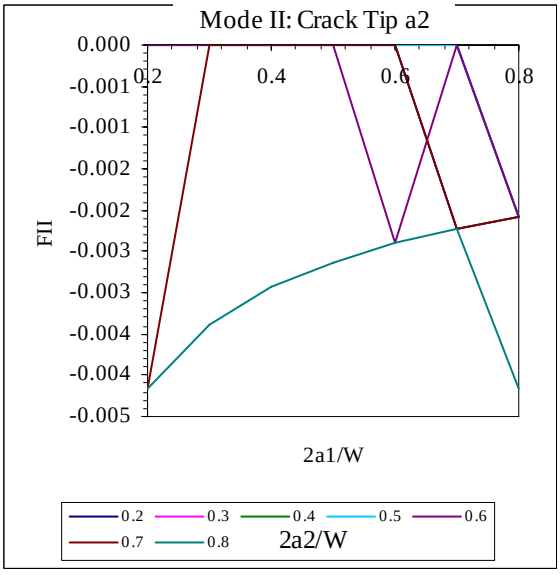

REPORT DOCUMENTATION PAGE

Form Approved
OMB No. 0704-0188

Public reporting burden for this collection of information is estimated to average 1 hour per response, including the time for reviewing instructions, searching existing data sources, gathering and maintaining the data needed, and completing and reviewing the collection of information. Send comments regarding this burden estimate or any other aspect of this collection of information, including suggestions for reducing this burden, to Washington Headquarters Services, Directorate for Information Operation and Reports, 1215 Jefferson Davis Highway, Suite 1204, Arlington, VA 22202-4302, and to the Office of Management and Budget, Paperwork Reduction Project (0704-0188), Washington, DC 20503

1. AGENCY USE ONLY *(Leave Blank)*	2. REPORT DATE	3. REPORT TYPE AND DATES COVERED
	July 2005	Contractor Report

4. TITLE AND SUBTITLE

The *M*-Integral for Computing Stress Intensity Factors in Generally Anisotropic Materials

5. FUNDING NUMBERS

NAS8–36801

6. AUTHORS

P.A. Wawrzynek,* B.J. Carter,* and L. Banks-Sills**

7. PERFORMING ORGANIZATION NAME(S) AND ADDRESS(ES)

*Fracture Analysis Consultants, Inc.
121 Eastern Heights Dr.
Ithaca, NY 14850

**Tel Aviv University
Tel Aviv, Israel

8. PERFORMING ORGANIZATION REPORT NUMBER

M–1141

9. SPONSORING/MONITORING AGENCY NAME(S) AND ADDRESS(ES)

NASA's Space Shuttle Main Engine (SSME) Program
George C. Marshall Space Flight Center
Marshall Space Flight Center, AL 35812

10. SPONSORING/MONITORING AGENCY REPO NUMBER

NASA/CR—2005–214006

11. SUPPLEMENTARY NOTES

Prepared for NASA's Space Shuttle Main Engine (SSME) Program by Fracture Analysis Consultants, Inc.
Technical Monitor: G.R. Swanson

12a. DISTRIBUTION/AVAILABILITY STATEMENT

Unclassified-Unlimited
Subject Category 39
Availability: NASA CASI 301–621–0390

12b. DISTRIBUTION CODE

13. ABSTRACT *(Maximum 200 words)*

Single-crystal super alloys are commonly used for components in the hot sections of contemporary jet and rocket engines. Due to the anisotropic nature of single-crystal materials the use of existing isotropic fracture mechanics calculations leads to errors in stress intensity factors. The difference can be substantial.

Presented in this report is the solution for calculating stress intensity factors in generally anisotropic materials using the *M*-integral. Included are examples of this solution applied to Brazilian disk crack growth specimens.

14. SUBJECT TERMS

single-crystal, anisotropic, fracture mechanics, Brazilian disk, stress intensity fractures

15. NUMBER OF PAGES

88

16. PRICE CODE

17. SECURITY CLASSIFICATION OF REPORT	18. SECURITY CLASSIFICATION OF THIS PAGE	19. SECURITY CLASSIFICATION OF ABSTRACT	20. LIMITATION OF ABSTRACT
Unclassified	Unclassified	Unclassified	Unlimited

National Aeronautics and
Space Administration
IS04
George C. Marshall Space Flight Center
Marshall Space Flight Center, Alabama
35812